12-2014

Physicocehmical Properties and Pre-Exposure Processes Govern Gold Nanoparticle Accumulation in Freshwater Species

Austin Thomas Wray
Clemson University

PHYSICOCHEMICAL PROPERTIES AND PRE-EXPOSURE PROCESSES GOVERN GOLD NANOPARTICLE ACCUMULATION IN FRESHWATER SPECIES

A Dissertation
Presented to
the Graduate School of
Clemson University

In Partial Fulfillment
of the Requirements for the Degree
Doctor of Philosophy
Environmental Toxicology

---

by
Austin Thomas Wray
December 2014

Accepted by:
Dr. Stephen Klaine, Committee Chair
Dr. Cindy Lee
Dr. Lisa Bain
Dr. Marie-Noele Croteau

ABSTRACT

Monitoring the distribution and subsequent effects of nanoparticle (NP) contaminants in aquatic ecosystems will be pivotal to developing regulations that minimize their environmental footprint. Regulators are in a unique position to take a proactive role in shaping how we produce and consume nanomaterials as opposed to the reactive role they have had to adopt with other contaminants. Over the last few decades, researchers have made great strides in describing the fate, behavior, and toxicity of NPs in environmental systems. Recent initiatives have made the transition to scenarios with greater environmental relevance, yet important aspects of fate and behavior remain unexplored. The goal of this dissertation research was to fill in several of those gaps, emphasizing relationships between gold NP characteristics, water chemistry and biodynamic parameters that will contribute to development of robust fate and behavior models. *Daphnia magna* and *Pimephales promelas* were used as model organisms to differentiate the impact of characteristics and water chemistry on two unrelated species residing in a common aquatic habitat.

Uptake and elimination rate constants were derived empirically for *D. magna* exposed to anionic spheres (4, 20 and 30 nm core diameter) anionic rods (18 x 58 nm) and cationic rods (18 x 58 nm) in moderately hard water (MHW). Size and surface charge greatly affected the uptake and elimination rate constant while shape had a relatively minor influence on accumulation. Multiple linear regression models revealed that *D. magna* favor accumulation of larger cationic NPs at high concentration exposures and larger anionic NPs at low concentration exposures**.** *D. magna* and *P. promelas* were then challenged with cationic and zwitterionic NPs in MHW and wastewater (WW) that represented a direct release scenario and a WWTP release scenario, respectively. Surface charge influenced not only the biodynamics in MHW exposures for both *D. magna* and *P. promelas* but also dictated the interactions between the NP and the wastewater components. Cationic NPs transformed in the presence of WW including an increase in size and a slight decrease in surface charge while zwitterionic NPs were unaffected. The influences of these transformations were species specific as *D. magna* experienced a significant decrease in the uptake rate constant while neither uptake nor elimination was affected in *P. promelas.* Finally, we exposed *P. promelas*

to a nano-pharmaceutical (doxorubicin-NP) and the free pharmaceutical (doxorubicin) to determine if the NP altered the distribution and accumulation patterns of the pharmaceutical. The intestine was the primary site of doxorubicin accumulation and the total accumulated content was not significantly affected by the form of the pharmaceutical. Despite a lack of statistical significance, several trends in my data suggest that nano-medicines do not behave like a standard pharmaceutical and, therefore, warrant further investigation to define its environmental impact.

Overall my data argue for prioritization of particle characteristics in risk assessment and inclusion of transformative pre-release processes in fate and behavior model development. At the moment releases of NPs into the environment are well below toxic thresholds. Yet as the popularity of nanotechnology further penetrates all aspects of society, engineered NPs will form a larger presence in environmental systems that could give rise to serious environmental consequences. Proactive regulation of NPs aided by comprehensive modeling initiatives are of paramount importance to making sure we use this technology responsibly or else we risk adding another name to the dubious pantheon of legacy contaminants.

DEDICATION

To Thomas and Judith Wray, the source of my enduring respect for and appreciation of nature without which I'd surely be lost. Their love and encouragement kept me motivated when problems seemed insurmountable and inspired me to accomplish more than I thought possible.

ACKNOWLEDGMENTS

I want to express my gratitude to family, friends, co-workers and collaborators whose influence radiates from the words in this dissertation. First to my advisor, Dr. Steve Klaine, for his guidance and encouragement throughout my graduate student career. His advice was integral to designing experiments, analyzing data, forming sound conclusions and improving the prose of my manuscripts. My committee members, Dr. Cindy Lee, Dr. Marie-Noele Croteau, and Dr. Lisa Bain, for their direction of my dissertation and for molding my manuscripts into concise, well-written, publishable work.

My parents, Thomas and Judith, for their support and encouragement during my five years at Clemson. Throughout my life they have supported my endeavors, trusting that I knew what I was doing and giving me the confidence to figure it out when I didn't. They have enabled me to take risks and to choose my own path, giving me the freedom to embrace my passions rather than settling for what is convenient. My brothers, Travis Wray and Tony Pingitore, for keeping my spirits elevated and reminding me why I chose this path. The best memories I have from the past five years were from the time spent during summer vacations and on impromptu visits with these two. I'm lucky to have two caring and supportive brothers who I also consider my best friends.

Norm Ellis, the lynchpin of the gold nanoparticle work, for analyzing my gold samples on the ICP-MS and giving suggestions on improving recovery and reducing analytical variability. Donald Mulwee and Dr. JoAn Hudson for turning what could have been dull tedious work into something just short of enjoyable. I want to thank them both for their instruction on operating the electron microscopes and for their patience during my struggles to produce the images found in this dissertation. Dr. Alaadin Alkilany for teaching myself and my lab mates how to synthesize gold nanorods and for imparting advice on the roles and responsibilities of a graduate student that stuck with me throughout my graduate career. Dr. Vincent Rotello, Daniel Moyano, and Gulen Yesilbag from the University of Massachusetts-Amherst for collaborating on my dissertation, synthesizing the gold nanomaterials and doxorubicin nanomaterials for the third and fourth chapters. Dr. Alan Jones, the resident analytical chemist, for training me on several analytical instruments and troubleshooting when the instruments were not cooperating.

The members of the Klaine lab, both past and present, for their feedback on the work presented in this dissertation and for helping me find enjoyment in the mundanity of laboratory work. Dr. Joe Bisesi, Dr. Aaron Edgington and Dr. Brandon Seda were excellent mentors during my first three years, teaching me the basics of toxicology lab work and giving me the courage to fail and the confidence to try again. Dr. Brad Glenn and Lauren Sweet were two of the best office mates I could have asked for. They listened attentively to my experimental woes and often led me to a solutions I would not have thought of myself. Katherine Johnson and Erica Linard for our daily chats on all things science and non-science that kept me sane even on the darkest days. Finally, I want to thank John Smink for teaching me the importance of proper lab etiquette and safety and for his help with establishing and maintaining animal cultures. I am nothing without those around me and I couldn't have asked for a better supporting cast.

TABLE OF CONTENTS

Page

Table of Contents (Continued)

Page

Table of Contents (Continued)

Page

Table of Contents (Continued)

Page

LIST OF TABLES

LIST OF FIGURES

List of Figures (Continued)

Figure Page

CHAPTER ONE

LITERATURE REVIEW

The advent of nanotechnology was a significant evolution in industrial design offering up a sophisticated toolset with which to improve and innovate on solutions to our most recalcitrant problems. Conceptually nanotechnology has near limitless potential. As a result, eager investors and government institutions have provided substantial capital contributions toward research and development. The fruits of these investments run the gamut from enhancements of more pedestrian consumer based products to unprecedented control over pharmaceutical administration and drinking water purification. Despite these auspicious beginnings, many remain wary of the possible negative consequences that will materialize if institutions are not in place to keep nanotechnology in check. In the past, unbridled technological progress has led to serious human and environmental health issues with repercussions that have persisted long after its discovery. Fortunately, we can use the lessons learned from these past mistakes to inform regulation of this burgeoning technology [1]. Addressing the implications of human and environmental exposure before nanotechnology reaches a critical mass is an absolute necessity so that our society can take advantage of this novel material while minimizing the repercussions.

Origins and Economics of Nanotechnology

The Origin of Nanotechnology

Nanotechnology has a diverse, storied history spanning centuries and numerous scientific disciplines. The concept of nanotechnology as the industrial powerhouse we know today originated from the simple notion of thinking large on a small scale. Amazingly artisans exploited this technology for centuries without this guiding principle. Between the 4th and 18th century, items such as the Lycurgus cup [2], stained glass windows, and “Damascus” saber blades [3] were produced using techniques reliant upon nanotechnology. These craftsmen recognized that certain processes bestowed unique properties to their works; processes that were years later revealed to integrate aspects of nanotechnology.

The birth of nanotechnology cannot be attributed to a single investigator or experimental result. Rather the arrival of nanotechnology is a product of several seminal discoveries during the 19th and 20th century that each contributed to the shifting technological landscape. Accounts of synthesized colloidal materials and their unique properties [4,5], alongside development of methods for near atomic level exploration [6,7] laid the technical groundwork for research in this field that had yet to attain universal acceptance. In 1960, a seminal presentation by Richard Feyman elevated the concept of atomic scale technology out of obscurity. He was the first to ruminate on the implications of exploiting materials at smaller scales in a manner that spoke toward mainstream application. In his speech, *There's Plenty of Room at the Bottom*, he envisioned manipulation and control occurring on a small scale, at the level of individual atoms, in a bottom up approach at synthesizing unique structures [8]. His speech was imbued with the essence of nanotechnology despite never mentioning the term. It was not until several decades later that the actual term nanotechnology was introduced into the collective consciousness.

Over several decades nanotechnology flourished into an industry standard as scientists and researchers realized the potential of a diminutive scale. The years succeeding Feyman's speech were incredibly fruitful resulting in the discovery of numerous novel nanomaterials [9,10] and methods to control the physicochemical characteristics of the final product [11-16]. The commercial applications of nanotechnology broadened as design methods became more sophisticated. In the 1990s and early 2000s nanomaterials started to appear in consumer products. In subsequent years nanotechnology expanded its reach into other disciplines including environmental remediation and biotechnology. As of 2013, 1,628 consumer products containing nanomaterials were commercially available according to a voluntary registration initiative [17]. This value likely only represents a small fraction of the current market penetration as nanotechnology carries significant clout in many industrialized countries. In the coming years the implementation of nanotechnology is expected to expand significantly, limited only by the imagination of its creators.

The Economics of Nanotechnology

The popularity of the nanotechnology industry has increased substantially over the last decade with an average annual growth of 25-30% [18]. This unprecedented pace is sustained by a strong flow of

capital from public, private and government investors. Federal investments through the National Nanotechnology Initiative (NNI) in the United States approach USD 1.8 billion annually, up from USD 463 million in 2001 at the inception of the initiative [19]. These investments consist of eight categories including basic research, nanomaufacturing, and environmental health and safety (EHS). Historically the gulf between EHS and nano-production allocations has been enormous. In 2006, only 2.8% of NNI designated funding was identified specifically for EHS research. However, growing concerns for human and environmental well-being have translated to increased EHS allocations upwards of 7% [20]. Not to be outdone, corporate investments in research, development, and commercialization were estimated at approximately USD 9 billion in 2010. Currently few sources of public funding exist due to the perception of risk associated with public nanotechnology [19]. This appears to be but a small setback that will likely be overcome in the near future further extending the reach of nanotechnology.

Synthesis of Metallic and Metal Oxide Nanomaterials

Nanotechnology owes much of its popularity to the unique properties that bequeath abilities and promote behavior not observed in its bulk counterpart. Unique synthetic nanomaterials are produced in laboratories through meticulous manipulations of the synthesis procedure in an engineering top-down, chemical bottom-up or hybrid approach [21]. Each method has its own idiosyncrasies that grant the manufacturer precise control over the characteristics of the nanomaterial. The following discussion of metal and metal oxide nanomaterials is not exhaustive as there are numerous subtypes of nanomaterials in each group. Instead the focus is held squarely on nanomaterials synthesized for commercial purposes. Moreover, the near infinite number of different techniques used for particle synthesis speaks to the diversity of particles in production and on the market. Accordingly, only the most important/common synthesis procedures will be discussed in this review

Metallic nanomaterials are constructed with either a metallic core or in the oxide form. These types of nanomaterials are found in a wide range of applications from transparent sunscreen to antimicrobials to drug delivery as discussed in the next section. Silver is the most popular metallic nanomaterial, at least for consumer applications, followed by titanium, zinc and gold [17]. Other metals,

including nickel, copper, cobalt, platinum, cadmium, lead, bismuth and tin have also been synthesized at the nanoscale though functionality is limited by the stability of the core metal [22-25]. The bottom up approach incorporates solvents, heat, surfactants and/or a strong reducing agent to convert a metal salt into a nanomaterial [14,16, 23, 26-29]. Metal ions are reduced to a zero valent state creating metal clusters that act as nucleation sites for additional metal attachment. The concentration and ratio of reagents, presence of certain reagents (such as $AgNO_3$ in gold rod synthesis), speed of reagent addition, and/or the temperature of the solution will determine the size and shape of the final product [12,13,30-33]. The top down approach involves reducing the bulk metal to a desired size and shape using lithography, laser ablation, emulsion or other processes [24,34].

Further control over the final configuration of the nanomaterial is accomplished through addition of a ligand molecule to the particle surface. Reagents that act as surface stabilizing ligands are often included to avoid immediate aggregation of the nanocores. In certain procedures a ligand has a dual role acting as the reducing agent and as a facilitator of size and shape [16,29]. The type of interaction between the ligand and nanomaterial core (i.e. electrostatic or covalent bond) is predetermined by the synthesis procedure. The identity of the surface ligand, however, is not restricted by the initial synthesis conditions and can be replaced through ligand exchange [26]. The advent of click chemistry in the material science community has further permitted greater control over ligand attachment. Material scientists select a base ligand that is covalently attached to the particle surface with an exterior moiety that allows for extension of the ligand with any number of compounds that chemically bond to the moiety [35]. Through click chemistry the surface ligand can be shaped, modified and extended infinitely so long as an exterior moiety is available. Regardless of how it is attached the presence of a ligand confers greater aqueous stability, either sterically or electrostatically, ensuring long-term viability in stock solutions. Surface ligands can likewise be added to nanomaterials made with top down methods if deemed necessary for stability [24].

Metal oxide nanomaterials are another subset of metallic nanomaterials that incorporate an oxygen moiety to improve stability of the metallic nanomaterial. The most common types of metal oxide particles are titanium dioxide (TiO_2), zinc oxide (ZnO), cerium oxide (CeO), magnetite (Fe_3O_4), and copper oxide (CuO). Much like the metallic nanomaterials, top down and bottom up approaches are used in synthesis.

Synthesis methods include combining chemical precursors, chemical and physical deposition, and thermal decomposition [36-39]. Modifications can likewise be introduced during the synthesis based on reagent selection or as a step in post-production.

A few metal-based nanomaterials exist beyond the traditional metallic and metal oxide forms. Quantum dots are constructed from a core and shell that are made of metal complexes, i.e. CdSe core with a ZnS shell. Bimetallic nanomaterials, as the name implies, consist of two metals layered together [40]. Lastly, metallic nanomaterials have been experimented in combination with other nano-constructions (such as dendrimers) to form hybrid nanostructures with idiosyncratic properties [41].

Applications of Metallic and Metal Oxide Nanomaterials

Consumer Based and Remediation Applications

Publically available data on nanomaterial market penetration indicate a strong presence of metal and metal oxide nanomaterials in consumer-based products [17]. Silver nanomaterials imbue textiles, washing machines, medical supplies, toothpaste, toys, shampoos and detergents with stronger antimicrobial defenses [42]. Nano-silver is also an excellent electricity conductor, which is exploited in electronics [43]. Titanium dioxide and zinc oxide nanomaterials are found in sunscreens [44], personal care products [45], and paints [46]. Titanium is also prevalent in the food production industry where it is used in bulk and nano form as a food pigment. Gold is primarily a biomedical tool but is also used liberally in cosmetics and in the construction of nano-electronics [47]. The reach of metal and metal oxide nanomaterial implementation extends beyond the improvement of conventional consumer products to more innovative and revolutionary applications. For example, nanomaterials have proven instrumental in developing unique solutions for environmental remediation. Iron-based particles in particular have shown great promise in removing arsenic from groundwater [48] and degrading organic chemicals such as carbon tetrachloride [49] and trichloroethylene [50].

Biomedical Applications

The biomedical field is perhaps the greatest benefactor of the nanotechnology movement. Significant resources have been devoted to developing more effective drug delivery systems, improving

resolution for imaging and revolutionizing cancer treatment procedures. The precision of nanoparticle manipulation supports the creation of drug and gene delivery systems that target specific tissues [51-53], cell types [54,55], and even cellular organelles [56]. In the design of the drug, consideration is also given to the method of drug attachment. Timed release of the drug can be tuned to physiological conditions [54,57] or external stimuli [58,59], and can be designed to resist metabolic pathways that often discourage proper pharmaceutical distribution [60,61]. Tissue- and cell-specific release of pharmaceuticals reduces the percentage of the dose that is metabolized before reaching the active site or activated at non-target sites. This allows for lower dosage requirements, fewer and less extreme side effects and minimizes drug excretion.

The optical properties of certain metallic nanomaterials make them suitable candidates for whole body imaging. Much like in the drug delivery scenario, the nanomaterials can be affixed with ligands that increase residence time and direct the nanomaterials to specific parts of the body. Gold and magnetite nanomaterials and quantum dots present a significant improvement over current imaging techniques as their unique optical properties contribute to enhanced resolution of tissues and cells [62-64]. Nanomaterials are also the building blocks of novel weaponry in the perpetual battle with cancer. Not only can nanomaterials carry chemotherapeutic drugs preferentially to tumors [65] and improve characterization and imaging [66], but the nanomaterial can also act as a tumor-suppressing agent itself. The absorbance properties of gold nanomaterials, for example, are being exploited in the creation of novel photo thermal cancer treatments [67].

Of the metallic nanomaterials, gold has garnered the most interest for biomedical applications because of its low toxicity, high biocompatibility, and optical properties [52]. Gold is not suitable for all applications and thus a number of other nanomaterial solutions exist for biomedical applications [68]. It remains to be seen which techniques rise above the rest and are adopted and standardized in the biomedical community.

Impact of Nano-Devices on Release and Toxicity of Anthracyclines

The specificity of nanomaterial drug delivery systems make them a great candidate for treating cancer [65]. Chemotherapy treatment using anthracycline compounds can benefit immensely from the nano-delivery system because these compounds are quite effective at suppressing tumor malignancies but are equally damaging to healthy tissues [69]. The primary mechanism of action for anthracyclines is intercalation into DNA strands causing deformation and strand breaks disrupting DNA synthesis. The less desirable mode of action is the production of free radicals that causes various forms of oxidative stress and leads to myelosuppression after acute exposures and irreversible cardiomyopathy from chronic exposures [69]. The nano-delivery systems are also designed to avoid early metabolism and excretion; a problem that reduces the effectiveness of anthracycline treatments [70].

Beyond the clear human health benefits, using nano-devices for drug delivery will also be a boon for the environment. Lower dose requirements and more efficient delivery to the active site will reduce the amount of pharmaceutical excreted into waste streams and minimize its environmental impact. Anthracyclines have a low environmental footprint from the conventional treatment thus the environmental benefits of attaching this compound to nano-devices will not be as obvious as with other over the counter and commonly prescribed pharmaceuticals. Wastewater treatment facilities range from highly efficient (>90%) to wholly inadequate (~0%) in their ability to remove anthracyclines from the influent [70, 71]; however, concentrations in the environment are not expected to exceed the ng/L range. For some perspective the EC50 for doxorubicin is 1.14 mg/L in exposed fish cell lines [72], 2 mg/L for *Daphnia magna*, 13 mg/L for *Pseudokirchneriella subcapitata*, and >1000 mg/L for *Pseudomonas putida* [73]. Using these exposure and effects data, risk quotients for doxorubicin were calculated to be well less than one for all organisms suggesting that doxorubicin is not a threat to the aquatic environment [71]. By all accounts the environmental impact of these compounds is expected to be minimal yet there are some residual concerns relating to the genotoxic potential of doxorubicin, which was demonstrated at concentrations as low as 0.074 mg/L [73].

A transition to nano-based delivery systems will come with its own set of issues that need to be addressed before commercial adoption. If traditional treatment of cancer transition to using nano-delivery systems the WWTP removal efficiency will then be a function of the nanomaterial, which could have ramifications for accumulation and toxicity of these compounds in aquatic organisms. As drug delivery systems become more reliant upon nano-based solutions the nanomaterials will need to be integrated into the pharmaceutical exposure paradigm as the combined contaminant could lead to higher than expected environmental concentrations and unanticipated toxicity.

Release of Metal and Metal Oxide Nanomaterials in the Aqueous Environment

The release of nanomaterial into aqueous and terrestrial environments is unavoidable considering the mass appeal and widespread use of nanotechnology [74-78]. Environmentally relevant simulations of weathered consumer products demonstrate the potential for substantial releases of nanomaterials or contaminants originating from nanomaterials (ions, aggregated nanomaterials) into aqueous ecosystems [42,46,79-81]. Discovery and identification of engineered nanomaterials in the environment will only become more frequent as production increases and monitoring techniques achieve greater sensitivity [82].

The identity and associated behavior of the nanomaterial in the environment will be closely linked to the route or routes through which it travels toward its inevitable environmental destination. Accordingly, Nowack et al. [83] categorized engineered nanomaterials into four subgroups that describe the modifications on the material occurring during production and after release. Pristine nanomaterials are the original stand-alone synthesized nanomaterial that are often a precursor to the final product. Product-modified nanomaterials are those that have been linked to a specific product, often embedded in the product matrix. As the environment takes its toll on the nano-enhanced product it transforms into a product-weathered nanomaterial. Finally, nanomaterials that undergo additional environmental transformation after dissociation from the product are categorized as environmentally-transformed nanomaterials [83].

The probability of pristine nanomaterials entering the environment intact is quite low [83]. A major reason is that the pristine nanomaterial is not often used in products without further manipulation. Designers select modifications that improve the compatibility of the nanomaterial with the intended matrix

[83,84], change the functionality of the particle [52,85] or reduce potential toxicity [44], among other reasons. The embedding process can even vary from product to product. Certain nanomaterials are loosely bound while others are locked into the product [81,86,87]. The degree of embedding is not necessarily the same for all products with a similar application, e.g. silver nanoparticles added in during textile production, further complicating attempts at developing comprehensive release models [81,87,88]. These design decisions can have a profound impact on the type of nanomaterial that enters the environment and the route of entry.

Scenarios for Direct Release

Nanomaterials destined to reach ecosystems have several pathways for environmental entry that are closely tied to the application of the product. Direct releases, while not common, do occur during production, manufacturing and use of products containing nanomaterials [89]. Certain applications require direct input of nanomaterials into the environment including remediation with zero valent iron and water purification. Nano-enhanced cosmetics or sunscreens can enter the environment directly if worn while swimming [90]. Likewise direct release could originate from using other nano-enhanced products in areas with proximity to the environment and no barrier to entry, i.e. no waste or storm treatment system. Overflow of sewage and storm water systems is another contributor of engineered nanomaterials in aquatic systems [89].

Transformation and Release During Waste Incineration

By far the more common release scenarios are the indirect pathways fundamentally tied to our waste disposal system. Wastewater treatment plants (WWTP), waste incineration and landfills are the three important waste disposal pathways that stand between a nanomaterial and the environment [83]. Each pathway is capable of transforming the material from a known quantity into a foreign entity.

The release of nanomaterials from landfill and waste incineration has not received as much attention as those originating from WWTPs. For waste incineration, this is likely because processing of nanomaterials in this manner is expected to contribute little to the overall nanomaterial burden in the environment [75,91]. Fully combusted nanomaterials, specifically carbon-based materials, are generally

reduced to their chemical components nullifying their threat to the environment [92]. Filter systems installed at waste incinerations sites retain ultrafine particles with 99.6 to 99.9%, efficiency, which prevents nanomaterials with a proclivity for volatilization from entering the atmosphere [75]. However, metallic nanomaterials are more stable and resistant to combustion; therefore, waste incineration is not an end of life process. One of the few published studies investigating the entire waste incineration process demonstrated that CeO_2 nanomaterials readily bind to solid residues and accumulate in the slag and fly ash rather than exit via flue gas [91]. The small fraction of CeO_2 that did escape into the flue gas was filtered out with 99.6-99.9% efficiency confirming the assumption that airborne nanomaterials present a minor threat. Mueller et al. published similar findings for titanium, zinc and silver nanomaterials based on a model constructed from available data [92]. Interestingly, CeO_2 nanomaterials retained their original physicochemical properties despite fluctuations in redox conditions that are known to alter properties in other scenarios [91]. This is likely a unique observation (possibly for CeO_2 exclusively) and it is expected that most nanomaterials will not be able to avoid transformation during the incineration process [92]. In their conclusions Walser et al. lamented that nanomaterials capable of withstanding combustion remain an environmental threat [91]. These materials may escape into the environment during handling, processing and storage of contaminated slag and ash. In many cases this nanomaterial burden is transferred to landfills where it joins a substantial nanomaterial conglomerate originating from biosolids, consumer products and other forms of solid waste [91,92].

Transformation and Release After Disposal in Landfills

Landfills will be a major sink for solid waste containing nanomaterials. In the landfill, these materials along with other forms of solid waste are at the mercy of extreme weather conditions. Landfill leachates originate from a combination of heavy rainfalls events, biochemical processes and water stored in the solid waste [93]. These leachates are known for mobilizing pollutants from their associated solid waste. If this occurs in a landfill without a system for leachate collection or if the leachate is treated improperly contaminants may leak into nearby surface water or percolate through soil into groundwater reservoirs.

Several studies have demonstrated that nanomaterials or contaminants with nanomaterial origin will partition into the leachate creating another route of environmental exposure. Benn et al. [42] observed

silver concentrations between 7 and 2900 ug/L in the leachate from textiles exposed to landfill-like conditions. The form of the silver was not characterized so this leachate may have contained both nanomaterials and ions. Regardless, these consumer products with nanomaterials present a contaminant risk. Bolyard et al. observed partitioning of silver, titanium and zinc nanomaterials into the leachate in both ion and colloidal form [94]. The authors noted that the extent of partitioning varied between particle types, which was attributed to the affinity of each coating for the leachate. The age, concentration of organic matter and chemical composition of the landfill is also known to affect the transport of nanomaterials [94,95]. Moreover, nanomaterials and ions that enter the leachate may not remain pure due to a number of elements that complex ions and high ionic strength that favors nanomaterial agglomeration. These transformations are more likely for certain elements (Ag) than others (Ti, Zn) [94]. Interestingly, one method of treatment involves reintroducing the leachate to wastewater treatment creating an enclosed loop between landfills and WWTP [93]. Though studies are sparse, the available evidence builds a case for landfill leachate as a viable transport mechanism to usher nanomaterials into the environment.

Transformation and Release During Wastewater Treatment

Many nanomaterial applications involve direct or indirect contact with a controlled urban water supply. Therefore, a significant effort has been put forth to characterize nanomaterials that undergo the treatment protocols for waste and storm water prior to environmental release. Consumer based nanomaterials are most likely to follow this route, whether it comes from washing nanomaterial laden textiles, liberation from painted facades during heavy rainfall or excretion of nano-medicines. Prior to arrival, nanomaterials can undergo several transformations in route to the treatment plant [96]. Waste and storm water contain a variety of chemical and physical substituents that can easily alter the appearance and behavior of the nanomaterial. Organic components, including macromolecules and organic pollutants, can attach to the surface of the nanomaterial if the ligand characteristics are compatible [37,97]. These organic coatings can limit the extent of nanoparticle aggregation and sedimentation in higher ionic strength conditions [37,98,99]. Alternatively, material properties and/or wastewater conditions may favor formation of complexes or sorption to larger suspended solids [96,100]. These pre-treatment interactions will greatly affect the reactivity of nanomaterials and the removal efficiency.

Each stage of treatment in a WWTP is capable of removing nanomaterials from wastewater with means that vary from settling to microbial interactions [100,101]. Taken together primary, secondary and tertiary treatment of wastewater is expected to remove >90% of the nanomaterial input into a wastewater treatment system though this amount can vary based on the design of the plant [101-104]. Primary treatment will remove nanomaterials associated with large debris and those that are highly susceptible to aggregation [100,103,105]. Moreover, treatment designs that utilize coagulants during this stage will foster greater particle removal [100,106]. Secondary treatment acts to breakdown pollutants that were not removed during primary treatment through combinations of aeration, microbial activity and activated sludge. In this stage, nanomaterials will be removed from the wastewater either through attraction to suspended biomass [37,96,105], entrapment in extracellular polymeric substances [99], and/or formation of complexes with inorganic elements such as sulfides residing in the sludge [96,102,107]. Further removal of nanomaterials can be achieved through micro or ultrafiltration of the suspended solids though few WWTPs incorporate utilize this additional filtration step [104].

The fate of nanomaterials in the WWTP can be predicted based on physicochemical properties of the material, residence time, and the chemistry of the wastewater [99]. Nanomaterials with properties that confer greater stability intrinsically will resist aggregation and sedimentation and remain in the water column while those with weaker stability attach to biological surfaces or complex with inorganic molecules and are relegated to the sludge. Nanomaterials that partition to the sludge often bear little resemblance to the original nanomaterial, having experienced a number of the aforementioned transformation processes. Materials that take the aggregation and sedimentation route to the sludge will likely have increased in size beyond the nano-scale. On the other hand, nanomaterials that take other routes to sludge are able to retain their size [37], even in scenarios where they complex with inorganic molecules [107]. The nanomaterial in the sludge may also have a different chemical structure. Kim et al. and Ma et al. [102,107] observed negligible concentrations of the original silver and zinc oxide nanomaterial in the biosolids. Instead these nanomaterials formed complexes with iron, phosphate and sulfide moieties. Furthermore, the processing of sludge for biosolid application can disrupt the speciation. Ma et al. noted that the Zn species distribution varied based on the redox conditions and moisture content in the production of sludge into Class A

biosolids while Ag sulfide complexes were unaffected [102]. Sludge that is appropriated for biosolid application is a direct source of nanomaterials for terrestrial environments and can contribute to aquatic exposures as runoff during heavy rainfall events.

Surface coating [37,99,105,108], size [99] and core chemistry [105] are particularly important to fate in a WWTP. Nanomaterials with a zeta potential, a characteristic tied to the surface chemistry, that is significantly greater or less than zero are more likely to appear in the effluent ([37,99,105]. Moreover, macromolecules and organic matter in the wastewater are capable of providing additional stability by coating receptive nanomaterials [37]. Nanomaterials that lack stability may still escape into the effluent partnered with suspended solids. In this scenario, the size, shape and surface coating of the nanomaterial is not a factor, instead the release is based on the percentage of contaminated sludge floc suspended during treatment [96].

Though only a small fraction of the nanoparticle input is expected to appear in the effluent, the relative loading of NPs may be such that 10% constitutes a significant environmental burden. This consideration is best illustrated with the two most popular nanomaterials, titanium and silver. Even with an expected removal efficiency of 90-99.5% of nanomaterial input, models predicted silver and titanium concentrations in wastewater effluent between 21 ng/L – 1.75 ug/L in the U.S [75]. These models recommended further risk evaluation of nanomaterials in sewage effluent for silver, titanium and zinc and surface water for silver because they calculated risk quotients to be greater than one [75]. Field measurements of WWTP effluent have validated these concerns. Kiser et al. recorded titanium particles (<0.7 um) at concentrations ranging from 5-15 ug/L in WWTP effluents [109]. Another study on titanium oxide nanomaterials in effluents determined that between <2 and 20 ug Ti/L was released from WWTP. In the second study, the released titanium was confirmed to retain their nano status with electron microscopy [104]. Furthermore the authors of the second study discovered the presence of silica nanoparticles in effluents at concentrations significantly higher than titanium oxide though lacked the proper analytical equipment to make more accurate estimates. Silver on the other hand was found at concentrations (<12 ng/L) lower than the model predictions in wastewater effluent from WWTP in Germany [110]. The authors stated that the input of Ag nanomaterials from WWTP effluents is of minimal concern; however, their

study is a snapshot of current use paradigms and does not take into account the possibility of increased usage as nanotechnology strengthens its foothold in consumer markets. Evidence of nanomaterial releases into the environment is significant and unequivocal, yet they only reveal part of the story. The transformed nanomaterials that were able to escape into the environment will face new challenges and conditions that will be the ultimate determinant of behavior, transport and fate.

Nanomaterial Behavior, Transport and Fate in the Environment

Nanomaterials from anthropogenic sources are not direct analogues of their naturally produced counterparts; therefore, releases of these nanomaterials into the environment cannot be dismissed as merely adding to the natural stock of colloidal materials. Engineered nanomaterials are constructed with stabilizing agents and, in some cases, from toxic materials, which organisms adapted to natural colloids may not be equipped to handle [111]. Engineered nanomaterials that enter the environment are at the mercy of the host system and its capricious nature. Behavior, transport, bioavailability, fate and ultimately toxicity of the nanomaterial are steered by the intrinsic and adopted properties of the nanomaterial, the biotic and abiotic factors inherent in the system and the physiology of the exposed organisms. These controlling forces work individually and in concert to guide the nanomaterial through to its environmental destination.

The Influence of Particle Characteristics

The properties of nanomaterials are a focal point throughout the published literature where they are often cited as an essential asset in the material design toolset but become more unpredictable once removed from the industrial setting. In consumer applications size, shape, surface chemistry/charge and core chemistry of a nanomaterial are manipulated to alter optical properties [112,113], reactivity [114], and cellular interaction and compatibility [113,115,116] amongst many other desired behaviors. Until recently, the environmental behavior of the nanomaterial was not considered during the design process [117]. In the environment these properties are known to dictate aggregation, sedimentation and mobility behavior, bioavailability and accumulation, dissolution and, ultimately, toxicity to exposed organisms.

As mentioned in the previous section, a majority of the nanomaterials that enter the environment will not resemble the nanomaterial produced in the laboratory. The properties adopted by the nanomaterial

from interactions either in route or upon entry into the environment are expected to exercise substantial control over the behavior and fate of the nanomaterial. Nanomaterials in aquatic environments with natural organic matter (NOM), for example, are expected to have greater stability and thus a lower propensity to aggregate. However, these added components also transform the characteristics of the nanomaterial. Using the NOM example again, nanomaterials associated with an organic carbon source will remain at the nanoscale; however, sorption of organic carbon to the surface will increase the size slightly, change the shape of the nanomaterial and fundamentally alter the surface chemistry and associated charge [98,118,119). For practical reasons a majority of the nanomaterial research to date has utilized pristine nanomaterials for behavior, fate and toxicity studies. Though not environmentally relevant, conclusions derived from observations on the influence of particle properties can be extrapolated to predict the behavior of transformed nanomaterials. This dissertation will focus on the four most studied properties: size, shape, surface charge/chemistry and core chemistry.

The size is the defining property of nanomaterials not only because it physically differentiates it from other colloidal materials but it also confers greater reactivity to the material. In the environment the greater surface area to volume ratio contributes to increased dissolution [120] and increased susceptibility to charge titration and thus aggregation [121]. Comparisons between nano and bulk materials demonstrated that the small size of the nanomaterial influences internal distribution [122,123], elimination efficiency [123], and toxicity to aquatic organisms [124]. For particles that remain in the nanoscale, the relationship between size and accumulation/toxicity is not as clear-cut. Size has a clear influence on accumulation though the patterns vary depending on the model organism [116,122,125-127]. Likewise, the mechanism of toxicity is size dependent creating a similar situation where certain organisms are more susceptible to larger nanomaterials [128] while others experience greater toxic responses when exposed to smaller nanomaterials [120,129].

Nanomaterials that have a proclivity for aggregation are likely to grow to sizes much larger than the nanoscale. For pelagic organisms this may decrease bioavailability and thus toxicity, yet may increase exposure for benthic organisms, biofilms and grazers after sedimentation [130]. Additionally, the lower surface area to volume ratio disrupts oxidation processes decreasing toxic ion release associated with

nanomaterials that dissolve [120]. However, if the aggregation is not succeeded by sedimentation, the larger sized particles can cause increased toxicity for pelagic organisms due to gut impaction as seen in *C. dubia* [131] and *D. magna* [132].

Shape by itself has not received the same attention as the other particle properties. However, according to the few available studies it is clear that this characteristic governs aggregation and deposition behavior [133] and accumulation in cells. Uptake of nanorods in cells is much slower compared to spherical particles with rates decreasing as aspect ratio increased [116]. Toxicity can also be shape-dependent as demonstrated in microbes [134] and marine diatoms [135].

The charge maintains particle stability through electrostatic repulsion thus the relative charge in the environment will control aggregation, sedimentation and interactions with surfaces and resident biota. The surface charge will determine the partitioning of nanomaterials into environmental compartments [136]. Much like size and shape, surface charge will dictate the mechanism and rate of endocytosis [85] and the mechanism of toxicity [137]. In general, materials with a cationic charge demonstrate greater accumulation in cells due to the attraction to the anionic cell surface [113,115]. In an estuarine mesocasm Burns et al. noted that a significant portion of the cationic nanorods remained in the water column resulting in higher cationic NP burdens for biofilms, clams, and snails [136]. Cationic NPs were also accumulated to a greater extent in fish due to an attraction to the negatively charged mucus lining the gills and gut [138]. In the estuarine mesocasm anionic nanomaterials exhibited greater partitioning into the sediment which fostered higher accumulation in rooted plants, and detritovores [136]. Cationic nanomaterials are associated with higher toxicity in cells [139], microbes [129,140], and daphnids [129]. One exception is a study by Lee et al. [141] that demonstrated enhanced zebrafish embryo biocompatibility for silver nanomaterials coated with a cationic peptide.

The charge on the material surface is clearly important to behavior, fate and toxicity. So, too, is the chemistry of the ligand that produces this charge. The chemistry of the ligand and the strength of the bond with the core of the nanomaterials can affect the chemical stability of the nanomaterial which in turn will control dissolution and phase partitioning. Moreover, accumulation [141-143] and internal distribution [138] are linked to specific surface moieties. Finally, toxicity of a nanomaterial can also be linked to the

surface chemistry, which can have intrinsic toxic potential [113], confer greater toxic action based on distribution [138], or change the stability and thus toxic impact of the nanomaterial [114,120,144].

Investigating the core chemistry alone is an important endeavor because core elements vary in reactivity and toxicity. Organisms on the receiving end of these nanomaterials tend to elicit unique responses for nanomaterials with different core chemistry [124,145]. Silver nanomaterials, for example, are used in medical settings and on textiles because it is well characterized as a bactericide. Gold, too, is utilized for its bactericidal properties; however, it is clearly less toxic than silver when exposed to non-target organisms [40]. The core chemistry of the nanomaterial is the determinant of the inherent nanomaterial reactivity and subsequent susceptibility to chemical destabilization. Bioavailability and toxicity of the nanomaterial is linked to chemical destabilization which can manifest as ion releases, catalytic activity or evolution of redox conditions on the particle surface [114].

The release of ions from nanomaterials is of great interest because the source of toxicity is important to evaluating risk and developing remediation strategies. Silver, zinc, and copper nanomaterials are readily dissolved in aqueous environments whereas gold and titanium are more stable. A number of studies have attempted to differentiate between ion toxicity and nano-specific toxicity for these materials though the picture remains muddled. Some studies have found the toxicity is solely a function of the ion concentration [146,147] while others have observed intrinsic nano-specific toxicity that is independent of the ion release [148-153].

The chemical stability of the core material is also linked to reactive oxygen species (ROS) production. Similar to dissolution, certain core materials (gold and titanium, for example) have a greater proclivity for ROS production compared to others [154]. Reactive oxygen species produced during nanoparticle exposure have been linked to toxic responses in microorganisms [154], filter feeding invertebrates [155,156] and fish [157,158]. Modifications are made to the material itself or the consumer product [44] to prevent chemical destabilization, yet in the environment these protective measures may be degraded, endangering exposed organisms [90].

The Influence of Water Chemistry

Nanomaterials and products containing nanomaterials will experience a number of physical and chemical processes in the environment that will fundamentally alter the appearance of the nanomaterial, its subsequent behavior and ultimately its fate. In aqueous environments ionic strength, pH and dissolved organic carbon are the three most important parameters [159]. Increased ionic strength can facilitate aggregation and sedimentation of the nanomaterials such that the bioavailability decreases for certain species that can no longer feed upon them but may increase for other species that were previously oblivious to their presence. Divalent cations are expected to have the greatest impact on particle stability, compressing the electronic double layer on the particle surface and on surrounding substrates [160]. Likewise, changes in pH that result in neutralization of the surface ligand lead to similar aggregation and sedimentation activity [160]. For metallic and metal oxide nanomaterials, the pH further governs the dissolution rate [159].

As mentioned previously, natural organic matter (NOM) and other carbon sources are known to increase stability of nanomaterials that have a penchant for aggregation and sedimentation. The natural organic matter can either replace or coat the existing ligand [98,119] depending on the strength of the bond between the ligand and particle surface. This protection can act as a buffer at extreme pH conditions and against increasing concentrations of monovalent ions. Interestingly, the NOM coating fosters greater aggregation as more divalent ions are introduced due to cation bridging between NOM molecules [98,119]. Bioavailability and toxicity are also affected by the presence and concentration of dissolved organic carbon (DOC) [161]. A consequence of increased stability is prolonged transport, greater bioavailability to organisms that reside in the water column, and an increase in the magnitude of the toxic response [161-163]. Dissolved organic carbon does not, however, increase nanomaterial bioavailability for all species as Glenn et al. [118] demonstrated with aquatic macrophytes. Moreover, the presence of dissolved organic carbon can mitigate dissolution of nanomaterials reducing the toxicity from harmful ions [144,164]. The properties of NOM are determined by the age and source, which can further impact the sorption activity of a given NOM molecule [159,165].

The state of the redox environment in an aquatic system exercises further control over metallic and metal oxide nanomaterial behavior. The redox conditions are tied to the rate of dissolution [114] and the probability of a nanomaterial forming complexes with elements (such as sulfur) residing in the sediments [102,166]. The presence of more complexing agents in the sediments will favorably remove metallic and metal oxide nanomaterials from the water column. Complexation was demonstrated to reduce oxidation rate and the resulting toxicity [166] of silver nanomaterials at the cost of persistence in the environment [102]. Temperature, season and the state of eutrophication can indirectly affect the metallic nanomaterial behavior by altering the redox conditions [166]. In addition to controlling the redox conditions, temperature is known to affect the release of toxic ions as mediated through seasonal mixing and altered reaction rates [166]

The Influence of Organism Physiology and Behavior

An exhaustive review of the available literature on nanomaterial accumulation, behavior, and toxicity studies revealed a number of discrepancies that may be explained by the selection of different model organism. The unique physiology and behavior of each organism will be influential in the interactions with nanomaterials and integral to accumulation mechanisms and any toxic response. To date, several studies have demonstrated species dependent uptake and accumulation of nanomaterials. One of the first mesocosm nanomaterial studies linked differential accumulation to the ecological niches of biofilms, plants, mollusks, grass shrimp, and fish [167]. Likewise, Glenn et al. attributed variable accumulation success among three species of aquatic macrophytes to evolution of unique salt tolerance mechanisms [125].

The route of exposure, as controlled by physiology and behavior, is fundamental to nanomaterial accumulation, distribution and toxicity. Nanomaterial waterborne exposures generally exhibit faster uptake and can introduce the nanomaterial to organs that are bypassed in dietborne exposures. [143]. However, dietborne exposures facilitate higher overall body burdens compared to waterborne exposures suggesting greater importance governing the accumulation rate [143,168,169]. Trophic transfer of nanomaterials was demonstrated in several small food chains [168-172], yet few examples exist for biomagnification [171]. More efficient elimination mechanisms adopted by higher trophic level organisms is one of the

hypothesized reasons behind the limited observed biomagnification [170,172]. Considering the obvious and discrete differences among organisms, creating broad accumulation and toxicity models will be a difficult endeavor. A study by Gaiser et al. [173] demonstrated similarities in toxicity for silver and cerium dioxide nanoparticles exposed to cells, daphnids and fish indicating that cross-species extrapolation is feasible. However, large discrepancies between studies suggest these types of cross-species extrapolations may not be appropriate for all types of nanomaterials.

Dissertation Goals and Objectives

Nanotechnology has progressed by leaps and bounds since Feyman's seminal speech in 1960. The specificity by which these particles can be manipulated gives designers a near infinite number of options and possibilities. This facet, amongst others, poses a peculiar problem for assessing human and environmental health risks from nanomaterial exposure and has impeded meaningful progress on regulatory action. Environmental and human health research has advanced well beyond its fledgling stages but gaps persist and a comprehensive modeling strategy remains elusive [174]. The aim of this dissertation was to demystify several of the many remaining unknowns obfuscating the relationship between particle characteristics, water chemistry and biota accumulation. This dissertation was intentionally constructed with a bottom up design. Each successive chapter iterated on the previous with additional considerations of particle sophistication, biological complexity and environmental relevancy. My goals for this dissertation were three fold. First, identify the specific characteristics of nanomaterials that most influenced accumulation in aquatic invertebrates. Second, examine the transformative effects of wastewater incubation on nanomaterials and how these changes impacted accumulation in a simple aquatic food chain. Finally, examine if attachment of pharmaceuticals to nanomaterials reshaped the prescribed risk to aquatic organisms for isolated pharmaceutical releases. To accomplish these goals I set out the following objectives:

1) Develop simple models that identify the impact of gold NP properties on *Daphnia magna* biodynamics and determine which characteristics are most influential in the accumulation processes

2) Simulate the particle-macromolecule interactions that occur in wastewater to identify the transformations that occur in route to environmental release and the consequences on accumulation in *D. magna* and *Pimephales promelas*.
3) Compare the accumulation and distribution patterns of nano-pharmaceuticals, lone pharmaceuticals and lone nanomaterials to evaluate the perceived risk to *P. promelas*.

The conclusions borne from this dissertation make up one of many necessary pillars that collectively will be integral in the development of a comprehensive regulatory strategy for engineered nanomaterials.

References

1. Hansen SF, Maynard A, Baun A, Tickner, JA. 2008. Late lessons from early warnings for nanotechnology. *Nat Nanotechnol* 3:444-447.

2. Freestone I, Meeks N, Sax M, Higgitt C. 2007. The Lycurgus Cup – a Roman nanotechnology. *Gold Bull* 40:270-277.

3. Reibold M, Paufler P, Levin AA, Kochmann W, Pätzke N, Meyer, DC. 2006. Materials: Carbon nanotubes in an ancient Damasucus sabre. *Nature* 444:286.

4. LaMer VK, Dinegar RH. 1950. Theory, production and mechanism of formation of monodispersed hydrosols. *J Am Chem Soc* 72:4847-4854.

5. Faraday M. 1857. The Bakerian lecture: Experimental relations of gold (and other metals) to light. *Philos T R Soc Lond* 147:145-181.

6. Binnig G, Rohrer H. 1983. Scanning tunneling microscopy. *Surf Sci* 126:236-244.

7. Müller EW, Bahadur K. 1956. Field ionization of gases at a metal surface and the resolution of field ion microscope. *Phys Rev* 102:624-631.

8. Feyman R.P. 1950. There's plenty of room at the bottom. Transcript. December 29, 1950. *Eng Sci* 22-36.

9. Iijima S. 1991. Helical microtubules of graphitic carbon. *Nature* 354:56-58.

10. Kroto HW, Heath JR, O'Brien SC, Curl RF, Smalley RE 1985. C_{60}: Buckminsterfullerene. *Nature* 318:162-163.

11. Lohse SE, Dahl JA, Hutchison JE. 2010. Direct synthesis of large water-soluble functionalized gold nanoparticles using bunte salts as ligand precursors. *Langmuir* 26:7504-7511.

12. Kimling J, Maier M, Okenve B, Kotaidis V, Ballot H, Plech A. 2006. Turkevich method for gold nanoparticle synthesis revisited. *J Phys Chem B* 110:15700-15707.

13. Jana NR, Gearheart L, Murphy CJ. 2001. Seeding growth for size control of 5-40 nm diameter gold nanoparticles. *Langmuir* 17:6782-6786.

14. Burst M, Walker M, Bethell D, Schiffrin DJ, Whyman R. 1994. Synthesis of thiol-derivatised gold nanoparticles in a two-phase liquid-liquid system. *J Chem Soc, Chem Commun* 7:801-802.

15. Murray CB, Norris DJ, Bawendi MG. 1993. Synthesis and characterization of nearly monodisperse CdE (E=S, Se, Te) semiconductor nanocystallites. *J Am Chem Soc* 115:8706-8715.

16. Lee PC, Meisel D. 1982. Adsorption and surface-enhanced Raman of dyes on silver and gold sols. *J Phys Chem* 86:3391-3395.

17. Project on Emerging Nanotechnologies (2014). Consumer Products Inventory. Retrieved 18 March 2014, from http://www.nanotechproject.org/cpi

18. Roco M.C. 2011. The long view of nanotechnology development: The National Nanotechnology Initiative at 10 years. *J Nanopart Res* 13:427-445.

19. OECD/NNI. 2013. Symposium on assessing the economic impact of nanotechnology: Synthesis report. 1-81.

20. Subcommittee on Nanoscale Science, Engineering and Technology, Committee on Technology, and National Science and Technology Council. 2013. The National Nanotechnology Inititative – Supplement to the President's 2014 budget. 1-81.

21. Teo B.K, Sun X. H. 2006. From top-down to bottom up to hybrid nanotechnologies: Road to nanodevices. *J Clust Sci* 17:529-540.

22. Park BK, Jeong S, Kim D, Moon J, Lim S, Kim JS. 2007. Synthesis and size control of monodisperse copper nanoparticles by polyol methods. *J Colloid Interf Sci* 311:417-424.

23. Kim K, Demberelnyamba D, Lee H. 2004. Size-selective synthesis of gold and platinum nanoparticles using novel thiol-functionalized ionic liquids. *Langmuir* 20:556-560.

24. Wang Y, Xia Y. 2004. Bottom-up and top-down approaches to synthesis of monodispersed spherical colloids of low melting-point metals. *Nano Lett* 4:2047-2050.

25. Sun S, Murray CB. 1999. Synthesis of monodisperse cobalt nanocrystals and their assembly into magnetic superlattices. *J Appl Phys* 85:4325-4330.

26. Woehrle GH, Hutchison JE. 2005. Thiol-functionalized undecagold clusters by ligand exchange: Synthesis, mechanism, and properties. *Inorg Chem* 44:6149-6158.

27. Caswell KK, Bender CM, Murphy CJ. 2003. Seedless, surfactantless wet chemical synthesis of silver nanowires. *Nano Lett* 3:667-669.

28. Creighton JA, Blatcford CG, Albrecht MG. 1978. Plasma resonance enhancement of Raman scattering by pyridine adsorbed silver or gold sol particles of size comparable to the excitation wavelength. *J Chem Soc, Faraday Trans 2* 75:790-798.

29. Turkevich J, Stevenson PC, Hillier J. 1951. A study of the nucleation and growth processes in the synthesis of colloidal gold. *Discuss Faraday Soc* 11:55-75

30. Wiley B, Sun Y, Mayers B, Xia T. 2005. Shape-controlled synthesis of metal nanostructures: The case of silver. *Chem Eur J* 11:454-463.

31. Jana NR, Gearheart L, Murphy CJ. 2001. Evidence for seed-mediated nucleation in the chemical reduction of gold salts to gold nanoparticles. *Chem Mater* 13:2313-2322.

32. Sau TK, Murphy CJ. 2004. Seeded high yield synthesis of short Au nanorods in aqueous solution. *Langmuir* 20:6414-6420.

33. Sun Y, Xia Y. 2002. Shape-controlled synthesis of gold and silver nanoparticles. *Scienc*e 298:2176-2179.

34. Amendola V, Polizzi S, Meneghetti M. 2007. Free silver nanoparticles synthesized by laser ablation in organic solvents and their easy functionalization. *Langmuir* 23:6766-6770.

35. Nandivada H, Jiang X, Lahann J. 2007. Click chemistry: Versatility and control in the hands of materials scientists. *Adv Mater* 19:2197-2208.

36. Croteau M, Dybowska AD, Luoma SN, Valsami-Jones E. 2011. A novel approach reveals that zinc oxide nanoparticles are bioavailable and toxic after dietary exposures. *Nanotoxicology* 5:79-90.

37. Limbach LK, Bereiter R, Muller E, Krebs R, Galli R, Stark WJ. 2008. Removal of oxide nanoparticles in a model wastewater treatment plant: Influence of agglomeration and surfactants on clearing efficiency. *Environ Sci Technol* 42:5828-5833.

38. Chen X, Mao SS. 2007. Titanium dioxide nanomaterials: Synthesis, properties, modifications and applications. *Chem Rev* 1017:2891-2959.

39. Sun S, Zeng H. 2002. Size-controlled synthesis of magnetite nanoparticles. *J Am Chem Soc* 124:8204-8205.

40. Li T, Albee B, Alemayehu M, Diaz R, Ingahm L, Kamal S, Rodriguez M, Bishnoi, SW. 2010. Comparative toxicity study of Ag, Au, and Ag-Au bimetallic nanoparticles on *Daphnia magna*. *Anal Bioanal Chem* 398:689-700.

41. Scott RWJ, Ye H, Henriquez RR, Crooks RM. 2003. Synthesis, characterization, and stability of dendrimer-encapsulated palladium nanoparticles. *Chem Mater* 15:3873-3878.

42. Benn T, Cavanagh B, Hristovski K, Posner JD, Westerhoff P. 2010. The release of nanosilver from consumer products used in the home. *J Environ Qual* 39:1875-1882.

43. Son Y, Yeo J, Moon H, Lim TW, Hong S, Nam KH, Yoo S, Grigoropoulos CP, Yang D, Ko SH. 2011. Nanoscale electronics: Digital fabrication by direct femtosecond laser processing of metal nanoparticles. *Adv Mater* 23:3176-3181.

44. Wakefield G, Green M, Lipscomb S, Flutter B. 2004. Modified titania nanomaterials for sunscreen applications—reducing free radical generation and DNA damage. *Mater Sci Technol* 20:985–988.

45. Weir A, Westerhoff P, Fabricius L, von Goetz N. 2012. Titanium dioxide nanoparticles in food and personal care products. *Environ Sci Technol* 46:2242-2250.

46. Kaegi R, Ulrich A, Sinnet B, Vonbank R, Wichser A, Zuleeg S, Simmler H, Brunner S, Vonmont H, Burkhardt M, Boller M. 2008. Synthetic TiO_2 nanoparticle emission from exterior facades into the aquatic environment. *Environ Pollut* 156:233-239.

47. Ko SH, Park I, Pan H, Grigoropoulos CP, Pisano AP, Luscombe CK, Frechet JMJ. 2007. Direct nanoimprinting of metal nanoparticles for nanoscale electronics fabrication. *Nano Lett* 7:1869-1877.

48. Kanel SR, Manning B, Charlet L, Choi H. 2005. Removal of arsenic (III) from groundwater by nanoscale aero-valent iron. *Environ Sci Technol* 39:1291-1298.

49. Vikesland P J, Heathcock AM, Rebodos RL, Makus KE. 2007. Particle size and aggregation effects on magnetite reactivity toward carbon tetrachloride. *Environ Sci Technol* 41:5277–5283.

50. He F, Zhao D, Liu J, Roberts CB. 2007. Stabilization of Fe-Pd nanoparticles with sodium carboxymethyl cellulose for enhanced transport and dechlorination of trichloroethylene in soil and groundwater. *Ind Eng Chem Res* 46:29-34.

51. Chen PC, Mwakwari SC, Oyelere AK. 2008. Gold nanoparticles: From nanomedicine to nanosensing, *Nanotech Sci Appl* 1:45–66.

52. Ghosh P, Han G, De M, Kim CK, Rotello VM. 2008. Gold nanoparticle in delivery applications. *Adv Drug Deliv Rev* 60:1307–1315.

53. Pissuwan D, Valenzuela SM, Killingsworth MC, Xu X, Cortie MB. 2007. Targeted destruction of murine macrophage cells with bioconjugated gold nanorods, *J Nanopart Res* 9:1109–1124.

54. Kim B, Han G, Toley BJ, Kim C, Rotello VM, Forbes NS. 2010. Tuning payload delivery in tumour cylindroids using gold nanoparticles. *Nat Nanotechnol* 5:465-472.

55. Weissleder R, Kelly K, Sun EY, Shtatland T, Josephson L. 2005. Cell-specific targeting of nanoparticles by multivalent attachment of small molecules. *Nat Biotechnol* 23:1418-1423.

56. Paulo CSO, Pires das Neves R, Ferreira LS. 2011. Nanoparticles for intracellular-targeted drug delivery. *Nanotechnology* 22:1-11.

57. Gupta P, Vermani K, Garg S. 2002. Hydrogels: From controlled release to pH-responsive drug delivery. *Drug Discov Today* 7:569–579.

58. Pissuwan D, Niidome T, Cortie M.B. 2011. The forthcoming applications of gold nanoparticles in drug and gene delivery systems. *J Control Release* 149:65-71.

59. Skirtach AG, Javier AM, Kreft O, Köhler K, Alberola AP, Möhwald H, Parak WJ, Sukhorukov GB, 2006. Laser-induced release of encapsulated materials inside living cells, *Angew Chem* 118:4728–4733.

60. Gu Y, Cheng J, Man CW, Wong W, Cheng SH. 2012. Gold-doxorubicin nanoconjugates for overcoming multidrug resistance. *Nanomed Nanotechnol* 8:204-211.

61. Li M, Al-Jamal KT, Kostarelos K, Reineke J. 2010. Physiologically based pharmacokinetic modeling of nanoparticles. *ACS Nano* 4: 6303-6317.

62. Boisselier E, Astruc D. 2009. Gold nanoparticles in nanomedicine: preparations, imaging, diagnostic, therapies and toxicity. *Chem Soc Rev* 38:1759-1782.

63. Kim S, Lim YT, Sotesz EG, DeGrand AM, Lee J, Nakayama A, Parker JA, Mihaljevic T, Laurence RG, Dor DM, Cohn LH, Bawendi MG, Frangioni JV. 2004. Near-infrared fluorescent type II quantum dots for sentinel lymph node mapping. *Nat Biotechnol* 22:93-97.

64. Nitin N, LaConte LEW, Zurkiya O, Hu X, Bao G. 2004. Functionalization and peptide-based delivery of magnetic nanoparticles as an intracellular MRI contrast agent. *J Biol Inorg Chem* 9:706-712.

65. Gu FX, Karnik R, Wang AZ, Alexis F, Levy-Nissenbaum E, Hong S, Langer RS, Farokhzad OC. 2007. Targeted nanoparticles for cancer therapy. *Nano Today* 2:14-21.

66. Gao X, Cui Y, Levenson RM, Chung LWK, Nie S. 2004. In vivo cancer targeting and imaging with semiconductor quantum dots. *Nat Biotechnol* 22:969-976.

67. Chen J, Glaus C, Laforest R, Zhang Q, Yang M, Gidding M, Welch MJ, Xia Y. 2010. Gold nanocages as photothermal transducers for cancer treatment. *Small* 6:811-817.

68. Gillies ER, Fréchet JMJ. 2005. Dendrimers and dendritic polymers in drug delivery. *Drug Discov Today* 10:35-43.

69. Hortobagyi GN. 1997. Anthracyclines in the treatment of cancer: An overview. *Drugs* 54:1-7.

70. Mahnik SN, Lenz K, Weissenbacher N, Mader RM, Fuerhacker M. 2007. Fate of 5-fluorouracil, doxorubicin, epirubicin, and daunorubicin in hospital wastewater and their elimination by activated sludge and treatment in a membrane-bio-reactor system. *Chemosphere* 66:30-37.

71. Martin J, Camacho-Munoz D, Santos JS, Aparicio I, Alonso E. 2014. Occurrence and ecotoxicological risk assessment of 14 cytostatic drugs in wastewater. *Water Air Soil Pollut.* 225:1896.

72. Caminada D, Escher C, Fent K. 2006. Cytotoxicity of pharmaceuticals found in aquatic systems: Comparison of PLHC-1 and TRG-2 fish cell lines. *Aquat Toxicol* 79:114-123.

73. Zounkova R, Odraska P, Dolezalova L, Hilscherova K, Marsalek R, Blaha L. 2007. Ecotoxicity and genotoxicity assessment of cytostatic pharmaceuticals. *Environ Toxicol Chem* 26:228-2214.

74. Gottschalk F, Sun T, Nowack B. 2013. Environmental concentrations of engineered nanomaterials: Review of modeling and analytical studies. *Environ Pollut* 181:287-300.

75. Gottschalk F, Sonderer T, Scholz RW, Nowack B. 2009. Modeled environmental concentrations of engineered nanomaterials (TiO_2, ZnO, Ag, CNT, fullerenes) for different regions. *Environ Sci Technol* 43:9216-9222.

76. Klaine SJ, Alvarez PJJ, Batley GE, Fernandes TF, Handy RD, Lyon DY, Mahendra S, McLaughlin MJ, Lead JR. 2008. Nanomaterials in the environment: Behavior, fate, bioavailability and effects. *Environ Toxicol Chem* 27:1825-1851.

77. Muller NC, Nowack B. 2008. Exposure modeling of engineered nanoparticles in the environment. *Environ Sci Technol* 42:4447-4453.

78. Scown TM, van Aerle R, Tyler CR. 2010. Do engineered nanoparticles pose significant threat to the aquatic environment? *Crit Rev Toxicol* 40:653-670.

79. Künniger T, Gerecke AC, Ulrich A, Huch A, Vonbank R, Heeb M, Wichser A, Haag R, Kunz P, Faller M. 2014. Release and environmental impact of silver nanoparticles and conventional organic biocides from coated wooden facades. *Environ Pollut* 184:464-471.

80. Kaegi R, Sinnet B, Zuleeg S, Hagendorfer H, Mueller E, Vonbank R, Boller M, Burkhardt M. 2010. Release of silver nanoparticles from outdoor facades. *Environ Pollut* 158:2900-2905.

81. Benn TM, Westerhoff P. 2008. Nanoparticle silver released into water from commercially available sock fabrics. *Environ Sci Technol* 42:4133–4139.

82. von der Kammer F, Ferguson PL, Hodlen PA, Masion A, Rogers KR, Klaine SJ, Koelmans AA, Horne N, Unrine JM. 2012. Analysis of engineered nanomaterials in complex matrices (environment and biota): General considerations and conceptual case studies. *Environ Toxicol Chem* 31:31-49.

83. Nowack B, Ranville JF, Diamond S, Gallego-Urrea JA, Metcalfe C, Rose J, Horne N, Koelmans AA, Klaine SJ. 2012. Potential scenarios for nanomaterial release and subsequent alteration in the environment. *Environ Toxicol Chem* 31:50-59.

84. Guo Z, Pereira T, Choi O, Wang Y, Hahn HT. 2006. Surface functionalized alumina nanoparticle filled polymeric nanocomposites with enhanced mechanical properties. *J Mater Chem* 16:2800–2808.

85. Sahay G, Alakhova DY, Kabanov AV. 2010. Endocytosis of nanomedicines. *J Control Release* 145:182-195.

86. Esawi AMK, Farag MM. 2007. Carbon nanotube reinforced composites: Potential and current challenges. *Mater Design* 28:2394-2401.

87. Windler L, Lorenz C, von Goetz N, Hungerbühler K, Amberg M, Heuberger M, Nowack B.2012. Release of titanium dioxide from textiles during washing. *Environ Sci Technol* 46:8181-8188.

88. Geranio L, Heuberger M, Nowack B. 2009. The behavior of silver nanotextiles during washing. *Environ Sci Technol* 43:8113-8118.

89. Gottschalk F, Nowack B. 2011. The release of engineered nanomaterials to the environment. *J Environ Monit* 13:1145-1155.

90. Auffan M, Pedeutour M, Rose J, Masion A, Ziarelli F, Borschneck D, Chaneac C, Botta C, Chaurand P, Labille J, Bottero J. 2010. Structural degradation at the surface of a TiO2-based nanomaterial used in cosmetics. *Environ Sci Technol* 44:2689-2694.

91. Walser T, Limbach LK, Brogioli R, Erismann E, Flamigni L, Hattendorf B, Juchli M, Krumeich F, Ludwig C, Prikopsky K, Rossier M, Saner D, Sigg A, Hellweg S, Günter D, Stark WJ. 2012. Persistence of engineered nanoparticles in a municipal solid-waste incineration plant. *Nat Nanotechnol* 7:520-524.

92. Mueller NC, Buha J, Wang J, Ulrich A, Nowack B. 2013. Modeling the flows of engineered nanomaterials during waste handling. *Environ Sci: Processes Impacts* 15:251-259.

93. Renou S, Givaudan JG, Poulain S, Dirassouyan F, Moulin P. 2008. Landfill leachate treatment: Review and opportunity. *J Hazard Mater* 150:468-493.

94. Bolyard SC, Reinhart DR, Santra S. 2013. Behavior of engineered nanoparticles in landfill leachate. *Environ Sci Technol* 47: 8114-8122.

95. Khan IA, Berge ND, Sabo-Atwood T, Ferguson PL, Saleh NB. 2013. Single-walled carbon nanotube transport in representative municipal solid waste landfill conditions. *Environ Sci Technol* 47:8425-8433.

96. Kaegi R, Voegelin A, Ort C, Sinnet B, Thalmann B, Krismer J, Hagendorfer H, Elumelu M, Mueller E. 2013. Fate and transformation of silver nanoparticles in urban wastewater systems. *Water Res* 47:3866−3877.

97. Röcker C, Pötzl M, Zhang F, Parak WJ, Nienhaus GU. 2009. A quantitative fluorescence study of protein monolayer formation on colloidal nanoparticles. *Nat Nanotechnol* 4:577-580.

98. Diegoli S, Manciulea AL, Begum S, Jones IP, Lead JR, Preece JA. 2008. Interaction between manufactured gold nanoparticles and naturally occurring organic macromolecules. *Sci Total Environ* 402:51-61.

99. Park H, Kim HY, Cha S, Ahn CH, Roh J, Park S, Kim S, Choi K, Yi J, Kim Y, Yoon J. 2013. Removal characteristics of engineered nanoparticles by activated sludge. *Chemosphere* 92:524-528.

100. Brar SK, Verma M, Tyagi RD, Surampalli RY. 2010. Engineered nanoparticles in wastewater and wastewater sludge – Evidence and impacts. *Waste Manage* 30: 504-520.

101. Westerhoff PK, Kiser MA, Hristovski K. 2013. Nanomaterial removal and transformation during biological wastewater treatment. *Environ Eng Sci* 30:109-117.

102. Ma R, Levard C, Judy JD, Unrine JM, Durenkamp M, Martin B, Jefferson B, Lowry GV. 2014. Fate of zinc oxide and silver nanoparticles in a pilot wastewater treatment plant and in processed biosolids. *Environ Sci Technol* 48:104-112.

103. Hou L, Li K, Ding Y, Li Y, Chen J, Wu X, Li X. 2012. Removal of silver nanoparticles in simulated wastewater treatment processes and its impact on COD and NH_4 reduction. *Chemosphere* 87:248-252.

104. Westerhoff P, Song G, Hristovski K, Kiser MA. 2011. Occurrence and removal of titanium at full scale wastewater treatment plants: Implications for TiO_2 nanomaterials. *J Environ Monit* 13:1195-1203.

105. Kiser MA, Ryu H, Jang H, Hristovski K, Westerhoff P. 2010. Biosorption of nanoparticles to heterotrophic wastewater biomass. *Water Res* 44:4105-4114.

106. Wang C, Dai J, Shang C, Chen G. 2013. Removal of aqueous fullerene n C60 from wastewater by alum-enhanced primary treatment. *Sep Purif Technol* 116:61-66.

107. Kim B, Park C, Murayama M, Hochella Jr, MF. 2010. Discovery and characterization of silver sulfide nanoparticles in final sewage sludge products. *Environ Sci Technol* 44:7509-7514.

108. Hendren CO, Badireddy AR, Casman E, Wiesner MR. 2013. Modeling nanomaterial fate in wastewater treatment: Monte Carlo simulation of silver nanoparticles (nano-Ag). *Sci Total Environ* 449:418-425.

109. Kiser MA, Westerhoff P, Benn T, Wang Y, Pe´rez-Rivera J, Hristovski K. 2009. Titanium nanomaterial removal and release from wastewater treatment plants. *Environ Sci Technol* 43:6757–6763.

110. Li L, Hartmann G, Doblinger M, Schuster M. 2013. Quantification of nanoscale silver particles removal and release from municipal wastewater treatment plants in Germany. *Environ Sci Technol* 47:7317-7323.

111. Handy RD, Owen R, Valsami-Jones E. 2008. The ecotoxicology of nanoparticles and nanomaterials: Current status, knowledge gaps, challenges, and future needs. *Ecotoxicology* 17:315-325.

112. Kelly KL, Coronado E, Zhao LL, Schatz GC. 2003. The optical properties of metal nanoparticles: The influence of size, shape, and dielectric environment. *J Phys Chem B* 107:668-677.

113. Alkilany AM, Nagaria PK, Hexel CR, Shaw TJ, Murphy CJ, Wyatt, MD. 2009. Cellular uptake and cytotoxicity of gold nanorods: Molecular origin of cytotoxicity and surface effects. *Small* 6:701-708.

114. Auffan M, Rose J, Wiesner MR, Bottero J. 2009. Chemical stability of metallic nanoparticles: A parameter controlling potential cellular toxicity in vitro. *Environ Pollut* 157:1127-1133.

115. Hauck TS, Ghazani AA, Chan WCW. 2007. Assessing the effect of surface chemistry on gold nanorod uptake, toxicity and gene expression in mammalian cells. *Small* 4:153-159.

116. Chithrani BD, Ghazani AA, Chan WCW. 2006. Determining the size and shape dependence of gold nanoparticle uptake into mammalian cells. *Nano Lett* 6:662-668.

117. Virkutyte J, Varma RS. 2011. Green synthesis of metal nanoparticles: Biodegradable polymers and enzymes in stabilization and surface functionalization. *Chem Sci* 2:837-846.

118. Glenn JB, Klaine SJ. 2013. Abiotic and biotic factors that influence the bioavailability of nanoparticles to aquatic macrophytes. *Environ Sci Technol* 47:10223-10230.

119. Stankus DP, Lohse SE, Hutchison JE, Nason JA. 2011. Interactions between natural organic matter and gold nanoparticles stabilized with different organic capping agents. *Environ Sci Technol* 45:3238-3244.

120. Allen HJ, Impellitteri CA, Macke DA, Heckman JL, Poynton HC, Lazorchak JM, Govindaswamy S, Roose DL, Nadagouda MN. 2010. Effects from filtration, capping agents and presence/absence of food on the toxicity of silver nanoparticles to *Daphnia magna*. *Environ Toxicol Chem* 29:2742-2750.

121. He YT, Wan J, Tokunaga, T. 2008. Kinetic stability of hematite nanoparticles: The effect of particle sizes. *J Nanopart Res* 10:321–332.

122. Scown TM, Santos EM, Johnston BD, Gaiser B, Baalousha M, Mitov S, Lead JR, Stone V, Fernandes TF, Jepson M, van Aerle R, Tyler CR. 2010. Effects of aqueous exposure to silver nanoparticles of different sizes in rainbow trout. *Toxicol Sci* 115:521-534.

123. Rosenkranz P, Chaudhry Q, Stone V, Fernandes TF. 2009. A comparison of nanoparticle and fine particle uptake by *Daphnia magna*. *Environ Toxicol Chem* 28:2142-2149.

124. Gaiser BK, Biswas A, Rosenkranz P, Jepson MA, Lead JR. Stone V, Tyler CR, Fernandes TF. 2011. Effects of silver and cerium dioxide micro- and nano-sized particles on Daphnia magna. *J Environ Monit* 13:1227-1235.

125. Glenn JB, White SA, Klaine SJ. 2012. Interactions of gold nanoparticles with freshwater aquatic macrophytes are size and species dependent. *Environ Toxicol Chem* 31:194-201.

126. Pan J, Buffet P, Poirier L, Amiard-Triquet C, Gilliland D, Joubert Y, Pilet P, Guibbolini, M, Risso de Faverney C, Roméo M, Valsami-Jones E, Mouneyrac C. 2012. Size dependent bioaccumulation and ecotoxicity of gold NPs in an endobenthic invertebrate: The Tellinid clam *Scrobicularia plana*. *Environ Pollut* 168:37-43.

127. Hull M, Chaurand P, Rose J, Auffan M, Bottero J, Jones JC, Schultz IR, Vikesland PJ. 2011. Filter-feeding bivalves store and biodeposit colloidally stable gold NPs. *Environ Toxicol Chem* 45:6592-6599.

128. Lee KJ, Browning LM, Nallathamby PD, Desai T, Cherukuri PK, Xu XN. 2012. In vivo quantitative study of sized-dependent transport and toxicity of single silver nanoparticles using zebrafish embryos. *Chem Res Toxicol* 25:1029-1046.

129. Silva T, Pokhrel LR, Dubey B, Tolaymat TM, Maier KJ, Liu X. 2014. Particle size, surface charge and concentration dependent ecotoxicity of three organo-coated silver nanoparticles: Comparison between general linear model-predicted and observed toxicity. *Sci Total Environ* 468-469:968-976.

130. Johnston BD, Scown TM, Moger J, Cumberland SA, Baalousha M, Linge K, van Aerle R, Jarvis K, Lead JR, Tyler CR. 2010. Bioavailability of nanoscale metal oxides TiO_2, CeO_2, and ZnO to fish. *Environ Sci Technol* 44:1144-1151.

131. McLaughlin J, Bonzongo JC. 2011. Effects of natural water chemistry on nanosilver behavior and toxicity to *Ceriodaphnia dubia* and *Pseudokirchneriella subcapitata*. *Environ Toxicol Chem* 31:168-175.

132. Zhu X, Chang Y, Chen Y. 2010. Toxicity and bioaccumulation of TiO2 nanoparticle aggregates in *Daphnia magna. Chemosphere* 78:209-215.

133. Afrooz ARMN, Sivalapalan ST, Murphy CJ, Hussain SM, Schlager JJ, Saleh NB. 2013. Spheres vs. rods: The shape of gold nanoparticles influences aggregation and deposition behavior. *Chemosphere* 91:93-98.

134. Pal S, Tak YK, Song JM. 2007. Does the antibacterial activity of silver nanoparticles depend on the shape of the nanoparticle? A study of the gram-negative bacterium *Escherichia coli. Appl Environ Microbiol* 73:1712-1720.

135. Peng X, Palma S, Fisher NS, Wong SS. 2011. Effect of morphology of ZnO nanostructures on their toxicity to marine diatoms. *Aquat Toxicol* 102:186-196.

136. Burns JM, Pennignton PL, Sisco PN, Frey R, Kashiwada S, Fulton MH, Scott GI, Decho AW, Murphy CJ, Shaw TJ, Ferry JL. 2013. Surface charge controls the fate of Au nanorods in saline estuaries. *Environ Sci Technol* 47:12844-12851.

137. Schaeublin NM, Braydich-Stolle LK, Schrand AM, Miller JM, Hutchison J, Schlager JJ, Hussain SM. 2010 Surface charge of gold nanoparticles mediates mechanism of toxicity. *Nanoscale* 3:410-420.

138. Zhu Z, Carboni R, Quercio Jr. MJ, Yan B, Miranda OR, Anderton DL, Arcaro KF, Rotello VM, Vachet RW. 2010. Surface properties dictate uptake, distribution, excretion, and toxicity of NPs in fish. *Small* 6:2261-2265.

139. Goodman CM, McCusker CD, Yilmaz T, Rotello VM. 2004. Toxicity of gold nanoparticles functionalized with cationic and anionic side chains. *Bioconjugate Chem* 15:897-900.

140. El Badawy AM, Silva RG, Morris B, Scheckel KG, Suidan MT, Tolaymat TM. 2011. Surface charge-dependent toxicity of silver nanoparticles. *Environ Sci Technol* 45:283-287.

141. Lee KJ, Browning LM, Nallathamby PD, Xu XN. 2013. Study of charge-dependent transport and toxicity of peptide functionalized silver nanoparticles using zebrafish embryos single nanoparticle plasmonic spectroscopy. *Chem Res Toxicol* 26:904-917.

142. Feswick A, Griffitt RJ, Siebein K, Barber DS. 2013. Uptake, retention and internalization of quantum dots in *Daphnia* is influenced by particle surface functionalization. *Aquat Toxicol* 130-131:210-218.

143. Croteau M, Misra SK, Luoma SN, Valsami-Jones E. 2011. Silver bioaccumulation dynamics in a freshwater invertebrate after aqueous and dietary exposures to nanosized and ionic Ag. *Environ Sci Technol* 45:6600-6607.

144. Bone AJ, Colman BP, Gondikas AP, Newton KM, Harrold KH, Cory RM, Unrine JM, Klaine SJ, Matson CW, Di Giulio RT. 2012. Biotic and abiotic interactions in aquatic microcosms determine fate and toxicity of Ag nanoparticles: Part 2 - toxicity and Ag speciation. *Environ Sci Technol* 46:6925-6933.

145. Montes MO, Hanna SK, Lenihan HS, Keller AA. 2012. Uptake, accumulation and biotransformation of metal oxide nanoparticles by a marine suspension-feeder. *J Hazard Mater* 225-226:139-145.

146. Adam N, Schmitt C, Galceran J, Companys E, Vakurov A, Wallace R, Knapen D, Blust R. 2013. The chronic toxicity of ZnO nanoparticles and $ZnCl_2$ to *Daphnia magna* and the use of different methods to assess nanoparticle aggregation and dissolution. *Nanotoxicology* 8:709-717.

147. Newton KM, Puppala HL, Kitchens CL, Colvin VL, Klaine SJ. 2013. Silver nanoparticle toxicity to *Daphnia magna* is a function of dissolved silver concentration. *Environ Toxicol Chem* 32:2356-2364.

148. Shaw BJ, Al-Bairuty G, Handy RD. 2012. Effects of waterborne copper nanoparticles and copper sulphate on rainbow trout, (*Oncorhynchus mykiss*): Physiology and accumulation. *Aquat Toxicol* 116-117:90-101.

149. Gomes T, Pinheiro JP, Cancio I, Pereira CG, Cardoso C, Bebianno MJ. 2011. Effects of copper nanoparticles exposure in the mussel *Mytilus galloprovincialis. Environ Sci Technol* 46:9356-9362.

150. Laban G, Nies LF, Turco RF, Bickham JW, Sepulveda MS. 2010. The effects of silver nanoparticles on fathead minnow (*Pimephales promelas*) embryos. *Ecotoxicology* 19:185-195.

151. Chae YC, Pham CH, Lee J, Bae E, Yi J, Gu MB. 2009. Evaluation of the toxic impact of silver nanoparticles on Japanese medaka. *Aquat Toxicol* 94:320-327.

152. Griffitt RJ, Hyndman K, Denslow ND, Barber DS. 2008. Comparison of molecular and histological changes in zebrafish gills exposed to metallic nanoparticles. *Toxicol Sci* 107:404-415.

153. Griffit RJ, Luo J, Gao J, Bozongo J, Barber DS. 2008. Effects of particle composition and species on toxicity of metallic nanomaterials in aquatic organisms. *Environ Toxicol Chem* 27:1972-1978.

154. Li Y, Zhang W, Niu J, Chen Y. 2012. Mechanism of photogenerated reactive oxygen species and correlation with the antibacterial properties of engineered metal-oxide nanoparticles. *ACS Nano* 6:5164-5173.

155. Tedesco S, Doyle H, Blasco J, Redmond G, Sheehan D. 2010. Oxidative stress and toxicity of gold nanoparticles in *Mytilus edulis*. *Aquat Toxicol* 100:178-186.

156. Kim KT, Klaine SJ, Cho J, Kim S, Kim SD. 2010. Oxidative stress responses of *Daphnia magna* exposed to TiO_2 nanoparticles according to size fraction. *Sci Total Environ* 408:2268-2272.

157. Xiong D, Fang T, Yu L, Sima X, Zhu W. 2011. Effects of nano-scale TiO_2, ZnO and their bulk counterparts on zebrafish: Acute toxicity, oxidative stress and oxidative damage. *Sci Total Environ* 409:1444-1452.

158. Federici G, Shaw BJ, Handy RD. 2007. Toxicity of titanium dioxide nanoparticles to rainbow trout (*Oncorhynchus mykiss*): Gill injury, oxidative stress, and other physiological effects. *Aquat Toxicol* 84:415-430.

159. Lin D, Tian X, Wu F, Xing B. 2010. Fate and transport of engineered nanomaterials in the environment. *J Environ Qual* 39:1896-1908.

160. Mukherjee B, Weaver JW. 2010. Aggregation and charge behavior of metallic and nonmetallic nanoparticles in the presence of competing similarly-charged inorganic ions. *Environ Sci Technol* 44:3332-3338.

161. Pokhrel LR, Dubey B, Scheuerman PR. 2013. Impacts of select organic ligands on the colloidal stability, dissolution dynamics, and toxicity of silver nanoparticles. *Environ Sci Technol* 47:12877-12885.

162. Wang Z, Li J, Zhao J, Sing B. 2011. Toxicity and internalization of CuO nanoparticles to prokaryotic alga *Microcystis aeruginosa* as affected by dissolved organic matter. *Environ Sci Technol* 46:6032-6040.

163. Gao J, Youn S, Hovsepyan A, Llaneza VL, Wang Y, Bitton G, Bonzongo JJ. 2009. Dispersion and toxicity of selected manufactured nanomaterials in natural river water samples: Effects of water chemical composition. *Environ Sci Technol* 43:3322-3328.

164. Blinova I, Niskanen J, Kajankari P, Kanarbik L, Kakinen A, Tenhu H, Penttinen O, Kahru A. 2013. Toxicity of two types of silver nanoparticles to aquatic crustaceans *Daphnia magna* and *Thamnocephalus platyurus. Environ Sci Pollut Res* 20:3456-3463.

165. Edgington AJ, Roberts AP, Taylor LM, Alloy MM, Reppert J, Rao AM, Mao J, Klaine SJ. 2010. The influence of natural organic matter on the toxicity of multiwalled carbon nanotubes. *Environ Toxicol Chem* 29:2511-2518.

166. Dale AL, Lowry GV, Casman EA. 2013. Modeling nanosilver transformations in freshwater sediments. *Environ Sci Technol* 47:12920-12928.

167. Ferry JL, Craig P, Hexel C, Sisco P, Frey R, Pennington P, Fulton M, Scott G, Decho A, Kashiwada S, Murphy C, Shaw TJ. 2009. Transfer of gold nanoparticles from the water column to the estuarine food web. *Nat Nanotechnol* 157:1-4.

168. Zhao C, Wang W. 2010. Biokinetic uptake and efflux of silver nanoparticles in *Daphnia magna*. *Environ Sci Technol* 44:7699-7704.

169. Zhu X, Wang J, Zhang X, Chang U, Chen Y. 2010. Trophic transfer of TiO_2 nanoparticles from daphnia to zebrafish in a simplified freshwater food chain. *Chemosphere*.79:928-933.

170. Lewinski NA, Zhu H, Ouyang CR, Conner GP, Wagner DS, Colvin VL, Drezek RA. 2011. Trophic transfer of amphiphilic polymer coated CdSe/ZnS quantum dots to *Danio rerio*. *Nanoscale* 8:3080-3083.

171. Werlin R, Priester JH, Mielke RE, Kramer S, Jackso S, Stoimenov PK, Stucky GD, Cherr GN, Orias E, Holden PA. 2010. Biomagnification of cadmium selenide quantum dots in a simple experimental microbial food chain. *Nat Nanotechnol* 6:65-71.

172. Holbrook RD, Murphy KE, Morrow JB, Cole KD. 2008. Trophic transfer of nanoparticles in a simplified invertebrate food web. *Nat Nanotechnol* 3:352-355.

173. Gaiser BK, Fernandes TF, Jepson MA, Lead JR, Tyler CR, Baalousha M, Biswas A, Britton GJ, Cole PA, Johnston BD, Ju-Nam Y, Rosenkranz P, Scown TM, Stone V. 2012. Interspecies comparisons on the uptake and toxicity of silver and cerium oxide nanoparticles. *Environ Toxicol Chem* 31:144-154
.

174. Klaine SJ, Koelmans AA, Horne N, Carley S, Handy RD, Kapustka L, Nowad B, von der Kammer F. 2012. Paradigms to assess the environmental impact of manufactured nanomaterials. *Environ Toxicol Chem* 31:3-14.

CHAPTER TWO

MODELING THE INFLUENCE OF PHYSICOCHEMICAL PROPERTIES ON PARTICLE UPTAKE AND ELIMINATION IN *DAPHNIA MAGNA*

Introduction

Over the last two decades capital investments in nanotechnology have surged in parallel with its growing popularity. The uses of nanotechnology are numerous and range from reinvention of consumer products such as sunscreens, makeup, and sporting equipment to development of more novel biomedical and remediation applications. Metals and metal oxide nanoparticles (NPs), in particular, have been exploited for their anti-bacterial, cellular recognition, and optical properties to develop innovative approaches to sanitation, drug delivery, and biomedical imaging, respectively. The potential of nanotechnology to revolutionize how we approach research and development is immense, but in order to maximize its usefulness we are compelled to document and minimize unintended consequences. We cannot dismiss the obvious potential for negative impacts on human and environmental health.

The swift rise of nanotechnology to this canonized status in industry has allowed product development to outpace research conducted on potential environmental and human impacts. Given the ubiquity of nanoparticle implementation it is inevitable that anthropogenic particles will be released into the environment [1]. Aquatic systems will act as the primary sink for many of these nanoparticle releases and, appropriately, the literature has devoted significant time to describing fate and effects of these particles in this environment.

The extent to which these particles are accumulated from both dietborne and waterborne exposures has received attention supported by concerns that NPs will mimic behavior of legacy persistent contaminants. Metal-based NPs have been observed to transfer from the water column into the resident biota [2-6], from producer to consumer [7], from decomposer to consumer [8], and from consumer to secondary consumer [9]. These patterns, however, are not universal for all particle types or organisms.

Holbrook et al. provided evidence against trophic transfer of metal nanomaterials from bacteria to ciliates, attributing the lack of accumulation to low sorption in the food [9]. Though nanomaterials are known to transfer across trophic levels, biomagnification is not often observed [7-9]. In many cases the lack of biomagnification was attributed to more proficient elimination mechanisms in the predator compared to their prey [7-9]. In contrast, Judy et al. [10] demonstrated biomagnification in a terrestrial food chain exposed to gold NPs. An additional and equally important consideration is the water chemistry to which nanomaterial fate and behavior is intrinsically linked [11,12]. Ultimately, the accumulation of nanomaterials in an organism will be a function of the environmental conditions, organism physiology and the intrinsic particle properties.

The effects of particle characteristics on behavior, interactions with the surrounding media and functionality have received considerable attention. *In vitro* studies have observed variable uptake rates and internal distribution patterns aligning to alterations in the size [13], shape [13,14] and surface chemistry [15]. Likewise whole organism studies concluded uptake to be dependent on particle size [10, 16-18] and surface chemistry [6,19-21]. These studies lay the groundwork for further investigation of property dependent uptake and elimination based on the assumption that organisms will reach an equilibrium state. Several studies have instead taken a kinetic approach to monitor uptake and elimination rates for predicting overall accumulation [4,5,9,22]. However, few studies have sought to describe the effect of particle characteristics on kinetic parameters [23]. To begin answering that question, my study investigated the role of particle size, shape and surface charge on the uptake and elimination of gold NPs by the cladoceran, *Daphnia magna*.

Materials and Methods

Nanomaterial Synthesis and Characterization

Chloroauric acid ($HAuCl_4.3H_20$, 99.9%), sodium citrate tribasic dihydrate ($Na_3C_6H_5O_7.2H_20$, 99%), sodium borohydride ($NaBH_4$ 99%), silver nitrate ($AgNO_3$, 99%), ascorbic acid (99%), poly (allylamine hydrochloride) (PAAH, MW~15000g/mole) and poly(acrylic acid, sodium salt) (PAA, MW

~15000 g/mole), cetyltrimethylammonium bromide (CTAB, 99%) were purchased from Sigma- Aldrich. All solutions were prepared in 18 MΩ ultrapure water.

Gold NPs were selected for our uptake and elimination studies due to the relative ease of production, lack of dissolution in typical environmental conditions, and negligible toxicity [3]. Simple spherical NPs used in this project were synthesized in our lab according to protocols modified from established methods [24,25]. Spheres with the approximate size of 6 nm were synthesized by combining 0.5 mL of 0.01 M $HAuCl_4$ with 0.5 mL of sodium citrate in 19 mL of purified Milli-Q water, followed by 0.6 mL of sodium borohydride and allowed to spin for two hours. Spheres with the approximate size of 20 nm were synthesized by adding 2.5 mL of 0.01 M $HAuCl_4$ to 97.5 mL of purified Milli-Q water, heating the solution to a boil, adding 3 mL of 1% sodium citrate and allowing the solution to boil for ten minutes. Spheres with approximate size of 30 nm were synthesized by adding 2.5 mL of 0.01 M $HAuCl_4$ to 97.5 mL of purified Milli-Q water, bringing to a boil, adding 10 mL of 1% sodium citrate and allowing the solution to boil for ten minutes.

Particles with aspect ratio greater than 1 were synthesized according to the procedure outlined in Alkilany et al. [15]. Briefly, nano-seeds were produced by combining 0.25 mL of 0.01M $HAuCl_4$ to 9.75 mL of 0.1M CTAB in a 50 mL falcon tube. To this mixture, 0.6 mL of 0.01M $NaBH_4$ was added and then the solution was allowed to spin for 30 minutes. In a 250 mL flask the following reagents were added in order: 95 mL 0.1M CTAB, 5 mL of 0.01 M $HAuCl_4$, 0.8 mL of 0.01M $AgNO_3$, 0.55 mL of 0.1 M ascorbic acid and 0.12 mL of the nano-seed solution prepared in the previous step. The solution was mixed gently for 30 seconds and allowed to sit undisturbed for 1 hour until complete color change. Following the color change, the particles were centrifuged and separated from the supernatant to remove excess CTAB. The particles were then separated and coated with poly(acrylic acid), centrifuged again to remove excess polymer then coated again either with poly(allylamine hydrochloride) to confer a positive charge to the rod or a second coating of poly(acrylic acid) for a negative charge. The end product was purified of excess polymer via centrifugation and re-suspended in Milli-Q water.

All stock solutions were characterized for size, shape, monodispersity and stability prior to exposures. Core diameter and shape were confirmed with transmission electron microscopy (Hitachi 7600

TEM). Monodispersity and stability of particles was determined initially based on absorbance spectrograph obtained from a Shimadzu UV-2501PC spectrophotometer and then confirmed from zeta potential measurements (Malvern Zetasizer). Hydrodynamic diameter measurements were taken at time 0 and 24 hours for citrate coated particles to assess the extent of aggregation in the presence of 1 mM citrate over the duration of the exposure.

Biodynamic Model

The biodynamic model described by Luoma and Rainbow [26] predicts the change in contaminant concentration in an organism over time (Equation 1). The model is used to describe the ability of an organism to sequester contaminants based on kinetic parameters attributed exclusively to that organism. Classically this model has been used for monitoring metal [34] and metalloid uptake and distribution but can be expanded to predict other suspended contaminants [4,22,23]. The model incorporates the competing influences of influx from waterborne (I_w) and dietborne (I_f) exposure and efflux of contaminant along with dilution from body growth.

$$d[M]_{org}/dt = I_w + I_f - (k_e + k_g)[M]_{org} \quad \textbf{(1)}$$

Influx of contaminants from the water column (Equation 2) is controlled by the unidirectional uptake rate constant (k_{uw}, L $g^{-1}d^{-1}$) from water-only and the concentration of contaminant in the water column (C_w, nM).

$$I_w = k_{uw} \text{ x } C_w \quad \textbf{(2)}$$

Influx of contaminant from the diet (Equation 3) is controlled by the unidirectional uptake rate constant for foodborne exposures (k_{uf}, g g^{-1} d^{-1}) and the concentration of the contaminant in the diet (C_f, nmols Au g^{-1}).

$$I_f = k_{uf} \text{ x } C_f \quad \textbf{(3)}$$

Efflux is a function of the elimination rate constant (k_e, d^{-1}), the growth of the organism (k_g, d^{-1}) when necessary, and the contaminant concentration in the organism [26].

Cultured Organisms

Daphnia magna cultures were housed at the Clemson University ENTOX facility and maintained according to standard protocols. *Pseudokirchneriella subcapitata* cells were grown in a nutrient solution for

one week under constant agitation, aeration and light to an approximate concentration of 5 $x10^5$ cells/mL. *D. magna* was cultured in synthetic moderately hard water (MHW, hardness ~108 mg $CaCO_3$/L, alkalinity ~ 60 mg $CaCO_3$/L, pH 7.2 – 7.8). Cultures were kept in incubator at 24 to 26 °C and under a 16:8 light/dark cycle. Organisms were fed daily and water was renewed on alternating days. All *D. magna* organisms used in uptake and elimination studies were 6-7 days old.

Daphnia magna Uptake

Daphnids from the culture were collected and allowed to depurate for two hours prior to exposure. Twenty daphnids were selected from our culture and exposed to each particle configuration at concentrations ranging from 29 - 2244 nM. Exposure solutions were created in MHW at a volume of 100 mL per replicate. After 24 hours of exposure, organisms were removed, washed twice in MHW for one minute and collected on mesh filters. Exposures were performed twice with three replications per concentration then combined to calculate the uptake rate constant (k_{uw}). The 20 nm exposures were performed a third and fourth time to acquire data at lower concentrations and then combined with the previous results.

Daphnia magna Elimination

Twenty daphnids were selected from our culture and exposed to 100 mL of each particle configuration at a concentration between 178 – 508 nM for the PAAH and PAA coated rods and between 2362 – 3102 nM for the citrate coated spheres. After 24 hours of exposure, organisms were removed, washed twice in MHW for one minute, transferred to clean MHW and fed uncontaminated algae at a concentration of 1.5 x 10^5 cells/mL. Organisms were removed at 0, 1, 3, 6, 12, 24, 36 and 48 hours post exposure, washed and collected as previously stated. At each time point the remaining organisms were transferred to fresh MHW inoculated with 1.5 x 10^5 cells/mL of fresh algae. Exposures were run in two trials with three replicates and then averaged.

Gold Analysis

After collection biological samples were dried for >24 hours at 60 °C, weighed, transferred to 15 mL centrifuge tubes and combined with 1.1 mL of 100% Aqua Regia (3 HCl: 1 HNO_3, 42 % acid).

Samples were digested for 90 minutes at 100 °C and then adjusted to 5% acid with Milli-Q water for analysis. Water samples of the exposure solutions were collected in 15 mL centrifuge tubes during each experiment, pre- and post-exposure. Each water sample was combined with 1.1 mL of 100% Aqua Regia for a final acid concentration of 5%, mixed well, and then analyzed. Gold analysis of all samples was performed on a Thermo Scientific XSeries2 Inductively Coupled Plasma Mass Spectrometer.

Imaging the Daphnia magna Gut Tract

Individual daphnids were removed from the highest concentration exposure and fixed in 2% gluteraldehyde. Samples were then dehydrated with alcohol, incubated for 40 minutes in a 50/50 mixture of propylene oxide:LR White for greater infiltration, and embedded in 100% LR White. Samples were cut into ultra-thin (90~110 nm) sections using an ultra-microtome and imaged on the Hitachi 7600 Transmission Electron or in the TEM setting on the Hitachi S4800 microscope. All identified nanostructures were separately confirmed to have gold signatures using energy dispersive X-ray analysis.

Data Analysis

All rate constants including standard error were derived using linear regression analysis with SAS 9.2 from the slope of the data displayed in native or transformed plots. The significance of three principle particle properties (size, shape and surface charge) was determined by combining data for all particle configurations in a multiple regression analysis with SAS 9.2. A comprehensive model was built from the quantitative (concentration) and qualitative (size, shape, surface charge) data to predict uptake and elimination rate constants based on initial particle characteristics. Analytical replicates that returned values below the detection limit of the ICP-MS (0.250 ug Au/L) were replaced with imputed values estimated from a linear regression analysis of the data after removing the data points that were below the detection limit. The imputed data points thus represent the theoretical values if they were consistent with the other data points. There is, of course, inherent bias in this method because I am assuming that the pattern of either elimination or uptake does not change drastically at concentrations below the detection limit. I selected this type of imputation because replacing the values with zero was not an option for the log transformed elimination plots and the use of singular values such as half the detection limit would greatly

skew the data toward that value, depreciating the rest of the data set. For all data analysis, a p value < 0.05 was considered statistically significant.

Results

Particle Characterization

Citrate capped gold nanospheres synthesis produced monodisperse stock solutions with core diameter of 5.67 $\pm$ 1.28 nm, 21.25 $\pm$ 2.5 nm, and 30.64 $\pm$ 6.00 nm (Figure 2.1a-c), hereafter referred to as 6, 20 and 30 nm, respectively. All citrate-capped nanospheres were stable in stock solutions and produced a negative zeta potential of -39.8 $\pm$ 9.94, -35.7 $\pm$ 19.5 and -38.9 $\pm$ 16.4 mV for 6, 20 and 30 nm stocks, respectively (Figure 2.2). All synthesized nanorods had dimensions of 17.82 $\pm$ 2.03 x 58.08 $\pm$ 5.31 nm with an average aspect ratio of 3.3 (Figure 2.1d-e). Nanorods coated with poly (acrylic acid) (PAA) held a negative zeta potential of -20.7 $\pm$ 9.33 mV while poly(allylamine hydrochloride) (PAAH) held a positive zeta potential of +38.8 $\pm$ 17.5 mV (Figure 2.2). Stability of the citrate capped particles decreased upon dilution in MHW causing noticeable aggregation over the duration of the exposure period. To minimize the effect of particle aggregation due to high cation concentration [27] exposure solutions and controls containing citrated-coated nanoparticles were supplemented with citrate at a final concentration of 1 mM without noticeable impact to organism health. Dynamic light scattering (DLS) was used to determine if particle size (measured as hydrodynamic diameter) changed significantly over the 24-hour exposure period (Figure 2.3). After 24 hours the 6, 20 and 30 nm spheres experienced marginal increases in size and a majority (over 99%) did not fall victim to aggregation. The 6 nm spheres changed the most, enduring an increase of 6.2 nm (from ~ 6.5 nm to ~ 13 nm). The 20 and 30 nm particles, on the other hand, remained fairly close to their original size or even seemed to decrease in size. The 20 nm particles increased 1.66 nm over 24 hours (from ~ 20.5 nm to ~ 22.5 nm) while the 30 nm particles either increased slightly (from ~ 41 nm to ~ 42 nm after 24 hours) or seemed to decrease to a size comparable to the first replicate (from ~ 53 to ~ 42 nm). Though we did observe changes in particle size during the 24 hours, the shifts were not enough to cause overlap between particle configurations enabling us to treat them separately in our models.

Exposure solutions of PAA and PAAH coated rods did not exhibit noticeable aggregation and were, therefore, prepared without additional reagents.

Derivation of Uptake Rate Constants

Influx of NPs by *D. magna* was plotted along a concentration gradient to empirically derive uptake rate constants for each particle configuration (Figure 2.4). Influx for all the negatively charged particles (6, 20 and 30 nm citrate capped gold nanospheres and PAA coated nanorods) was linear with respect to concentration. Daphnids exposed to 6 nm citrate coated particles exhibited the largest uptake rate constant of the citrate-coated spheres. Uptake rate constants for the 20 and 30 nm citrate coated particles were both statistically different from the 4 nm exposure but not from each other. Daphnids exposed to the PAA coated nanorods exhibited the slowest rate constant of all the configurations tested. In contrast to the other particles examined, daphnids exposed to the PAAH coated rods exhibited a biphasic uptake pattern along the concentration gradient. The PAAH exposure plot was separated into low and high concentration data sets to linearize the slope and simplify analysis. The low concentration rate constant mirrored that of the 4 nm citrate coated spheres. However the high concentration uptake rate constant was significantly greater than the rate constants derived for all other particle configurations. All uptake rate constants are presented in Table 1 including standard error.

Derivation of Elimination Rate Constants

Upon transfer into clean medium the elimination of particles from the daphnids was quantified. Particle body burden remaining in *D. magna* was plotted against depuration time to assign the appropriate elimination model and empirically derive elimination rate constants for each particle configuration (Figure 2.5). Elimination of NPs in the presence of food adhered to the two-compartment model: a significant portion of the body burden (70- 90%, Figure 2.5) is removed within the first 3-6 hours (fast compartment), followed by a steady removal of the remaining NPs over the next 42 - 45 hours (slow compartment). PAAH coated rods and 6 nm spheres exhibited statistically similar elimination rate constants that were greater than the other particle configurations. These elimination rate constants indicate that daphnids exposed to PAAH coated rods and 6 nm citrate coated spheres were able to eliminate 50% of the body burden every 6 hours.

PAA coated rods had the next largest elimination rate constant followed by 20 nm spheres and 30 nm spheres. These elimination rate constants translated to a half-life of 8 hours, 9 hours and 14 hours for PAA coated rods, 20 nm citrate coated spheres and 30 nm citrate coated spheres, respectively. All elimination rate constants are provided in Table 1 including standard error.

Modeling the Influence of Particle Properties on Biodynamic Parameters

The influence of core diameter, shape and surface charge on uptake and elimination rates was determined using multiple linear regression analysis with data collected for each particle configuration. Similarities in size (diameter 6, 20 or 30 nm), shape (rod or sphere), and surface charge (cationic or anionic) enabled fundamental comparisons of each particle property with respect to uptake and elimination patterns. While there is no consensus on a definitive concentration metric in the literature, our choice to use gold mass concentration rather than gold NP concentration was a practical consideration. The concentration range for our data converted to NP concentration spanned several orders of magnitude and returned dubious statistical results. Accurate statistical comparisons could, therefore, only be conducted using mass data.

Due to the biphasic response elicited by PAAH coated rods the PAAH uptake data were divided into separate high (solid line, Figure 2.4e) and low (dashed line, Figure 2.4e) concentration data sets to linearize the plots. The data for the other particle configurations were not separated because they were linear across the entire concentration range. The two PAAH datasets were incorporated into separate models to determine slope differences for high and low PAAH concentration exposures with respect to the other particle configurations. Overlapping concentration ranges were chosen so as to include three concentrations for both data sets. The low PAAH dataset was combined with the full dataset for the other particle configurations to create the low concentration model (Equation 4). Likewise, the high PAAH dataset was combined with the full dataset for the other particle configurations to create the high concentration model (Equation 5).

$$\text{Influx} = 0.88 + 2.80\,(\text{concentration}) - 238.07\,(\text{small}) + 2.33\,(\text{small}*\text{concentration}) \quad \textbf{(4)}$$

Influx = -2.48 + 2.81 (concentration) -234.70 (small) - 3247.31 (surface charge) + 2.33 **(**small*concentration) + 89.69 (surface charge*concentration) **(5)**

Both uptake models were created using multiple linear regression analysis with the appropriate datasets described above. Concentration was the quantitative variable and size, shape and surface charge were the qualitative variables. The qualitative variables were converted to fabricated numerical values that allowed the model to group the data according to the particle characteristics. Size had to be separated into two sub-variables "small" and "large" because there were three possible diameters (i.e. either 6, 20 or 30 nm). The “small” variable was coded as 6 nm = 1, 20 nm = 0, and 30 nm = 0 and this variable identified differences between NPs with a 6 nm diameter and NPs larger than 4 nm. The “large” variable was coded as 6 nm = 0, 20 nm = 0, and 30 nm = 1 and this identified differences between NPs with a diameter of 30 nm and NPs smaller than 30 nm. Using these two sub-variables the model could signify if there was a significant influence from very small particles (6 nm), large particles (30 nm) and if both were significant, then it can be assumed the medium particle (20 nm) is different from the others as well. The shape and surface charge variables were not broken into sub-variables because there were only two possible designations for each. The “shape” variable was coded as sphere = 0 and rod =1. The “surface charge” variable was coded as anionic = 0 and cationic = 1.

When I used the low concentration PAAH data (Equation 4), particle size was the only characteristic influential to uptake (Table 2). Surface charge did not appear to exercise influence over uptake at low concentrations, as the cationic rods are taken up at a rate identical to the anionic particles of similar size. Shape was likewise ruled out as an important characteristic with the low concentration PAAH data. An important distinction to make is that the size effect is only statistically significant for small particles (4-6 nm) in relation to particles of larger size (20-30 nm) as represented by the “small” qualitative variable. The impact of particle size is not as strong when comparing uptake of particles with diameter 30 nm to the smaller particles as represented by the “large” qualitative variable. Inclusion of the high concentration PAAH data into my model (Equation 5), revealed that surface charge exercised considerable

influence over uptake after a certain threshold, operationally defined in my study as 148 nM (Table 2). Once again changes in shape and a shift in particle diameter from 6 nm to 20 or 30 nm had minimal impact.

Analysis of the elimination data mirrored the procedure employed on uptake data except in this time is the quantitative variable rather than concentration. The combined elimination model (Equation 6) compared the natural log transformed slow exchange compartment (hours 3-48) for all configurations, as that will dictate the rate of depuration. The model (Table 2) indicated that all sizes (both "small" and "large") and surface charge were influential to the depuration process. Shape again appeared to have a negligible impact.

$$\text{Ln (\% remaining)} = 2.94 - 1.93\,(\text{time}) + 0.90\,(\text{small}) - 0.11\,(\text{large}) + 0.01\,(\text{surface charge}) - 0.99\,(\text{small*time}) + 0.81\,(\text{large*time}) - 0.81\,(\text{surface charge*time}) \quad \textbf{(6)}$$

Using these three equations and the numerical values assigned to each variable, theoretical rate constants were derived for all iterations of size and surface charge (Table 3) for a hypothetical gold NP construction. These rate constants were then used to calculate the steady state bioconcentration factor (Table 3). According to the model predictions, *D. magna* exposed to larger cationic particles at concentrations exceeding 148 nM are expected to achieve the highest body burden of NPs at steady state while *D. magna* exposed to smaller anionic particles and smaller cationic particles at concentrations below 148 nM will accumulate the lowest concentrations (Table 3). The fact that cationic particles are both the most accumulated and least accumulated seems counterintuitive. However, at low concentrations the influence of charge on uptake is negligible compared to the influence of charge on elimination. Therefore, the faster elimination rate for cationic particles dictates the overall accumulation. At high concentrations, the contribution from the large uptake rate constant overshadowed the faster elimination rate constant accounting for the higher predicted accumulation.

A cationic nanosphere is noticeably absent from the particle catalogue. Regretfully, I did not have the means required to synthesize cationic spheres with the PAAH surface chemistry at a size similar to any of our citrate coated spheres. Therefore, my models are used to extrapolate the data for this particle type. In

a subsequent experiment for Chapter 3 I exposed *D. magna* to 2 nm (core size) cationic particles (quaternary amine surface coating) for 24 hours and derived uptake and elimination rate constants. The data for these particles confirmed the biphasic uptake pattern for daphnids exposed to cationic particles and further indicated a saturation point for particle uptake. Interestingly, uptake (k_{uw} = 110.31 $\pm$ 10.77 L g^{-1} d^{-1}) and elimination (k_e = 2.93 $\pm$ 0.13 d^{-1}) rate constants did not directly align with those predicted for small cationic spheres from my model though this may be attributed to the lack of similarity in particle characteristics and ligand chemistry. The discrepancies with my model predictions and this unrelated particle illustrate the difficulties in developing a robust model that is inclusive to all particle configurations

Particle Internalization

Transmission electron microscopy was used to qualitatively assess the localization of each gold nanoparticle configuration in the gut tract and surrounding tissues of an exposed *D. magna* (Figure 2.6a-e). Identifiable gold NPs were found in the lumen of the gut tract in various states of aggregation for each treatment. The presence of gold in the gut tract confirmed ingestion as a viable route of uptake for gold NPs in *D. magna*. After a thorough examination of the gut sections I did not find evidence to indicate translocation across epithelial membranes into cells for any of the treatments. I did witness several treatments (7a-d) where gold NPs were in association with or in proximity to the microvilli suggesting that these particles may be in route to internalization. Furthermore, the NPs that did cross membrane barriers were likely individual particles and at extremely low concentrations as evident from our elimination experiments. It is entirely possible that the narrow scope of my TEM examination overlooked areas where these NPs were stored internally. With these considerations in mind I cannot completely rule out the possibility of NP accumulation for the particle configurations selected for my study.

Elemental analysis was conducted on each *D. magna* gut tract micrograph to confirm the presence of gold (Figure 2.7). Elemental analysis utilized the Energy Dispersive X-ray (EDX) technique, producing spectra that identified the elemental array present at a selected site on the micrograph. Gold peaks were present in each spectra along with other element peaks including carbon and copper. The carbon and copper peaks were part of an expected array associated with the grid itself. For each micrograph, several particle groupings were analyzed to confirm the presence of gold NPs.

Discussion

The models derived from my data indicated that surface charge and core diameter were the dominating properties controlling accumulation in *D. magna.* The underlying influence of these two particle properties is best explained through separate examination of uptake and elimination pathways and the mechanistic role of charge and size in these processes.

Influx of NPs by *D. magna* is a measure of the ingested nanomaterial, nanomaterial absorbed across the gut tract and nanomaterial adsorbed or trapped by the carapace. The pattern of influx with respect to concentration will reflect the mechanism(s) of uptake over a given concentration range [4]. Uptake of negatively charged NPs (citrate coated spheres and PAA coated rods) followed first order uptake kinetics indicating a single dominant uptake mechanism (Figure 2.2). Evidence from microscopy analysis pointed to ingestion as the dominant mechanism for anionic NPs (Figure 2.6a-d). Furthermore, adsorption of anionic gold NPs is expected to contribute little to the overall body burden [27,28]. In contrast, we observed a biphasic uptake pattern for cationic NPs. A biphasic influx pattern often indicates the presence of binding sites with different characteristics (affinity and capacity). However, this explanation is not a perfect fit for the PAAH data because I did not find evidence of PAAH rods adsorbing to cell surfaces (Figure 2.6e). The biphasic pattern may instead represent a shift in the dominant influx mechanism [4]. Qualitative observations and microscopy analysis indicated significant particle content in the gut tract of daphnids exposed to elevated concentrations suggesting that ingestion is the dominant mechanism for high concentration exposures. Though it was not quantified, adsorption of PAAH coated rods to the carapace or trapping of rods under the carapace likely contributed to overall accumulation at both high and low concentrations, possibly representing the dominant influx mechanism for low concentration exposures [4].

Even though overall accumulation was greatest for larger cationic particles, the smaller cationic particles exhibited the highest uptake rate constant. This preferential uptake gives insight into the filtering and ingestion mechanisms of *D. magna* and other cladocerns. The NPs used in our exposures were natively smaller than the average mesh filter size of *Daphnia* species; therefore, capture and ingestion of these particles must occur incidentally via a pressure gradient produced by the filtration process, incidentally via

physicochemical interactions with the mesh filter, in association with other suspended debris, or actively in an aggregated form [29-31]. Aggregation did not seem to play a role in uptake as particle size did not have significant fluctuations in the exposure media over the 24-hour exposure period. Furthermore the exposure solutions were prepared with 18 MOhm water and without food, keeping miscellaneous debris to a minimum. Therefore, particle uptake must have been primarily through incidental ingestion. Particles smaller than the mesh filter can still be captured through gravitational deposition, inertial impaction, motile-particle deposition and electrostatic interaction [32]. Uptake of smaller sized particles is expected to be greater for uptake mechanisms involving either diffusion particle deposition or electrostatic interaction implying that one or both may be the dominant mechanism of uptake in my study [32].

The acknowledgement of surface charge as influential to uptake of NPs lends further credence to the presence of an electrostatic component in the *D. magna* uptake mechanism for gold NPs. For particles smaller than the filter mesh size, Gerritsen and Porter adamantly argued that the electrostatic interaction between the particle and the filter surface dictated ingestion rates [31]. They observed that a reduction in negative charge through addition of amine groups to the surface of the particle resulted in higher uptake efficiency by *D. magna*. The ingestion of more PAAH coated particles at higher concentrations could thus be explained by a stronger attraction to the filter surface enhancing uptake rate. Hammer et al. noted a similar trend for dinoflaggelates concluding that particles with a charge opposite of the organism would have a higher probability of being ingested [33]. Neglecting uptake of negatively coated particles could also be an evolutionary advantage for obligate filter feeders such as *Daphnia*. Most particles in the aqueous environments carry a negative charge [34]; having an extra layer of defense against particles smaller than their filter mesh would ensure ingestion of fewer unnecessary particles. While statistically significant, the particle size contribution to the model may not be as important as the connection between initial surface charge and particle uptake. Due to the large uptake rate constant for cationic particles, the impact of surface charge may have greater biological significance when considering the enormous energetic requirements and associated toxicity of clearing a gut filled with nanomaterials [5,11].

Uptake rate constants do not distinguish between NPs absorbed, adsorbed, or those unassociated in the gut tract. The elimination rate constants were, therefore, derived to intuit the behavior of the particle

after ingestion and relate it to the daphnids ability to eliminate the NPs. Furthermore the link between elimination rates, surface charge and size can be used to describe the interaction between NPs and defensive mechanisms in the gut of cladocerns.

Similar to uptake, elimination rate constants were greatest for smaller cationic particles. The fact that larger sized particles produced higher predicted BCFs implied that, with respect to size, elimination is a more important mechanism than uptake. In lieu of evidence to suggest internal accumulation, we attributed differences in efflux rates to internal aggregation and interactions with debris and internal structures in the gut. Based on the microscopy images I speculated that the fast and slow exchanging compartment were related to the location of the particles in the gut tract. The fast exchanging compartment was the middle of the gut tract where algae could easily and quickly push the particles along. The slow exchanging compartment was the surface of debris, microvilli and peritrophic membrane where particles were more difficult to remove. The size of the particle, for example, will determine if a particle or aggregate can penetrate barriers [13,35]. Larger sized particles have a greater probability for deposition on gut surfaces that would retard the daphnids ability to push these particles through the gut [32]. This reasoning aligns well with my observations. However, most particle configurations aggregated to some degree after ingestion (Figure 2.6b-e). Widespread aggregation was not observed, which may have resulted from sample preparation. While most particles were found in proximity to the microvilli, the 4 nm spheres were the only particle type that was clearly associated. Despite this association, daphnids were able to eliminate 4 nm particles quickly implying the association was tenuous or the fraction adsorbed to the microvilli was negligible.

Surface charge, on the other hand, controls particle-particle and particle-surface interactions two processes that influence elimination by *D. magna* [12,36]. All anionic particle configurations were observed in proximity to or associated with the microvilli (Figure 2.6a-c) or associated with the peritrophic membrane (Figure 2.6d) inhibiting elimination. The cationic NPs, however, exclusively formed aggregates around cellular debris as opposed to contact with the peritrophic membrane, microvilli or other cellular structures (Figure 2.6e). The lack of interaction with the peritrophic membrane or microvilli would intuitively favor quicker peristaltic removal in the presence of food. The interaction of anionic particles

with negatively charged microvilli and peritrophic membrane surfaces implies a change in NP surface charge upon ingestion or depression of the electronic double layer around the particle surface [37]. This assumption is further supported by a proclivity to aggregate noted to varying degree for all particle configurations. However, smaller particle sizes are well documented to be more susceptible to aggregation disagreeing with my visual results [12]. At this point it is unclear why the 6 nm particle configurations did not demonstrate an aggregated state in the daphnid gut tract (Figure 2.6a-c). One possible explanation is that our TEM images were not of an entire daphnid and, therefore, it would have been easy to miss aggregates in other sections of the daphnid gut tract. Alternatively it is possible that the sample preparation process induced aggregation of some particles and not others. My observations indicate that in the gut, surface charge dictates where the NPs absorb, and similar to size, the ability to traverse peritrophic and epithelial membranes. Shape is known to have an impact on aggregation behavior and particle-surface interactions as well [13,38]. However, my results downplayed the significance of shape with respect to size and surface charge on interactions that would control accumulation.

The NP body burden predicted by my model represents particles that are associated to external structures (carapace, gut tract) rather than a significant internalized fraction as is often the case when modeling metal exposures. The lack of gold NP internalization in my experiments is not unprecedented [28,39]. Yet, *D. magna* have been previously reported to translocate NPs to secondary storage depots and internal tissues indicating the presence of a mechanism for absorption [18,19]. The visual and empirical evidence produced in this study suggested that our particle types and those in the other studies were not suited for absorption, however other configurations of gold NPs may possess the ability to translocate into epithelial cells and other internal tissues [28,39].

The BCFs calculated (Table 3) from my empirical rate constants and lack of evidence to indicate internal translocation downplay the threat of significant accumulation for all particles configurations except the PAAH rods. However, even elimination of the PAAH rods approached the detection limit of the ICP-MS ([Au] ~ 0.25 ppb) after 48 hours in presence of a food source suggesting limited assimilation. These results are in stark contrast to several other studies that observed long- term particle retention after transferring to fresh moderately hard water [4,5,18,19,21]. Variation in particle retention across these

studies could be suggestive of a separate consideration for particle accumulation: gut tract interactions that are distinctive to the core composition of a particle. A study on gold nanoparticle depuration in *D. magna* without food by Lovern et al. revealed a temporal change in gut particle content that is consistent with my experimental results [28]. At 24 hours the bulk of the nanoparticle body burden was present in the tail region indicating rapid removal irrespective of food availability. A similar study by Khan et al. observed a similar trend to the Lovern et al. study and my own though elimination from the slow compartment proceeded an order of magnitude slower than I observed [28,39]. The relative ease of removing gold NPs could explain why I observed much quicker elimination rates for gold NPs and minimal long-term accumulation.

The visual and empirical evidence produced in this study argued against but did not rule out the possibility of gold NP translocation into epithelial cells and other internal tissues. *Daphnia magna* have been previously reported to translocate NPs to secondary storage depots and internal tissues suggesting the presence of a mechanism for absorption in the gut tract [18,19]. Furthermore, several other species have been reported to accumulate gold NPs in tissues outside of the gut tract. Particles ranging from 5 – 50 nm in diameter were detected throughout internal tissues of tobacco worms from dietborne exposure and endobenthic bivalves from waterborne exposures [10,17,40]. In a study investigating the role of surface chemistry on uptake in Japanese medaka, Zhu et al. witnessed systemic distribution of gold NPs with a hydrophobic surface coating [6]. In support of my study they did note that, of the hydrophilic surface ligands, the cationic particles were ingested at the highest frequency establishing the highest particle accumulation in the intestinal tract and gills. Mammalian species have likewise demonstrated the ability to absorb gold NPs, a fact oft exploited in biomedical applications [16]. Based on my experiments and those in the literature it is unclear if absorption is restricted to a particle type with a specific set of attributes and if these attributes fall outside of the configurations chosen in my experiment. It is conceivable that *D. magna* possess mechanisms to translocate gold NPs but I was unable to detect the low levels that constitute the accumulated fraction.

Despite the species and particle specific nature of my models, the broader trends are consistent with several studies on different organisms and particle types. My model predicted that larger (30 nm)

cationic NPs would achieve greater accumulation at steady state compared to smaller (<30 nm) anionic NPs. In the literature larger particles have been reported to have greater accumulation in clams, and hornworms [10,17,40]. Likewise cationic NPs have exhibited greater accumulation in mammalian cells, biofilms, clams, snails, fish, and hydroponic plant roots [2,6,15,20]. This information could be useful for predictive modeling, risk assessment, NP regulations, and in particle fabrication aimed at minimizing environmental impact. Yet the complexity of nanoparticle exposures and organism physiology precludes indiscriminate use of my models for predicting accumulation. For example, results from daphnids exposed to quantum dots, cells exposed to gold NPs, estuarine rooted plants and detritovores exposed to gold NPs, and the internalized concentration of gold NPs in hydroponic plants defy the trends postulated by my models [2,13,14,20,21].

My models were not intended to be comprehensive, rather they were designed to illustrate which, of three, properties was the most important to accumulation. The particles selected for this experiment did not cover the entire defined range for nanomaterials (1-100 nm), yet it did cover the size range ($\leq$30 nm) where metallic nanomaterials exhibit unique properties that can increase their toxicity [41]. My models could be strengthened by the inclusion of more sizes, shapes and surface charges to see if the patterns persist beyond the particle configurations chosen for this experiment. Evaluating other characteristics, such as core chemistry, surface chemistry, and surface area, with a similar approach may also resolve the discrepancies noted from other experiments [19,23,41]. Finally, the concentration metric selected for our models was done out of necessity but it may not be the best option for assessing risk of nanomaterials [10,41]. Ultimately it may be inappropriate, even impossible to produce a single model for all nanoparticle types and species of concern. Smaller more focused models for each model organism, such as the one produced from my data, will then find a place among the larger framework of modeling initiatives.

Conclusions

This study examined the influence of three principle particle characteristics on accumulation in *D. magna*. Models of the data suggest that surface charge and particle size are the dominant properties controlling accumulation in *D. magna*. When challenged in environmental conditions similar to those in my

experiments, *D. manga* will accumulate a higher particle body burden from exposure to larger positively coated NPs compared to smaller negatively coated particles. No evidence was found to indicate that the NPs were absorbed across epithelial membranes. Rather particle accumulation was observed primarily in the gut tract and was likely controlled by interactions with permanent (gut wall including microvilli) and transient (peritrophic membrane and debris) structures. The models derived from my data set were designed as initial indicators of the influential nature of particle properties on uptake and elimination mechanisms and are by no means exhaustive. Future work with more particle configurations will be required to develop more robust and defendable models.

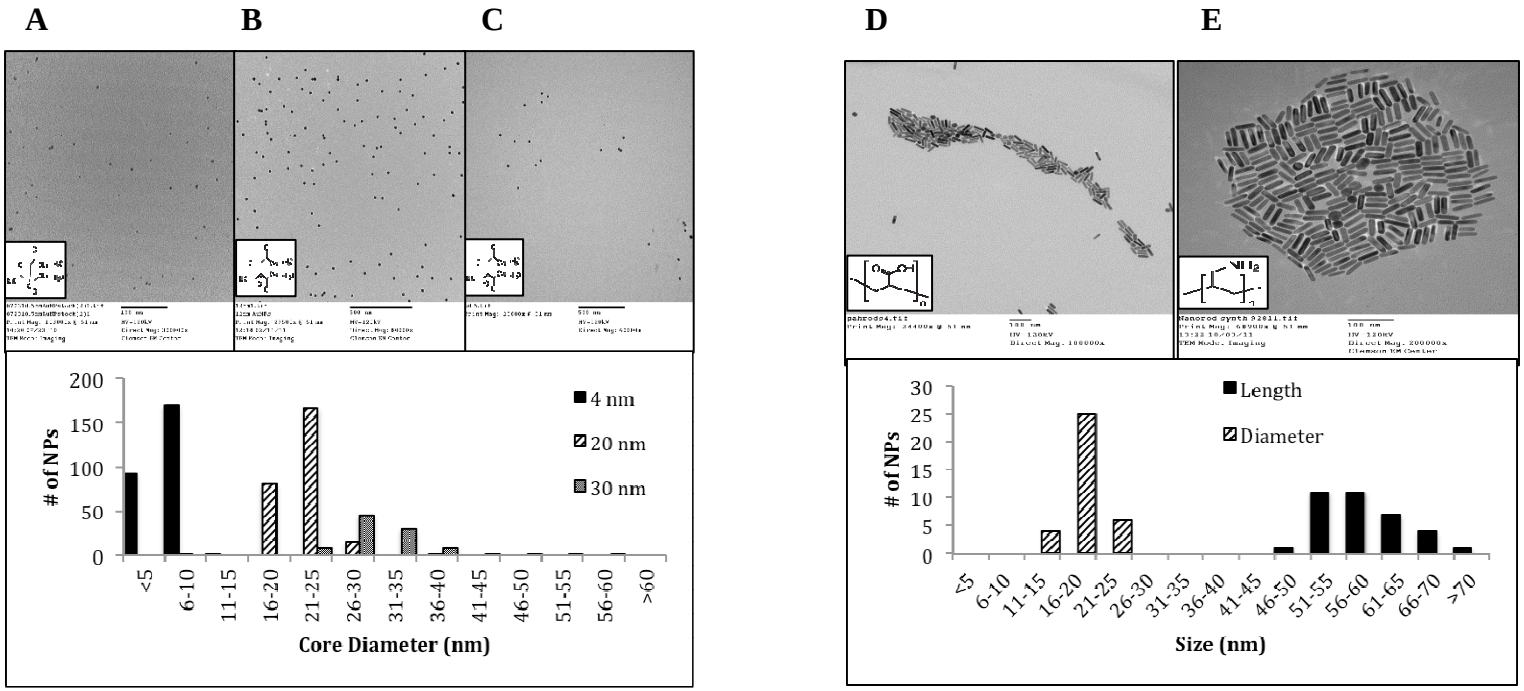

Figure 2.1: TEM images of gold nanoparticle configurations with distribution histograms
TEM imaging of 6 nm (A), 20 nm (B), and 30 nm (C) citrate coated spheres, PAA coated rods (D), and PAAH coated rods (E) with the chemical structure of the surface coating (insert). Histograms present the distribution of core diameter for each particle configuration based on Image J analysis of > 30 particles. The PAAH and PAA rods were produced from the same stock of nanorods, therefore, the particle length and width are combined in a single histogram.

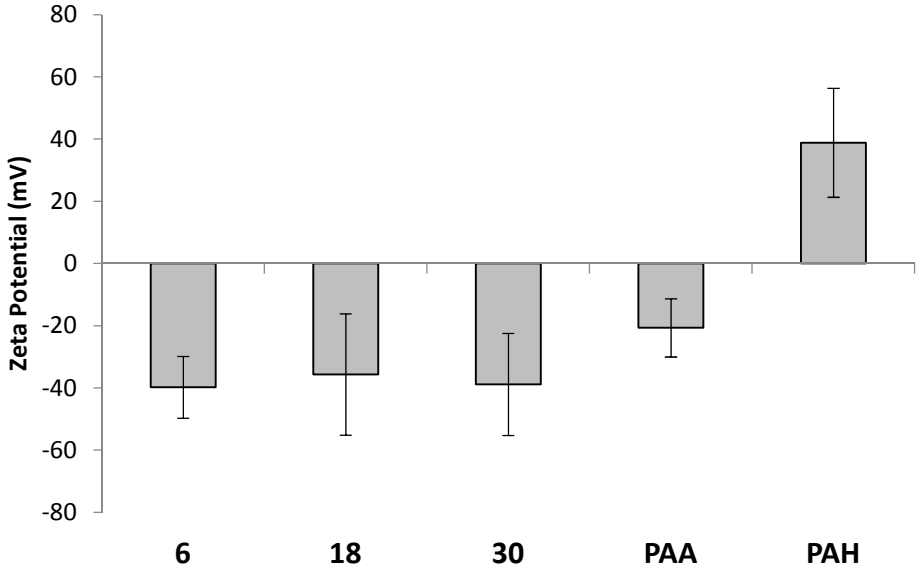

Figure 2.2: Zeta potential of the stock solution for each particle configuration
Zeta potential measurements of each particle configuration in Milli-Q water. Error bars represent one standard deviation.

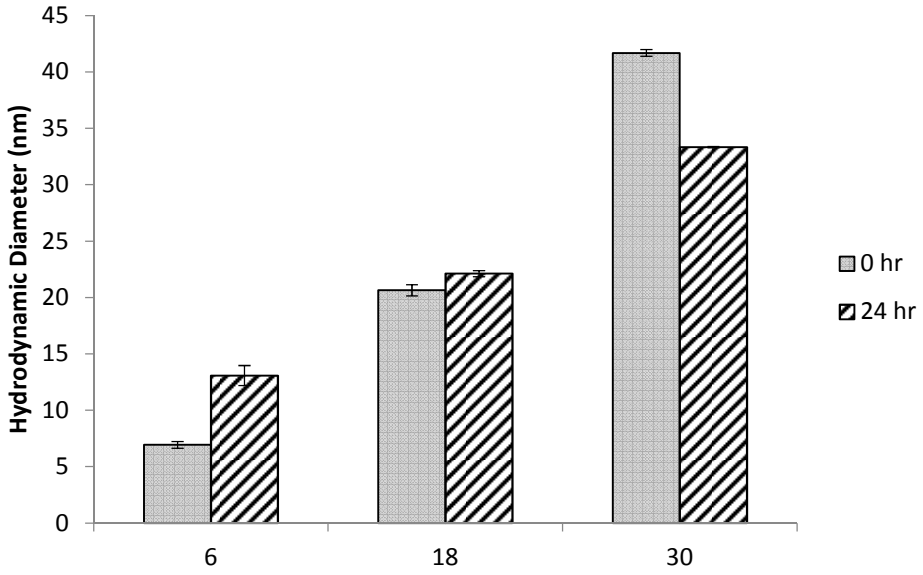

Figure 2.3: Hydrodynamic diameter of citrate coated particles at the beginning and end of the exposure

Aggregation experiment with citrate coated nanomaterials in MHW supplemented with 1 mM citrate. Dynamic light scattering (DLS) measurements were taken immediately after adding NPs to moderately hard water (solid-0 hr) and at the end of the uptake experiment (striped- 24 hr). Error bars represent one standard deviation. PAA and PAAH nanorods did not exhibit visible aggregation in MHW and, therefore, are not included in this DLS

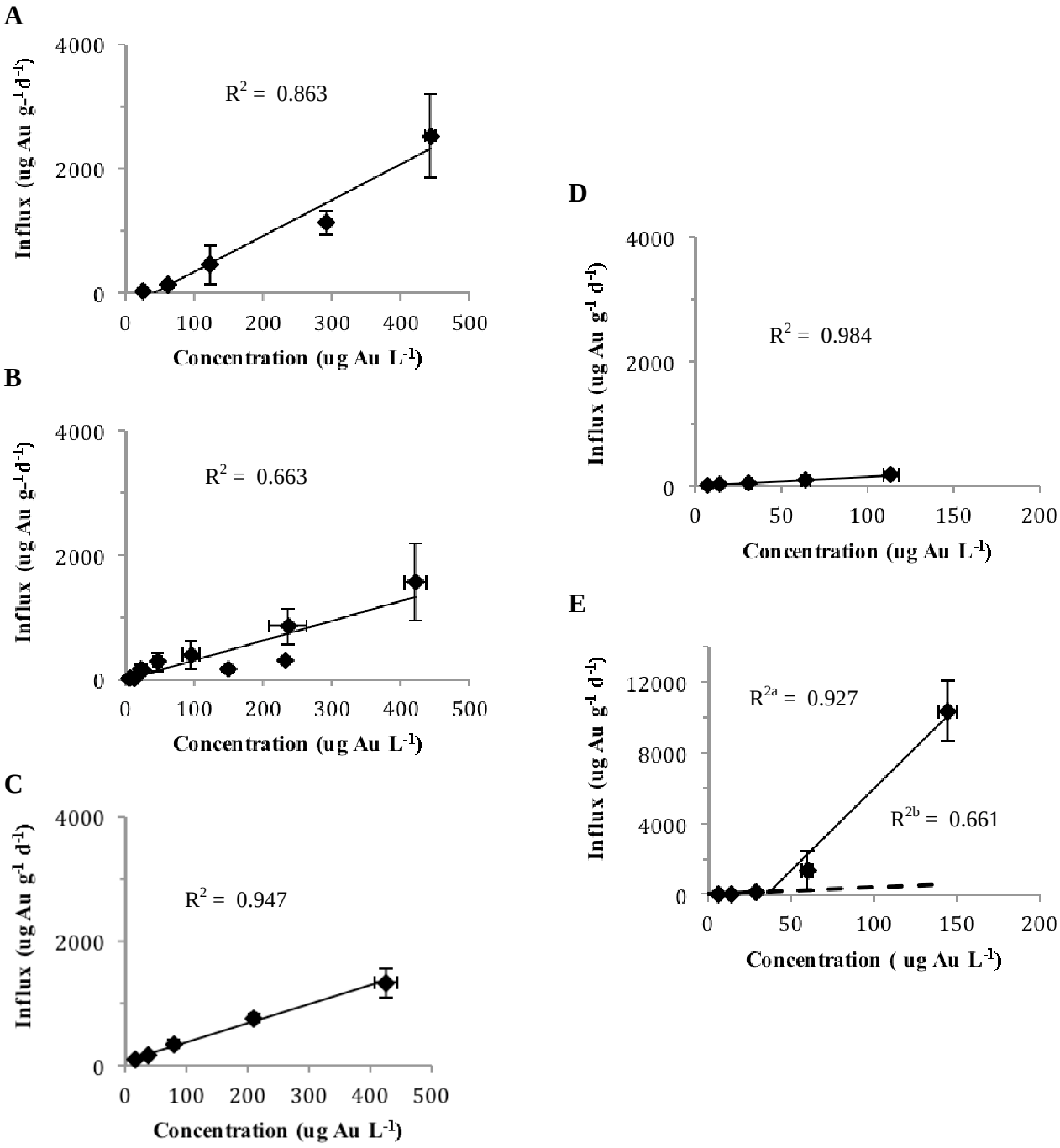

Figure 2.4: Uptake of five different gold nanoparticle configurations by *Daphnia magna*

Uptake plots for each gold nanoparticle configuration: (A) 6 nm citrate coated nanospheres, (B) 20 nm citrate coated nanospheres, (C) 30 nm citrate coated nanospheres, (D) PAA coated nanorods, and (E) PAAH coated nanorods with R^2 values for the regression line used to derive the uptake rate constants. All data points are averages of six replicates $\pm$ 1 standard deviation. Dashed line in the PAAH graph (E) represents the low concentration uptake rate constant (R^{2b}) and the solid line represents the high concentration uptake rate constant (R^{2a}).

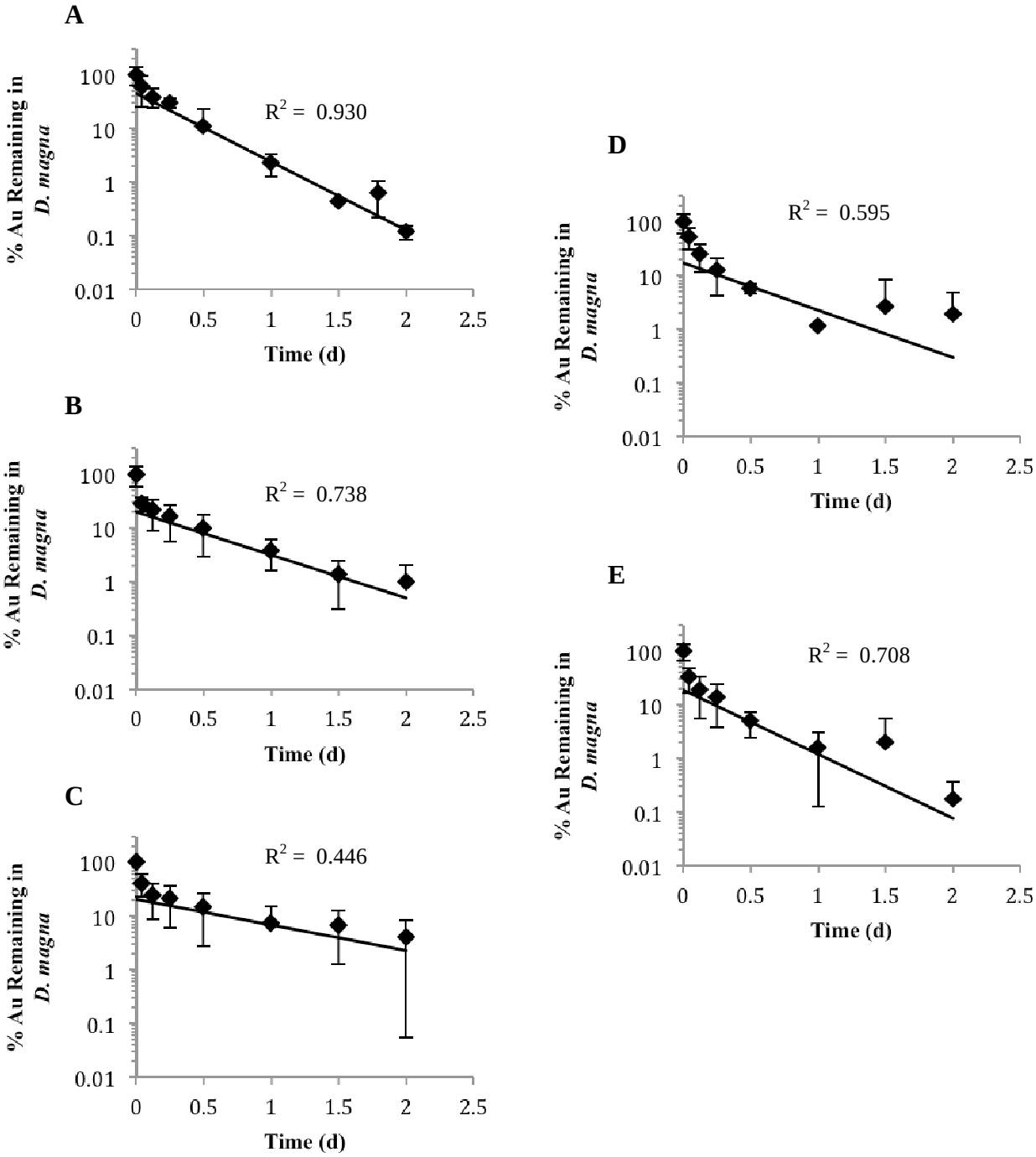

Figure 2.5: Elimination of five different gold nanoparticle configurations by *Daphnia magna*

Full elimination plots for each gold nanoparticle configuration: (A) 6 nm citrate coated spheres, (B) 20 nm citrate coated spheres, (C) 30 nm citrate coated spheres, (D) PAA coated rods and (E) PAAH coated rods with R^2 values for the regression line used to derive the elimination rate constant. All plots are log transformed in accordance with the two-compartment elimination model. Each value represents the average of six replicates $\pm$ 1 standard deviation. All values below the limit of detection (0.250 ug/L Au) were replaced using regression imputation. Data points without a lower bound indicate a range that encloses zero.

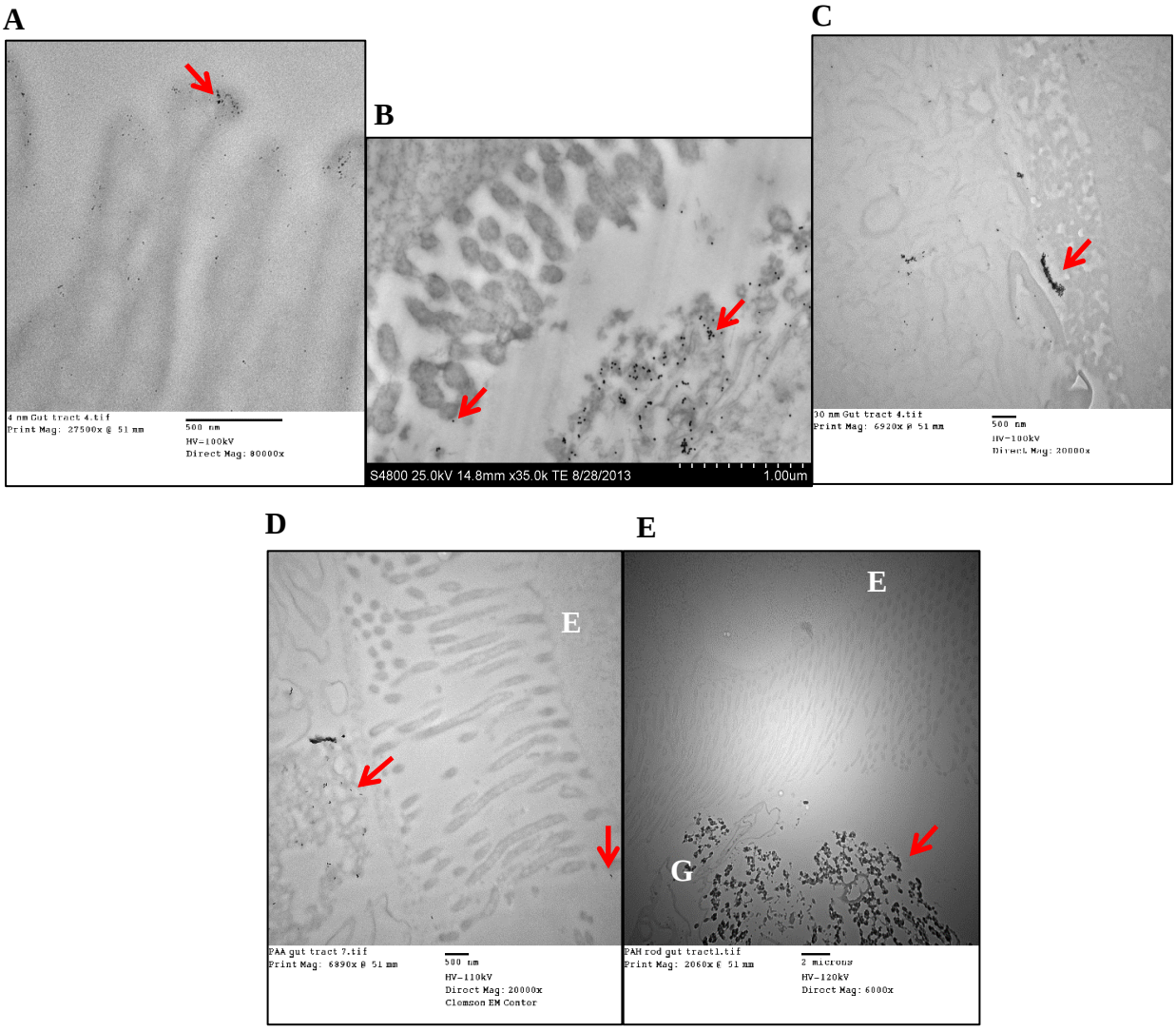

Figure 2.6: TEM images of *Daphnia magna* gut tract
Gut tract of *Daphnia magna* exposed to 6 nm (A), 20 nm (B), and 30 nm (C) citrate coated spheres, PAA coated gold nanorods (D) and PAAH coated gold nanorods (E). All identified nanostructures were separately confirmed to have gold signatures with EDX analysis. G = gut lumen, E = epithelial cells, arrows = gold nanoparticles.

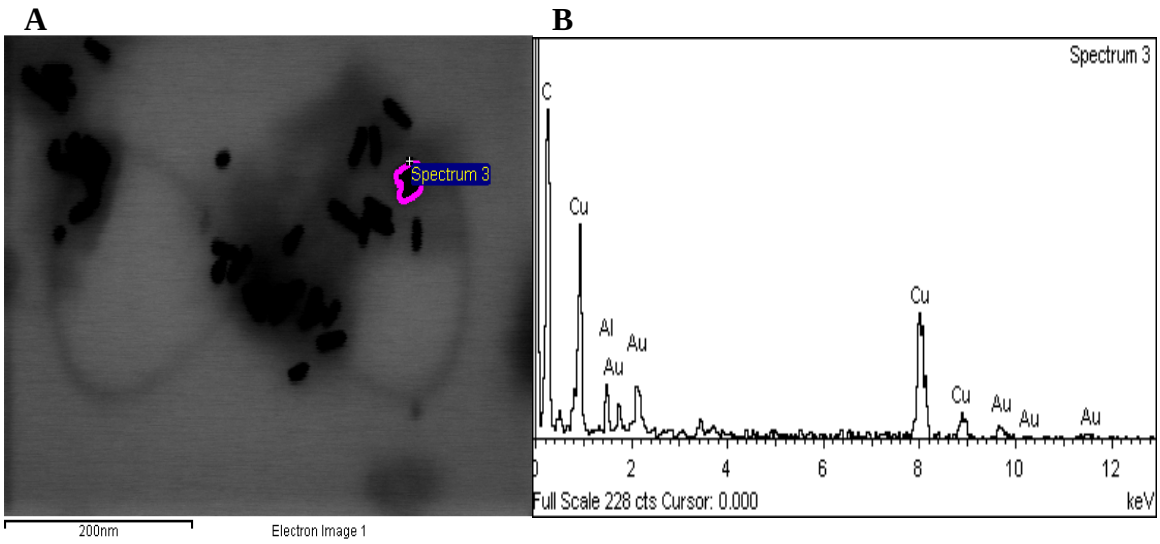

Figure 2.7: Representative elemental analysis of Daphnia magna gut tract exposed to PAAH rods

Representative micrograph of *D. magna* gut tract exposed to PAAH gold nanorods (A) and the resulting EDX spectra (B) for the selected area on the image. The spectra indicated the presence of gold signatures in the selected area confirming that the rod shaped objects contained gold. The carbon and copper peaks were expected background signatures. Several particles were analyzed from each treatment to rule out the possibility that these nanostructures were artifacts of TEM prep.

Size (nm)	Shape	Surface Ligand	k_{uw} (L g_{org}^{-1} d^{-1}) [a]	k_e (d^{-1})
6	Sphere	Citrate	5.139 ± 0.388	2.929 ± 0.140
20	Sphere	Citrate	2.772 ± 0.247	1.840 ± 0.190
30	Sphere	Citrate	2.679 ± 0.120	1.119 ± 0.213
18 x 58	Rod	Poly(acrylic acid)	1.548 ± 0.038	2.025 ± 0.287
18 x 58	Rod	Poly(allylamine hydrochloride)	L: 4.632 ± 0.830 H: 92.494 ± 6.504	2.746 ± 0.303

Table 2.1: Uptake and elimination rate constants for *Daphnia magna* exposed to each nanoparticle configuration
Size, shape, surface ligand, uptake and elimination rate constants (± standard error) for each nanoparticle configuration.
[a] *D. magna* exposed to PAH coated rods demonstrated a unique biphasic uptake pattern therefore a high and low elimination rate constant was derived exclusively for that exposure.

	Low Concentration Uptake Model [a]R^2= 0.84		High Concentration Uptake Model [a]R^2= 0.94		Elimination Model [a]R^2 = 0.70	
Parameter	**Full**	**Reduced[c]**	**Full**	**Reduced[c]**	**Full**	**Reduced[c]**
intercept	0.9922	0.9723	0.9961	0.9647	<0.0001	<0.0001
conc/time[b]	0.1721	<0.0001	0.4955	<0.0001	<0.0001	<0.0001
small	0.0032	0.0014	0.1379	0.1164	0.1718	0.0401
large	0.3211	-	0.6208	-	0.5713	0.8809
shape	0.9745	-	0.9873	-	0.3844	-
sc	0.9187	-	<0.0001	<0.0001	0.2083	0.3455
small*conc/time	<0.0001	<0.0001	0.0004	<0.0001	0.0009	0.0006
large*conc/time	0.7769	-	0.8878	-	0.0128	0.0016
shape*conc/time	0.2875	-	0.5958	-	0.5538	-
sc*conc/time	0.6169	-	<0.0001	<0.0001	0.0036	0.0003

Table 2.2: P values for the low and high concentration uptake models and the elimination model

P values for each parameter of multiple linear regression models of the low concentration uptake data set, high concentration uptake data set and the elimination data set. The low concentration model was developed using the PAAH data for exposures $\leq$ 148 nM and the entire data set for the other four particles while the high concentration model was developed using the PAAH data for exposures $\geq$ 148 nM and the entire data set for the other four particles. The elimination model used the complete data set for each particle.

[a]R^2 values were calculated from the reduced model.

[b]concentration is the quantitative parameter for the uptake model, time is the quantitative parameter for the elimination model.

[c]parameters that had a p value >0.05 in the full model were removed to optimize the reduced model. If the interactive parameter was significant the individual qualitative parameter was kept in the model even if it wasn't significant. The reduced version of each model was used to predict uptake and elimination rate constants.

Diameter (nm)	Surface Charge	k_{uw} (L g_{org}^{-1} d^{-1})	k_e (d^{-1})	BCF
6	Anionic	5.14	2.93	1750[a]
20	Anionic	2.81	1.93	1460[a]
30	Anionic	2.81	1.12	2510[a]
6	Cationic	L: 5.14 H: 94.83	3.74	L: 1370 H: 25400
20	Cationic	L: 2.80 H: 92.02	2.75	L: 1020 H: 33500
30	Cationic	L: 2.80 H: 92.02	1.93	L: 1450 H: 47700

Table 2.3: Predicted rate constants and bioconcentration factors for different nanoparticle configurations
Rate constants were predicted using the reduced multiple linear regression models for uptake at low ($\leq$ 148 nM) and high ($\geq$ 148 nM) concentrations and elimination. Bioconcentration factors were calculated using these predicted rate constants.
[a]Based on our models the high and low concentration exposures produce near identical rate constants for NPs with a anionic surface charge therefore it was unnecessary to calculated separate BCFs.

References

1. Gottschalk F, Nowack B. 2011. The release of engineered nanomaterials to the environment. *J Environ Monit* 13:1145-1155.

2. Burns JM, Pennignton PL, Sisco PN, Frey R, Kashiwada S, Fulton MH, Scott GI, Decho AW, Murphy CJ, Shaw TJ, Ferry JL. 2013. Surface charge controls the fate of Au nanorods in saline estuaries. *Environ Sci Technol* 47:12844-12851.

3. Li T, Albee B, Alemayehu M, Diaz R, Ingahm L, Kamal S, Rodriguez M, Bishnoi, SW. 2010. Comparative toxicity study of Ag, Au, and Ag-Au bimetallic nanoparticles on *Daphnia magna*. *Anal Bioanal Chem* 398:689-700.

4. Zhao C, Wang W. 2010. Biokinetic uptake and efflux of silver nanoparticles in *Daphnia magna*. *Environ Sci Technol* 44:7699-7704.

5. Zhu X, Chang Y, Chen Y. 2010. Toxicity and bioaccumulation of TiO_2 nanoparticle aggregates in *Daphnia magna. Chemosphere* 78:209-215.

6. Zhu Z, Carboni R, Quercio Jr. MJ, Yan B, Miranda OR, Anderton DL, Arcaro KF, Rotello VM, Vachet RW. 2010. Surface properties dictate uptake, distribution, excretion, and toxicity of NPs in fish. *Small* 6:2261-2265.

7. Bouldin JL, Ingle TM, Sengupta A, Alexander R, Hannigan RE, Buchanan RA. 2008. Aqueous toxicity and food chain transfer of quantum dots in freshwater algae and *Ceriodaphnia dubia*. *Environ Toxicol Chem* 27:1958-1963.

8. Werlin R, Priester JH, Mielke RE, Kramer S, Jackso S, Stoimenov PK, Stucky GD, Cherr GN, Orias E, Holden PA. 2010. Biomagnification of cadmium selenide quantum dots in a simple experimental microbial food chain. *Nat Nanotechnol* 6:65-71.

9. Holbrook RD, Murphy KE, Morrow JB, Cole KD. 2008. Trophic transfer of nanoparticles in a simplified invertebrate food web. *Nat Nanotechnol* 3:352-355.

10. Judy JD, Unrine JM, Bertsch PM. 2011. Evidence for biomagnification of gold NPs within a terrestrial food chain. *Environ Sci Technol* 45:776-781.

11. Edgington AJ, Roberts AP, Taylor LM, Alloy MM, Reppert J, Rao AM, Mao J, Klaine SJ. 2010. The influence of natural organic matter on the toxicity of multiwalled carbon nanotubes. *Environ Toxicol Chem* 29:2511-2518.

12. Hotze EM, Phenrat T, Lowry GV. 2010. Nanoparticle aggregation: Challenges to understanding transport and reactivity in the environment. *J Environ Qual* 39:1909-1924.

13. Chithrani BD, Ghazani AA, Chan WCW. 2006. Determining the size and shape dependence of gold nanoparticle uptake into mammalian cells. *Nano Lett* 6:662-668.

14. Hauck TS, Ghazani AA, Chan WCW. 2007. Assessing the effect of surface chemistry on gold nanorod uptake, toxicity and gene expression in mammalian cells. *Small* 4:153-159.

15. Alkilany AM, Nagaria PK, Hexel CR, Shaw TJ, Murphy CJ, Wyatt, MD. 2009. Cellular uptake and cytotoxicity of gold nanorods: Molecular origin of cytotoxicity and surface effects. *Small* 6:701-708.

16. Schleh C, Semmler-Behnke M, Lipka J, Wenk A, Hirn S, Schaffler M, Schmid G, Simon U, Kreyling WG. 2012. Size and surface charge of gold NPs determine absorption across intestinal barriers and accumulation in secondary target organs after oral administration. *Nanotoxicology* 6:36-46.

17. Hull M, Chaurand P, Rose J, Auffan M, Bottero J, Jones JC, Schultz IR, Vikesland PJ. 2011. Filter-feeding bivalves store and biodeposit colloidally stable gold NPs. *Environ Toxicol Chem* 45:6592-6599.

18. Rosenkranz P, Chaudhry Q, Stone V, Fernandes TF. 2009. A comparison of nanoparticle and fine particle uptake by *Daphnia magna*. *Environ Toxicol Chem* 28:2142-2149.

19. Feswick A, Griffitt RJ, Siebein K, Barber DS. 2013. Uptake, retention and internalization of quantum dots in *Daphnia* is influenced by particle surface functionalization. *Aquat Toxicol* 130-131:210-218.

20. Zhu Z, Wang H, Yan B, Zheng H, Jiang Y, Miranda OR, Rotello VM, Xing B, Vachet RW. 2012. Effect of surface charge on the uptake and distribution of gold NPs in four plant species. *Environ Sci Technol* 46:12391-12398.

21. Lewinski NA, Zhu H, Jo H, Pham D, Kamath RR, Ouyang CR, Vulpe CD. Colvin VL, Drezek RA. 2010. Quantification of water solubilized CdSe/ZnS quantum dots in *Daphnia magna*. *Environ Sci Technol* 44:1841-1846.

22. Khan FR, Misra SK, Garcia-Alonso J, Smith BD, Stekopytov S, Rainbow PS, Luoma SN, Valsami-Jones E. 2012. Bioaccumulation dynamics and modeling in an estuarine invertebrate following aqueous exposure to nanosized and dissolved silver. *Environ Sci Technol* 46:7621-7628.

23. Croteau M, Misra SK, Luoma SN, Valsami-Jones E. 2011. Silver bioaccumulation dynamics in a freshwater invertebrate after aqueous and dietary exposures to nanosized and ionic Ag. *Environ Sci Technol* 45:6600-6607.

24. Kimling J, Maier M, Okenve B, Kotaidis V, Ballot H, Plech A. 2006. Turkevich method for gold nanoparticle synthesis revisited. *J Phys Chem B* 110:15700-15707.

25. Burst M, Walker M, Bethell D, Schiffrin DJ, Whyman R. 1994. Synthesis of thiol-derivatised gold nanoparticles in a two-phase liquid-liquid system. *J Chem Soc, Chem Commun* 7:801-802.

26. Luoma SN, Rainbow PS. 2005. Why is metal bioaccumulation so variable? Biodynamics as a unifying concept. *Environ. Sci. Technol.* 39:1921-1931.

27. Lee B, Ranville JF. 2012. The effect of hardness on the stability of citrate-stabilized gold nanoparticles and their uptake by *Daphnia magna*. *J Hazard Mater* 214:434-439.

28. Lovern SB, Owen HA, Klaper R. 2008. Electron microscopy of gold nanoparticle intake in the gut of *Daphnia magna*. *Nanotoxicology* 2:43-48.

29. Gophen M, Geller W. 1984. Filter mesh size and food particle uptake by *Daphnia*. *Oecologia* 64:408-412.

30. Gillis PL, Chow-Fraser P, Ranville JF, Ross PE, Wood CM. 2005. *Daphnia* need to be gut-cleared, too: The effect of exposure to and ingestion of metal –contaminated sediment on the gut-clearance patterns of *D. magna*. *Aquat Toxicol* 71:143-154.

31. Gerritsen J, Porter KG. 1982. The role of surface chemistry in filter feeding by zooplankton. *Science* 216:1225-1227.

32. Rubenstein DI, Koehl MAR. 1977. The mechanisms of filter feeding: Some theoretical considerations. *Am Nat* 111:981-994.

33. Hammer A, Gruttner C, Schumann R. 1999. The effect of electrostatic charge of food particles on capture efficiency by *Oxyrrhis marina Dujardin* (Dinoflagellate). *Protist* 150:375-382.

34. Gerritsen J, Bradley SW. 1987. Electrophoretic mobility of natural particles and cultured organisms in freshwaters. *Limnol Oceanogr* 32:1049-1058.

35. Hegedus D, Erlandson M, Gillott C, Toprak U. 2009. New insights into peritrophic matrix synthesis, architecture, and function. *Annu Rev Entomol* 54:285-302.

36. Bowen WR, Filippov AN, Sharif AO, Starove VM. 1999. A model of interaction between a charged particle and a pore in a charged membrane. *Adv Colloid Interfac* 81:35-72.

37. Barbehenn RV, Martin MM. 1994. Tannin sensitivity in larvae of *Malacosoma disstria* (Lepidoptera): Roles of the peritrophic envelope and midgut oxidation. *J Chem Ecol* 20:1985-2001.

38. Zhou D, Keller AA. 2010. Role of morphology in the aggregation kinetics of ZnO nanoparticles. *Water Res.* 44:2948-2956.

39. Khan FR, Kennaway GM, Croteau M, Dybowska A, Smith BD, Nogueira AJA, Rainbow PS, Luoma SN, Valsami-Jones E. 2014. *In vivo* retention of ingested Au NPs by *Daphnia magna*: No evidence for trans-epithelial alimentary uptake. *Chemosphere* 100:97-104.

40. Pan J, Buffet P, Poirier L, Amiard-Triquet C, Gilliland D, Joubert Y, Pilet P, Guibbolini, M, Risso de Faverney C, Roméo M, Valsami-Jones E, Mouneyrac C. 2012. Size dependent bioaccumulation and ecotoxicity of gold NPs in an endobenthic invertebrate: The Tellinid clam *Scrobicularia plana*. *Environ Pollut* 168:37-43.

41. Auffan M, Rose J, Bottero JY, Lowry GV, Jolivet JP, Wiesner MR. 2009. Towards a definition of inorganic nanoparticles from an environmental, health and safety perspective. *Nat Nanotechnol* 4: 634-641.

CHAPTER THREE

TRANSFORMATION OF NANOPARTICLES IN THE PRESENCE OF WASTEWATER AND ITS IMPACT ON ACCUMULATION IN *DAPHNIA MAGNA* AND *PIMEPHALES PROMELAS*

Introduction

For millions of years an untapped technology has existed beyond the boundaries of human perception. Physical and chemical processes originating from natural mechanisms and, more recently, anthropogenic intervention gave rise to nano-sized colloids equipped with unique properties that distinguished them from their macro-sized counterparts. Within the last century the perceived benefits of operating at smaller scales spurred development of methods for engineering nanomaterials. This new technology brought forth a surge of innovation and invention from private corporations, academic institutions, and government organizations. These innovations have led to cosmetic and structural changes in everyday consumer products as well as technological leaps in imaging and drug delivery fidelity. Minute changes in synthesis procedure can produce distinct differences in the resulting properties, which in turn could change the behavior of the particle and its implementation into a product. The sheer number of possibilities for implementation seems limitless given the aforementioned malleability of the nanomaterial construction. However, engineered nanomaterials only vaguely resemble their natural counterparts and in many cases lack a naturally produced analogue. Wildlife that is unfortunate enough to be on the receiving end of nanomaterial release may, therefore, lack the defensive mechanisms to withstand the toxic insult. From an environmental and human health standpoint the evolution of nanomaterial construction may be as much a burden as a boon.

The ubiquitous presence of nanotechnology in the toolset of industrial innovators will lead to inevitable environmental release. The release of nanomaterials from consumer-based products in environmentally relevant conditions is already well documented [1-5]. Moreover, life cycle analysis of several popular nanomaterials predicted concentrations of nanomaterials in surface waters and sewage

treated effluent that approached or exceeded a previously defined toxic threshold [6]. The threat of nanomaterial release to aquatic organisms is covered in detail in the literature [7-12]. These studies examined the impact of pristine nanomaterials whose fate and behavior is solely dependent on the abiotic conditions of the exposure media and interactions with biota in the system of interest. Utilizing pristine nanomaterials as a model is useful in establishing a foundation for nanomaterial regulation; however, these exposure scenarios neglect possible transformation steps in route to environmental release. Nanomaterials are clearly susceptible to their surroundings [13-20] and pre-release processes may introduce the nanomaterial to conditions that are not typical in an aqueous environment. The nanomaterial that enters the environment via an indirect pathway is, therefore, likely to have an appearance and behavior that are distinct from the original pristine nanomaterial.

Most commercially available nanomaterials will take an indirect pathway to the environment that is tied to waste disposal and treatment processes [6,21]. Nanomaterials that are collected by wastewater are thrust into an environment with substantial ionic strength, inorganic substituents and high concentrations of dissolved organic carbon [22]. These initial conditions are likely to alter the appearance of the nanomaterial either inducing aggregation and sedimentation or enhancing water column stability [23]. Though not designed specifically for nanomaterial purification, modern WWTPs are capable of removing > 90% of nanomaterials from the influent [24]. The removal efficiency can vary based on the design of the plant [25-27] and the type of nanomaterial [28-29]. Generally the removal of nanomaterials is carried out through particle aggregation, adsorption to biomass that settles into the sludge, and complexation with inorganic molecules in the sludge [23,25,26,29]. Though no longer a threat for release in the effluent, the conversion of the sludge to bio solids and subsequent application to agricultural land presents a viable route for nanomaterial transfer into the terrestrial environment and possible conduit for exposure to nearby aqueous environments.

Not all nanomaterials are relegated to the sludge giving them a chance to escape in the effluent [20,27]. The ability of nanomaterials to avoid falling out of the water column is related to the intrinsic nanomaterial properties [28-30] and the presence of organic macromolecules in the system [20,23]. Nanomaterials that make their way into the effluent are able to do so because they are intrinsically stable,

are receptive to organic matter coating limiting aggregation or pass through sorbed to suspended solids [20,22,31]. Transformation of these nanomaterials will become even more important to monitor upon release into the receiving stream because nanomaterial characteristics are a key component in how the material behaves and its interactions with aquatic organisms. For example accumulation and toxicity of nanomaterials is dependent on size [10, 32-38], shape [39-40], surface charge [11, 41-42], and surface chemistry [8,11,41,43-44].

A survey of WWTPs in the United States revealed nano titanium and silica in wastewater effluent demonstrating that this is a viable route for nanomaterials to enter the environment [27]. Despite evidence demonstrating environmental release, there is a paucity of information on how wastewater transforms the particle and the subsequent effects on biota in the receiving streams. The following study investigated how incubation in wastewater affects the characteristics of spherical gold nanoparticles with different surface charges and how these transformations change accumulation patterns in a simple aquatic food chain consisting of a pelagic filter feeder, *Daphnia magna*, and pelagic secondary consumer, *Pimephales promelas*. Gold nanoparticles (NPs) were chosen based on their low toxicity, low dissolution rate in typical freshwater systems and optical properties, which make them ideal for modeling accumulation in the test organisms.

Materials and Methods

Synthetic Wastewater

Synthetic wastewater (WW) was formulated following a recipe outlined in the EPA guidelines for simulating aerobic treatment in wastewater treatment studies [45]. The contents were as follows: peptone casein pancreatic digest (Sigma), 144 mg; meat extract (Sigma), 99 mg; urea (Sigma), 27 mg; dipotassium hydrogen phosphate (Fisher), 25 mg; sodium chloride (Fisher), 7 mg; calcium chloride (Fisher), 4 mg; magnesium sulfate (Sigma), 2 mg; brought to a final volume of 900 mL with Milli-Q water. The stock WW (~100 mg/L DOC) was then diluted to ~6.5 mg DOC/L with moderately hard water (MHW) and filter sterilized through a 0.22 um Supra® membrane before introducing NPs.

Cultured Organisms

Daphnia magna were cultured at Clemson University ENTOX facility following standard protocols [46]. *D. magna* was cultured in synthetic moderately hard water (MHW, Hardness ~108 mg CaCO3/L, Alkalinity ~ 60 mg CaCO3/L, pH 7.5 – 8.5). Cultures were kept in incubator with temperature of 25 $\pm$ 1 °C and under a 16:8 light/dark cycle. *Pseudokirchneriella subcapitata* cells were grown in a nutrient solution for one week under constant agitation, aeration and light to an approximate concentration of 5 $x10^5$ cells/mL. Organisms were fed *P. subcapitata* and YCT daily and renewed on alternating days. All *D. magna* organisms used in uptake and elimination studies were 6 – 7 days old.

Pimephales promelas were cultured in accordance with an animal use protocol approved by the Clemson University Animal Use Committee that followed established protocols [46]. *P. promelas* were grown and bred in a spacious flow through system that maintained temperature at 25 $\pm$ 2 °C, pH between 7.5 – 8, and minimized nitrate and ammonia levels. Organisms were fed daily and kept under a 16:8 light/dark cycle. All fish were allowed to acclimate to the exposure containers and moderately hard water for 24 - 48 hours prior to exposure in order to alleviate any stress induced by the change in water hardness and alkalinity, and the additional stress caused by the transfer process. All adult fish used in uptake, elimination and organ accumulation experiments were 8 – 10 months old.

Gold Nanoparticle Synthesis and Characterization

The Rotello lab at the University of Massachusetts-Amherst prepared all nanomaterials used in this study. Particle synthesis followed methods outlined in published literature [11]. The particles were coated with either a cationic or zwitterionic ligand and were spherical with a 2 nm core diameter. The ligand was composed of three regions: an alkyl chain for stability, a polyethylene glycol molecule for biocompatibility, and an interchangeable molecule on the surface that conferred charge to the particle. The cationic charge was produced by a quaternary amine molecule and the zwitterionic charge was produced by the combination of sulfite and quaternary amine molecules. Size and surface charge of stock NPs, NPs diluted in MHW and NPs diluted in WW were characterized prior to exposure. Hydrodynamic diameter and zeta potential were calculated with a Malvern Zetasizer in triplicate. Core diameter was confirmed with

transmission electron microscopy (Hitachi 7600 TEM). Hydrodynamic diameter and zeta potential was measured at time zero and after the first hour to monitor the nanomaterial-wastewater equilibrium. Zeta potential was also measured for cationic particles after 24 hours and five days to assess temporal trends in WW transformation. Sedimentation was measured by determining the percentage of the initial nanomaterial concentration that was no longer suspended at the end of the exposure. Exposure media was placed into separate exposure containers without organisms to quantify the loss of nanomaterials from the water column that was associated with sedimentation and binding to the exposure container. These data were plotted as a function of exposure concentration and fit to the Michaelis-Menten model. The model calculated the maximum percent of particles lost from solution, which was used to assess the relative stability of the different treatments.

Daphnia magna Uptake

Daphnids collected for experimentation from the culture were allowed to depurate in clean MHW for two hours prior to exposure. Daphnids were then divided into replicates of 10-20 individuals and placed into either polypropylene or glass acid washed exposure containers containing 100 mL of gold NPs in MHW or WW, respectively. Nanoparticle concentrations covered several orders of magnitude, from 9.72–4369 nmoles Au/L. Exposures were conducted for 13-14 hours to minimize particle elimination and ensure sufficient accumulation for instrument detection at the lower concentration exposures. At the end of the exposure period organisms were removed, washed twice in MHW for 30 seconds and collected on mesh filters. Each concentration contained three replicates from which I derived uptake rate constant(s). A second set of experiments increased the exposure time to 24 hours and was processed in the same manner.

Daphnia magna Elimination

Daphnids were selected from the mass culture and separated into the appropriate acid washed container for the initial 14-hour uptake period. All containers within an experiment received the same nominal NP concentration (634 nmoles Au/L). The measured concentration across all exposures was 550 $\pm$ 143 nmoles Au/L. After 14 hours of exposure, organisms were removed, washed twice in MHW for 1 minute, transferred to clean MHW and fed uncontaminated algae at a concentration of 1.5×10^5 cells/mL.

Three replicates consisting of twenty organisms were removed at 0, 1, 3, 6, 12, 24, 36 and 48 hours post exposure, washed and collected as previously stated. At each time point the remaining organisms were transferred to fresh MHW inoculated with 1.5 x 10^5 cells/mL of fresh algae. Depuration experiments were run in duplicate and data were averaged to determine a single elimination rate constant for each treatment. A second set of experiments increased the initial exposure time to 24 hours followed by a 48 hour depuration period and were processed in the same manner.

Daphnia magna Distribution

Individual daphnids were removed from the highest concentration exposure and fixed in 2% gluteraldehyde. Samples were then dehydrated with alcohol, incubated for 40 minutes in a 50/50 mixture of propylene oxide:LR White for greater infiltration, and embedded in 100% LR White. Samples were cut into ultra-thin (90~110 nm) sections using an ultra-microtome and imaged on the Hitachi 7600 Transmission Electron or in the TEM setting on the Hitachi S4800 microscope. All identified nanostructures were separately confirmed to have gold signatures using energy dispersive X-ray analysis. The scope of the *D. magna* distribution experiment focused exclusively on the gut tract and epithelial membrane interface to determine if gold nanomaterials could cross from the gut tract into epithelial cells. Each treatment was identified as either providing evidence that the NPs crossed the gut tract or not providing any visible indication that particle translocation had taken place. I did not track post uptake localization to determine the terminal distribution of the nanomaterial after traversing epithelial membranes.

Pimephales promelas Uptake

Individual *P. promelas* were transferred into either polypropylene (MHW exposure) or glass (WW exposure) acid washed exposure containers after the initial acclimation period. Each container held 350 mL of gold NPs in MHW or WW with concentrations ranging from 98 - 2580 nmoles Au/L. Exposure water was aerated for the duration of the exposure to ensure dissolved oxygen did not drop below acceptable levels. After 14 hours, fish were removed, euthanized with 4 % Tricane MS-222. Each concentration was run in triplicate with one fish per replicate. Exposures were run twice and the data were combined.

Pimephales promelas Elimination

Individual *P. promelas* were acclimated to exposure jars using the aforementioned method. Fish were exposed in triplicate to gold nanomaterials in 1.2 L of exposure solution at nominal concentration of 634 nmols Au/L with measured concentrations of 638 $\pm$ 81 nmoles Au/L for 24 hours. Organisms were then transferred to individual glass jars containing 500 mL of clean MHW and fed flake food at 0, 12, 24 and 36 hours after the transfer. At 0, 1, 3, 12, 24, and 48 hours after transfer three fish were removed and euthanized with buffered 4 % Tricane MS-222. Water changes were conducted at hours 3, 12, and 24 to minimize the amount of gold re-ingested after excretion. Water samples and feces were collected at the time of exposure and at each time point during the depuration period.

Pimephales promelas Tissue Distribution

Six fish were exposed to each gold NP treatment at a nominal concentration of 1269 nmoles Au/L (measured concentration: 986 $\pm$ 141 nmoles Au/L) along with six control fish for 48 hours. After exposure fish were euthanized with buffered 4 % Tricane MS-222 and dissected to remove the brain, heart, gills, liver/gallbladder and intestines. Brain, heart and liver/gall bladder were pooled in sets of two to maximize possibility of obtaining a signal on the ICP-MS. Intestine and gills were analyzed separately. The wet weight of each organ was recorded and then the organs were digested for gold analysis.

All fish uptake, elimination and distribution experiments were performed with constant aeration to prevent maintain high dissolved oxygen concentrations during the exposure. Clemson Animal Use Committee (IACUC) approved the experimental design and euthanasia procedure used in all vertebrate testing for this study.

Digestion and Gold Analysis

Whole organisms were dried to constant weight for >24 hours at 60 °C, weighed and then prepped for gold analysis. *D. magna* samples were transferred to 15 mL centrifuge tubes and combined with 100% Aqua Regia (3 HCl: 1 HNO_3, 46 % acid). Samples were digested for 30 minutes at 100 °C and then adjusted to 5% acid with Milli-Q water for analysis. Complete digestion of whole *P. promelas* samples required a more complicated method. Several methods were used to digest fish tissues each with apparent

returns of 70-90% from percent recovery experiments (Table A.1). Fish from pristine MHW uptake exposures were homogenized and placed in 50 mL digestion chambers with 6 mL of 35% Aqua Regia and 1 mL hydrogen peroxide (TraceGrade 30% v/v). Samples were microwave digested at 170 °C for 25 minutes then diluted to 30 mL with Milli Q. Initial percent recovery experiments returned 89.44 $\pm$ 36.17% for this digestion method. All MHW waterborne uptake experiments were digested in this manner. However, despite high recovery it was obvious that this method did not completely digest the tissues, which is most likely, the cause of the high variability. The inability of this method to completely digest the tissues was not ideal as it could potentially miss nanomaterials associated with lipids in the uptake, elimination and distribution experiments.

A second digestion method was employed for fish from wastewater uptake exposures and all elimination exposures to ensure complete digestion of the fish tissue. Fish from these experiments were dry ashed in the muffle furnace at 450 °C for 26 hours. Ash of the fish was dissolved into 5 mL concentrated nitric acid (TraceGrade 70% v/v) then diluted with Milli-Q water to 35% acid. Digestions were then performed with the aid of a microwave digester using the following procedure: 30 minute ramp to 175 °C at 300 W, then hold at 175 °C and 300 W for 20 minutes. Digested samples were transferred to PFA digestion chambers. Five mL of 100% Aqua Regia was added to each digestion chamber and allowed to evaporate to near dryness. Residue was then taken up into 0.710 or 1.1 mL of 100% Aqua Regia and then diluted with Milli-Q water to 6 or 10 mL, respectively. Fish tissue injected with known concentration of gold NPs was included in each digestion to ensure digestion method was reproducible. Method two provided a 73.03 $\pm$ 3.58% recovery of gold from sample fish injected with 65 ppm gold NPs. Pristine uptake experiments were performed again with fewer replicates and digested using the second method to validate the efficacy of the first digestion method.

Organs dissected from *P. promelas* were digested using two methods based on the size of the organ. Intestines and gills were immersed in 5 mL concentrated nitric acid and allowed to sit overnight (TraceGrade 70% v/v). Two (2) mL hydrogen peroxide and 3 mL Milli-Q water were added the next day to achieve a final acid concentration of 35%. These organs were digested in a microwave digester using the previously described procedure. Digested samples were then transferred to 30 mL PFA digestion chambers,

combined with 5 mL of 100% Aqua Regia and evaporated to near dryness (<1 mL). Intestine and gill residue was dissolved in 0.710 mL or 1.1 mL of 100% Aqua Regia and diluted with Milli-Q water to 6 mL and 10 mL, respectively. Brain, heart and liver/gallbladder tissues were pooled in sets of two and transferred to sealed 7 mL acid washed PFA digestion containers with 2 mL nitric acid and allowed to sit overnight. The following day 1 mL of hydrogen peroxide was added and organs were further digested at 100 °C for 30 minutes on a hot plate. Samples were then evaporated to less than 1 mL. Residue was dissolved in 0.710 mL of 100% Aqua Regia then diluted to 6 mL with Milli-Q water.

Water samples of all exposure solutions were collected in 15 mL centrifuge tubes prior to and after each experiment. Water samples were acidified with 100% Aqua Regia for a final acid concentration of 5%, mixed well, and then analyzed. Gold analysis of all samples was performed on a Thermo Scientific XSeries2 Inductively Coupled Plasma Mass Spectrometer.

Model Selection

The biodynamic model and its parameters were described in detail in the previous chapter. Uptake and elimination rate constants were derived using the same methods as in that chapter and are described briefly in the data analysis section below. Unlike the previous chapter, most of our uptake plots achieved saturation in the concentration window, thus I was able to calculate equilibrium binding constants using non-linear regression analysis. I selected either the Michaelis-Menten model (Equation 1) or sigmoidal model (Equation 2) for each uptake plot based on the model fit that produced the lowest RSME.

$$\text{Influx} = (B_{max} \times [C_w])/(K_d + [C_w]) \quad \textbf{(1)}$$

$$\text{Influx} = (B_{max} \times [C_w]^h)/(K_d^{\,h} + [C_w]^h) \quad \textbf{(2)}$$

Both models use binding site capacity (B_{max}), binding affinity (K_d), and the waterborne NP concentration (C_w) to predict the influx rate. The sigmoidal model incorporates a fourth variable, hill slope (h) that accounts for the change in slope between low and high concentration exposures.

Data Analysis

All data were fit to linear and the most appropriate non-linear regression model when appropriate. All rate constants (k_{uw}, k_e) with standard error were derived from the linear portion of each data set in native or transformed plots using JMP 10.0. Analytical replicates that returned values below the detection limit of the ICP-MS (0.250 ug Au/L) were replaced with imputed values estimated from a linear regression analysis of the data after removing the data points that were below the detection limit. The imputed data points thus represent the theoretical values if they were consistent with the other data points. I selected this type of imputation because replacing the values with zero was not an option for the log transformed elimination plots and the use of singular values such as half the detection limit would greatly skew the data toward that value, depreciating the rest of the data set. The two fish zwitterionic elimination data sets were exceptions that encountered considerable bias when utilizing the imputation method above due to a higher number of non-detects. Instead the values below the detection limit were replaced with one-half the detection limit (0.125 ug/L). Binding site capacity (B_{max}), and binding affinity (K_d) with standard error was derived for each treatment when appropriate using nonlinear regression analysis in JMP 10.0. Slope comparison to identify statistical differences in rate constants between treatments was performed with JMP 10.0. Organ data below the detection limit were used without imputation correction or data replacement. Unequal variance test was performed on the organ data prior to mean comparisons to choose the best statistical method. If variances were equal a one-way ANOVA test was conducted on the data followed by a Tukey HSD post-hoc test if necessary. If the variances were unequal Welch's test was performed followed by the Dunnetts method post-hoc test if necessary. All mean comparisons were performed in JMP 10.0. For all data analysis, a p value ≤ 0.05 was considered statistically significant.

Results

Particle Characterization in the Exposure Media

Both nanomaterials of interest in this study were spherical with a reported core diameter of 2 nm (Figure 3.1a - d) in the stock solution. The hydrodynamic radius and zeta potential data for each particle configurations in both treatment scenarios along with the intrinsic stock values are visualized in Figure 3.2.

The cationic nanomaterials had an intrinsic hydrodynamic diameter of 18.3 ± 4.09 nm and maintained a zeta potential of +40.3 ± 23 mV. The zwitterionic nanomaterials had an intrinsic hydrodynamic diameter of 5.48 ± 0.844 nm and a surface zeta potential of -4.38 ± 7.07 mV. Incubation of these nanomaterials in the two exposure medias (MHW and WW) had a significant impact on the characteristics of the cationic particles but did not drastically affect the zwitterionic NPs. The size of the cationic NPs increased slightly to 23.66 ± 7.3 nm in MHW and significantly to 75.82 ± 16.23 nm when incubated with wastewater. On the other hand, the zwitterionic NPs diameter remained constant across treatments. Zeta potential was not altered enough to indicate statistically significant changes across the two exposure medias yet both NPs trended toward more negative zeta potential in the WW exposure media compared to the MHW treatment and the stock solution. Zeta potential for the cationic NPs was +14.3 ± 7.78 mV and +8.84 ± 2.68 mV for MHW and WW treatments, respectively. Zeta potential for the zwitterionic NPs was -6.35 ± 6.61 mV and -12.9 ± 7.14 mV for MHW and WW treatments, respectively.

Electron microscopy images of the particles in MHW (Figure 3.1b and e) and WW (Figure 3.1c and f) corroborate my DLS and zeta potential data. Core diameter was unaffected in the MHW treatment for both particle types and in the WW treatment for the zwitterionic NPs. The micrographs of the cationic NPs in WW demonstrate both an increase in core diameter and a strong association between the NPs and organic matter present in the WW media. Both of these transformations are likely the cause of the observed size increase in the DLS data. Stability, as measured by the amount of gold remaining in the water column in the absence of organisms, was similarly influenced by the presence WW (Figure 3.3). Aqueous stability of cationic NPs increased significantly in the presence of WW, most notably at higher concentrations. Sedimentation, quantified as the percent of particles no longer in suspension, reached a plateau at 69.9 ± 15.7% in MHW exposures compared to 13.4 + 1.1% in the WW exposure. Zwitterionic NPs experienced a minor yet statistically significant decrease in stability in the presence of WW. Sedimentation in the MHW and WW exposures reached a plateau at approximately 45.5 ± 4.4% and 60.9 ± 2.3% of the initial exposure concentration, respectively. Stability did seem to increase at higher concentrations in the zwitterionic MHW exposure; however, I cannot make any direct comparisons due to a lack of WW data above 1500 nM. Notable also is the difference between the MHW exposures of the cationic and zwitterionic

nanomaterials. At low concentrations (<500 nM) the cationic nanomaterials appear more stable. However, as concentration increased the percentage of cationic NP falling out of suspension was more similar to the zwitterionic treatments.

Daphnia magna Uptake

Uptake of gold NPs by *D. magna* was affected by both the charge of the ligand attached to the particle and the presence of wastewater in the exposure media. All uptake rate constants and equilibrium binding constants detailed below are presented in Table 2 with standard error.

Cationic gold NPs exhibited different patterns of influx based on the treatment (Figure 3.4a-b). The MHW exposure fit well to the Michaelis-Menten saturation model while the sigmoidal model was deemed more appropriate for data collected from the WW treatment. The MHW uptake rate constant was 218 $\pm$ 16 L g^{-1} d^{-1}. The uptake rate constant for the WW treatment, 110 $\pm$ 11 L g^{-1} d^{-1}, was significantly different from the MHW exposure suggesting a disruptive influence from the WW on uptake. Furthermore, daphnids exposed to the WW treatment demonstrated a biphasic influx pattern prior to saturation similar to the PAAH rods from the previous chapter. Therefore, a second uptake rate constant, 2.95 $\pm$ 0.26 L g^{-1} d^{-1}, was derived for low concentration exposures of cationic gold NPs in WW. The membrane binding characteristics for both treatments were derived using non-linear regression modeling. The binding site capacity (B_{max}) and binding affinity (K_d) were calculated for each treatment based on a sigmoidal model. Daphnids exposed in the WW treatment had a greater capacity for gold NPs with a B_{max} of 12200 $\pm$ 5450 nmol g^{-1} compared to 43400 $\pm$ 5400 nmol g^{-1}. However, cationic NPs incubated in WW had a larger K_d, 729 $\pm$ 46 nmol L^{-1}, compared to the NPs in the MHW exposure, 138 $\pm$ 70 nmol L^{-1}. A higher K_d translates to a weaker binding affinity; therefore, the cationic NPs in MHW had a greater affinity for binding sites on *D. magna*.

Similar to the cationic MHW exposure, the data fit well to the Michaelis-Menten saturation model (Figure 3.5a). Likewise rate constants for the zwitterionic particles were derived from the linear section of the saturation curve. Daphnids exposed to zwitterionic NPs in MHW exhibited an uptake rate constant of 1.32 $\pm$ 0.14 L g^{-1} d^{-1}. Binding site capacity, 1520 $\pm$ 287 nmol g^{-1}, was much lower compared to both cationic treatments. Likewise, binding affinity, 988 $\pm$ 407 nmol L^{-1}, was weaker for the zwitterionic MHW

exposures compared to the MHW cationic exposures though it was not significantly different from the cationic WW exposure. The presence of wastewater elevated the uptake rate constant to 2.63 $\pm$ 0.26 L g^{-1} d^{-1} (Figure 3.5b). However, this change was not statistically significant compared to the MHW exposure. Uptake of zwitterionic particles in the presence of wastewater did not reach saturation in the selected concentration range prohibiting calculation of binding site capacity and binding affinity constants. Nevertheless the patterns exhibited by the wastewater-exposed daphnids suggested a lower binding affinity and higher binding site capacity consistent with the cationic exposure.

Twenty-four hour exposures were also conducted for each treatment to investigate the temporal nature of the uptake and elimination rate constants and shed light on the role of bacteria growth in the WW treatments. The dichotomy between the uptake patterns for each treatment remained after the longer exposure period (Figure 3.4c and d). Uptake rate constants for MHW and WW cationic treatments decreased significantly from the 14-hour exposure to 111 $\pm$ 13 L g^{-1} d^{-1} and 26.5 $\pm$ 2.3 L g^{-1} d^{-1}, respectively. Furthermore, the WW uptake rate constant was significantly lower than the MHW treatment mirroring the trends observed in the 14-hour exposure. Both binding site capacity, 37700 $\pm$ 3710 nmol g^{-1}, and binding affinity, 241 $\pm$ 93 nmol L^{-1}, decreased for the MHW exposure though neither change was statistically significant. Saturation was not reached in the 24 hour WW treatment; therefore, equilibrium binding constants were not calculated.

In contrast to the cationic exposures, and quite unexpectedly, the uptake rate constants for the 24-hour zwitterionic exposure did not change significantly from the 14-hour exposure (Figure 3.5c and d). The uptake rate constant for zwitterionic MHW and WW exposures was 1.46 $\pm$ 0.24 L g^{-1} d^{-1} and 3.28 $\pm$ 0.12 L g^{-1} d^{-1}, respectively. Moreover the 24-hour MHW and WW rate constants were significantly different reversing the trend observed in the 14-hour exposure. Another difference present in the 24-hour exposure is a Michaelis-Menten saturation fit to both the zwitterionic WW and MHW whereas saturation kinetics was observed only in the MHW treatment from the 14-hour exposure. Compared to the 14-hour exposure binding site capacity in the MHW exposures increased to 4190 $\pm$ 717 nmol g^{-1} while binding affinity decreased to 3400 $\pm$ 1020 nmol L^{-1}. The binding characteristics of 24-hour zwitterioinc WW treatment lack an analogous measure in the 14-hour exposure rendering it impossible to determine if values increased or

decreased with an extended exposure period. Nevertheless the binding site capacity of the 24-hour zwitterionic WW exposure was 3240 $\pm$ 653 nmol g^{-1} and the binding affinity was 704 $\pm$ 426 nmol L^{-1}.

Daphnia magna Elimination

Unlike uptake, elimination of cationic (Figure 3.6a-d) and zwitterionic nanomaterials (Figure 3.7a-d) was unaffected by the presence of wastewater in both 14 and 24 hour exposures (Table 2). Elimination of cationic NPs followed a biphasic pattern dominated by the fast exchange compartment from hour 0 to hour 3 with control over efflux rate transitioning to the slow exchanging compartment from hour 3 onward. Elimination rate constants from the slow exchanging compartment were 2.64 $\pm$ 0.08 d^{-1} and 2.73 $\pm$ 0.14 d^{-1} for 14 hour MHW and WW treatments, respectively. These rate constants indicated that *D. magna* eliminated 50% of the cationic NP body burden every 6 - 6.5 hours. Slow exchange compartment elimination rate constants increased for the 24-hour exposure to 2.93 $\pm$ 0.13 d^{-1} and 2.90 $\pm$ 0.21 d^{-1} for MHW and WW treatments, respectively. These rate constants translate to a shorter half-life, ~5.7 hours, compared to the 14-hour exposure. Interestingly the MHW elimination rate constant changed significantly based on the initial exposure duration while the WW did not. At the start of depuration the daphnids exposed to MHW cationic NPs for 14 hours partitioned 54% of the NP body burden to the fast exchanging compartment and 45% to the slow exchanging compartment. After a 24-hour exposure the initial distribution of MHW cationic NPs shifted in favor of the slow exchange compartment (61%) decreasing the fast exchanging compartment to 39%. Daphnids exposed to WW cationic NPs exhibited the opposite trend. The accumulated fraction in the slow exchange compartment, 53%, was greater than the fast exchange compartment, 47%, after 14 hour. During the longer exposure the majority of the NPs resided in the fast exchange compartment, 75%, leaving only 25% of the NP body burden in the slow exchange compartment.

Elimination of zwitterionic NPs accumulated from MHW was significantly slower compared to the cationic particles and demonstrated a more pronounced biphasic elimination pattern with a similar delineation between the fast and slow compartment at hour 3 (Figure 3.7a and c). The rate constants for the 14 hour MHW exposure was 1.96 $\pm$ 0.07 d^{-1} which decreased significantly to 1.18 $\pm$ 0.10 d^{-1} following a 24-hour exposure. The distribution of the NP body burden remained consistent between the 14 and 24-hour MHW exposures with approximately 56% residing in the fast exchanging compartment and 44% in the

slow exchanging compartment. The WW elimination rate constant was nearly identical to the MHW exposure in the 14-hour and 24-hour exposure (Figure 3.7b and d) with reported values of 1.98 $\pm$ 0.09 d^{-1} and 1.08 $\pm$ 0.13 d^{-1}, respectively. Similar to the MHW exposures, the slow compartment elimination rate constant decreased significantly with increased exposure duration. Despite these similarities, however, the slow exchanging compartment clearly held a larger proportion of NPs at the onset of the depuration period. The slow exchanging compartment for the 14-hour exposure accounted for 68% of the total body burden, which increased, to 97% in the 24-hour exposure. The high percentage of NPs in the slow exchange compartment in the 24-hour exposure indicated that there might only be one compartment involved in the elimination. Based on these rate constants the half-life of zwitterionic NPs in *D. magna* was ~8.5 hours and ~15 hours for 14 and 24-hour exposures, respectively.

Steady-state bioconcentration factors were calculated for each exposure using the derived values for the uptake and elimination rate constants. For both the 14 and 24 hour exposure the order of BCFs was identical (Table 2). Cationic MHW exposures produced the highest BCF, followed by the cationic WW, zwitterionic WW and finally the zwitterionic MHW. Despite maintaining the same order, the temporal BCF trends were diametrically opposed between the two particle configurations. Cationic BCF values decreased substantially with longer exposure time while the zwitterionic BCFs increased. Elimination rate constants, fast and slow compartment partitioning percentages, and BCFs for *D. magna* are presented in Table 2.

Distribution in Daphnia magna

Microscopic analysis of gut sections from exposed *D. magna* demonstrated a clear translocation of gold nanomaterials from the lumen into epithelial cells for both cationic treatments (Figure 3.8a-d). The size of the identified gold NPs both in the gut tract and in epithelial cells was perceptibly larger (~20 nm) than the average core diameter in the stock solutions. It is worth noting that the larger particles would be easier to identify and it is possible that I overlooked smaller particles that crossed as well. The relative concentration of internalized nanomaterials was difficult to assess with this technique but the type of pre-treatment and the ligand chemistry did not appear to discourage or prevent translocation. Regrettably I was unable to find gold nanomaterials in the sections of *D. magna* exposed to zwitterionic nanomaterials. The lack of discernable NPs may have been due to the lower accumulation of particles in the gut tract compared

to the cationic exposures or that most of the particles retained their small size and could not be detected in the biological matrix (Figure 3.9). Elemental analysis of several spherical objects in the micrographs of *D. magna* exposed to cationic NPs confirmed that the particles contained gold (Figure 3.10 and 3.11).

Pimephales promelas Uptake

The waterborne uptake rate constants for *Pimephales promelas* were several orders of magnitude smaller than the rate constants derived for *D. magna*. Uptake rate constants presented below are compiled in Table 3 with standard error. The cationic uptake rate constants were 0.215 ± 0.025 L g^{-1} d^{-1} and 0.228 ± 0.059 L g^{-1} d^{-1} for MHW and WW treatments, respectively (Figure 3.12a and b). The zwitterionic uptake rate constants were 0.0037 ± 0.001 L g^{-1} d^{-1} and 0.0023 ± 0.0006 L g^{-1} d^{-1} for MHW and WW treatments, respectively (Figure 3.12c and d). The influence of WW on particle uptake was not a universal trend as noted there were no statistically differences between treatments for either particle configuration. One common theme between *D. magna* and *P. promelas* was the stark difference in uptake between the two particle configurations. In both treatments, the cationic uptake rate constant was significantly larger than that for the zwitterionic. Additionally, the biphasic uptake model observed for the cationic WW *D. magna* exposure persisted in the *P. promelas* cationic WW exposure. The second uptake rate constant, 0.017 + 0.004 L g^{-1} d^{-1}, was also significantly smaller than the *D. magna* constant. None of our treatments reached influx saturation in the chosen concentration range precluding estimation of membrane binding constants. High variability, especially in the zwitterionic exposures, may have concealed important differences between the two types of exposures. Both digestion methods utilized were shown to be reasonably consistent (as highlighted in the methods) indicating that the source of variability is likely the fish themselves.

Pimephales promelas Elimination

Elimination of cationic NPs by *P. promelas* mimicked the lack of treatment disparity observed in the uptake experiments. Elimination rate constants, fast and slow compartment partitioning percentages and BCFs presented below for *P. promelas* are compiled in Table 3. In both exposures the elimination followed the common biphasic pattern noted also in the *D. magna* experiments with a fast compartment that

dominated for 3 hours and the slow compartment dominating for hours 3-48 (Figure 3.13a and b). The body burden of NPs in the fish was either below or near the detection limit for both treatments by hour 48 of the depuration. The slow exchanging compartment rate constant was 1.11 $\pm$ 0.44 d^{-1} and 1.00 $\pm$ 0.22 d^{-1} for MHW and WW cationic treatments, respectively. Surprisingly, the elimination of cationic NPs was slower in the *P. promelas* compared to *D. magna* across both treatments. The half-life for cationic NPs accumulated in *P. promelas* was approximately 15 - 15.5 hours for both treatments. In both treatments the percent of NPs in the slow compartment was lower than in *D. magna* accumulating 12.5 and 21% in the MHW and WW treatments, respectively. Each time point contained significant variability in the depuration efficiency especially in the MHW exposure. Likewise, elimination of zwitterionic NPs was rife with variability (Figure 3.13c and d). Unfortunately, this confounded the ability to accurately derive an elimination rate constant. Over 30% of the data for each treatment was below the detection limit forcing the use of the data replacement method outlined in the data analysis section. Using this method the zwitterionic elimination rate constants were 1.93 $\pm$ 0.52 and 2.05 $\pm$ 0.57 for MHW and WW exposures, respectively. Due to the inherent bias that accompanies data replacement of this magnitude these elimination rate constants should be considered vague approximations and may underestimate the true elimination efficiency. Despite these considerations there are still several noteworthy trends in the data. The elimination rate constant was not affected by the treatment; however, the demarcation between the two compartments was not as obvious after introducing wastewater. Elimination of zwitterionic NPs by *D. magna* exhibited a similar trend after a 24-hour exposure. Furthermore, the elimination rate constants were similar to the 14-hour *D. magna* values. Regardless of the high variability, it is clear that zwitterionic NPs were eliminated much faster than cationic NPs contrary to our *D. magna* results. The half-life for accumulated zwitterionic NPs in *P. promelas* was 8 - 8.5 hours in both treatments. Bioconcentration factors were two orders of magnitude greater for the cationic NPs with values of 194 and 228 compared to the zwitterionic treatments with values of 1.92 and 1.12 for the MHW and WW exposures, respectively.

Distribution in Pimephales promelas

Waterborne gold NPs taken up by *P. promelas* were distributed almost exclusively to the intestine and gills for all treatments (Table 4). Accumulation in these organs was affected by the charge on the

nanomaterial and was consistent with the trends from the *P. promelas* uptake data. The accumulation of gold was significantly higher in the gills and intestines for the cationic MHW exposures compared to the zwitterionic MHW exposures. Likewise, accumulation was greater in the intestine of fish exposed to cationic NPs in WW compared to fish exposed to zwitterionic NPs in the same media; however, accumulation on the gills was not significantly different. The exposure media did have an impact on accumulation of cationic NPs in the gills though there was no difference between cationic treatments in the intestine. Fish exposed to zwitterionic NPs accumulated measureable amounts of gold in their gills and intestine but were not statistically different from the controls nor did the exposure media affect the concentration of gold found in these organs. None of our replicates produced a measurable signal in the brain or heart indicating that these two organs were likely spared from the gold NPs used in our experiments. Several liver/gallbladder replicates in the cationic MHW, one replicate in the cationic WW and one replicate in the zwitterionic MHW exposure contained concentrations of gold above the detection limit. Despite measureable gold in this organ, the average accumulation in liver/gallbladder was not significantly different from the controls due to high variability between replicates.

Discussion

Previous research has implicated water quality, intrinsic particle properties, adopted particle properties and organism physiology as important influences on the rate and extent of nanomaterial accumulation in aquatic organisms [7-11,32-34,37,38,41,43,44]. Many of these previous studies examined the nanomaterials at the point of entry into the environment with minimal consideration for the transformative possibilities that preceded release. Most consumer-based nanomaterials will follow the traditional waste treatment regime prior to environmental release and in most cases this includes a sojourn in a wastewater treatment plant. A considerable amount of time has been devoted to evaluating the ability of conventional wastewater treatment designs to remove NPs from effluents and how the NPs themselves influence removal efficiency. The goals of this study were designed to bridge the gap between the well-characterized influence of pre-exposure processes on particle characteristics and the downstream consequences of these changes upon environmental release.

Nanomaterials that are subjected to wastewater treatment processes are highly susceptible to transformation initiated by organic components and other waste products that are found in waste streams and wastewater treatment systems. Even in media with a low DOC concentration (~6.5 mg DOC/L), the cationic NPs from my experiment experienced a substantial increase in particle size with minimal change in particle charge within an hour. Based on microscopy images (Figure 3.1c) the change is size appears to be a consequence of the interaction between the organic components and the cationic NPs. A study by Limbach et al. using a similar synthetic wastewater recipe observed a decrease in the zeta potential of cerium oxide particles [20]. The authors combined the cerium particles with each component separately and found that the peptone was the principle cause of the reduced zeta potential [20]. I did not examine the WW components individually but it is likely that peptone contributed to the slight decrease in zeta potential observed for the cationic NPs. Furthermore, proteins are known to rapidly coat nanomaterials when in proximity to one another [18,47]. This knowledge along with the observed NP-organic agglomerates (Figure 3.1b) in our WW treatment suggested that the proteins from the meat extract play a role in the cationic transformations as well. Despite a minimal change in zeta potential in the WW treatment and a measured zeta potential well below the stability threshold of $\pm$ 30 mV, the cationic NPs demonstrated greater stability in suspension compared to the more transient NPs of the MHW exposure. Rather than strictly an electrostatic stabilization the sorption of organic components likely conferred stabilization through steric interactions similar to the stabilizing effect of bovine serum albumin and NOM coatings [19,48].

Cationic NPs were combined with high DOC WW to test the limits of stabilizing effect. Stability disappeared when the concentration of DOC was increased to ~80 mg DOC/L. The cationic NPs aggregated rapidly to sizes that were easily visible without the aid of a microscope. The loss of suspension stability is likely due to an abundance of organic matter that cross-linked nanomaterials into NP clusters. Gold NPs demonstrated a similar clustering mechanism in the presence of blood proteins [47] and NOM [9]. Microscopy images of NP-organic agglomerates at low DOC concentrations demonstrated similar particle gathering behavior though the reduced organic matter and NP concentration precluded formation of larger agglomerates (Figure 3.1c).

The influence of WW on particle transformations was also shown to be a function of the original particle characteristics, specifically particle charge. Except for a minimal decrease in surface charge, the zwitterionic NPs were unaffected by the organic components in the WW treatment. Microscopy images of the zwitterionic WW treatment provided visual confirmation that zwitterionic NPs did not change from the MHW treatment (Figure 3.1e-f). The lack of organic matter interaction with zwitterionic NPs was expected. The zwitterionic ligand is well known for its ability to resist protein attachment and is often utilized by particle manufacturers to improve success rate in drug delivery applications [49]. Despite no visible interaction between the WW components and the zwitterionic particles, sedimentation increased significantly in the WW exposure. Zwitterionic particles have demonstrated strong resilience to aggregation pressures in high ionic strength solutions [50] yet my observations suggested that their mechanism for resistance was rendered ineffective after introducing a DOC source. My data indicated that the cause of the increased sedimentation is not a loss of electrostatic stability nor is it related to particle aggregation (Figure 3.2). The interactions between the zwitterionic particles and the exposure container provided one possible explanation for the increased sedimentation. I used plastic beakers for the MHW exposures and glass beakers for the WW exposures to minimize the loss of nanomaterials as a result of surface adsorption. Metals have a greater affinity for glass surfaces over plastic surfaces; yet when coated by an organic layer the affinity for the glass surface is reduced. In the WW exposure, the zwitterionic NPs did not show signs of being coated by an organic layer. In the absence of an organic coating the zwitterionic NPs would be free to interact with the glass walls of the exposure container. This additional sorption mechanism may account for the increased sedimentation in the zwitterionic WW exposure compared to the zwitterionic MHW exposure.

Daphnia magna exposed to cationic NPs exhibited two different patterns of uptake depending on the treatment. The Michaelis-Menten saturation model proved a better fit for the MHW exposure data deviating from the biphasic uptake model observed for cationic PAAH-coated nanorods in the previous chapter. There does appear to be a small concentration window in which influx does not increase rapidly with concentration; however, that window was considered too small to be a significant contribution in the shape of the model. Alternatively, the WW exposure data aligned well with the previously described

biphasic uptake pattern. In the 14-hour exposure the biphasic uptake took a sigmoidal shape reaching a saturation point whereas the 24-hour exposure mirrored the PAAH data from the previous chapter. This biphasic pattern is largely unique to cationic NPs as zwitterionic NPs in this study, anionic NPs from a previous study and other biodynamic investigations of silver NPs with anionic charge [44,51] remained consistent with the more common monophasic uptake model. A study by Zhao and Wang is the lone exception, demonstrating biphasic uptake of anionic silver NPs by *D. magna* [52].

Few other examples of biphasic uptake as a function of concentration are available in the literature and often these are associated with ionic metals and cellular uptake [53-54]. Uptake of PAAH coated rods in my previous work adhered to the biphasic model without any evidence of internalization ruling out absorption as the foremost instigator. This pattern may instead reflect adsorption to multiple binding sites in the gut tract or on external surfaces of the daphind that vary in affinity for cationic NPs. The low concentration uptake rate could represent binding to low capacity high affinity sites up to a threshold that indicates saturation of these sites. After this threshold cationic NPs switch to low affinity high capacity sites until reaching complete saturation [54]. Alternatively, the biphasic uptake pattern observed in the WW exposures may reflect changes that occur during the filtering process. Zhao and Wang [52] and my previous work posited that the dramatic change in influx after a threshold concentration marked a transition in the dominant uptake mechanisms from carapace adsorption to ingestion.

The uptake rate constant for cationic NPs was clearly impacted by the presence of wastewater. The decrease in uptake rate constant was likely a direct repercussion of the wastewater induced NP transformation. The models derived in the previous chapter as well as numerous other studies [7,33-34,38,44,55-56] demonstrate a clear link between uptake and the size and surface charge of the NP. The uptake model for *D. magna* predicted that increasing particle size and decreasing surface charge would reduce the uptake rate constant aligning well with my observations. Furthermore, the zwitterionic NPs did not experience any characteristic transformation in WW and subsequently the uptake rate constant did not change significantly from the MHW treatment.

For the cationic NPs, the change in equilibrium binding characteristics can also be attributed to the transformative properties of WW. The increase in binding site capacity could be a consequence of

increased particle stability promoting an environment with a higher concentration of NPs in suspension for the *D. magna* to ingest. The decrease in binding affinity is likely a result of the loss of surface area and decreasing surface charge, both related to particle coating by wastewater components. Lee et al. postulated that NOM mediated interference of the particle-epithelial cell surface reduced the toxicity of quantum dots [57]. Likewise NPs with a humic acid ligand mimicking a NOM coating elicited an increase in binding site capacity and decrease in binding affinity [44]. Based on the changes to binding affinity the protein coating likely played a similar role in the cationic exposure disrupting the interactions between the particles and the gut surfaces at least initially. TEM images of *D. magna* gut exposed to cationic NPs in WW revealed NPs trapped in an organic matrix in proximity to microvilli (Figure 3.8c and d) though not directly interacting with the microvilli surface. A similar organic matrix was not observed in the cationic MHW exposure (Figure 3.8a and b) suggesting that it was not an artifact of the TEM preparation. While there was no significant change in uptake rate constant or characteristic transformations from the WW, the zwitterionic equilibrium binding constants followed the same trends as the cationic NPs. The higher binding site capacity of the WW treatment in this case was not a function of the available NP concentration in suspension as a higher percentage of the zwitterionic NPs fell out of suspension in the WW treatment. The zwitterionic results may instead indicate an indirect effect of WW on binding interactions that is independent of the particle surface charge.

The WW media contained components that are found in bacteria growth media and the exposures were conducted in non-sterile environments so it came as no surprise that bacteria colonized the WW treatments. Twenty-four hour exposures were conducted to investigate the changes in accumulation and retention patterns over a longer exposure period to identify possible biodynamic aberrations that could arise from increased bacteria growth. It is recommended that uptake rate constants be derived from the shortest possible exposure period thus eliminating any influence from depuration, which can artificially decrease the rate constant. The uptake rate constants decreased significantly in both treatments with a longer exposure period as expected. The binding affinity decreased in the MHW exposure as elimination exerted more influence over influx; yet, the binding site capacity of the MHW exposure did not change significantly based on exposure duration suggesting that *D. magna* has a finite number of sites for cationic

NPs. In addition, this constant saturation point may indicate that the percent of cationic NPs no longer in suspension does not change dramatically from the 14-hour exposure. The WW treatment did not achieve saturation in the concentration window; therefore, it is difficult to predict with accuracy the true binding site capacity and binding affinity of this treatment. Even though it cannot be calculated directly, the pattern of the 24-hour WW uptake data implied that the binding affinity decreased from the 14-hour exposure. Moreover, the influx rate did not exceed that observed at saturation in the 14-hour exposure suggesting a possible finite number of sites for cationic NPs incubated with WW as well. The similarities in pattern between the two suggested that bacteria had a minimal impact on the influx of cationic NPs. Furthermore, microscopy images of *D. magna* from the cationic WW treatment (Figure 3.8c and d) noticeably lack bacteria ruling out bacteria assisted NPs ingestion.

The patterns exhibited by the 24-hour zwitterionic exposures did not conform to our expectations as neatly as the cationic exposures. The uptake rate constants for both treatments did not change significantly during the extended exposure period; however, the gulf between the WW and MHW rate constant widened such that the WW exposure was no longer statistically similar to the MHW exposure. No evidence was found to indicate that the zwitterionic NPs were transforming over the 24-hour period and the zwitterionic ligand is expected to repel bacteria surfaces [58] thus the increased separation is unlikely a result of bacterial contamination. *D. magna* are known to filter and ingest DOC [59]; therefore, the increase in uptake may be related to an increase in filtration rate in the presence of DOC and other organic material in the water. Because they did not have a strong electrostatic attraction for the filter comb ingestion would be largely passive as with the anionic particles observed in the previous chapter. If the daphnid is increasing its filter rate it would thus increase the amount of water passing over its filter comb facilitating greater incidental ingestion of the zwitterionic NPs.

The biphasic uptake pattern for cationic NPs persisted in the *P. promelas* experiments though the uptake rate constants were several orders of magnitude smaller than the *D. magna* constants. This species discrepancy was attributed to differences in organism behavior. *D. magna* perpetually filter the water column, pushing food and other particulates into their food groove which is then directed toward the gut tract. *P. promelas*, on the other hand, draw water across their gills at a rate that is necessary for proper

ventilation and rarely swallow water diminishing its chances of accumulating NPs. The transformation in particle characteristics did not impact the rate constant though I did notice a shift in the threshold value that separated the two phases of the uptake model. The shift is analogous to our observations for *D. magna* and though they did not achieve saturation it is likely that the binding affinity decreased in the *P. promelas* cationic WW treatment. DOC can inhibit binding of metals to gill surfaces [60] and my results suggested that it may play a similar role for NP binding. A lack of significant difference between the two cationic treatments suggested that *P. promelas* were not as sensitive as *D. magna* to the particle transformations induced by WW incubation. The change in surface charge was slight and likely did not impact the attraction of the particle for mucus surfaces. The size transformation, however, was significant but also had no apparent impact on the uptake rate constant. Scown et al. [38] and Gaiser et al. [55] both demonstrated size related differences in accumulation for silver NPs. The particles in the Scown et al. study were highly polydispersed with a near 4-fold difference in hydrodynamic diameter [38]. Likewise, the average size of the two particles in the Gaiser et al. study were separated by >200 nm [55]. The difference in hydrodynamic diameter in the MHW and WW treatments of my study was negligible compared to these studies and may not have been enough to elicit a similar size-dependent effect.

The strength of the wastewater influence on uptake appeared to be species specific; however, discrepancies between uptake and intrinsic particle characteristics remained consistent across species. The cationic NPs were taken up at a rate significantly higher than the zwitterionic NPs identical to the trend observed for *D. magna*. Furthermore the 48-hour distribution study found significantly greater accumulation of cationic NPs in the intestine compared to the zwitterionic exposures. In a separate study using NPs with similar ligand chemistry, Japanese medaka was shown to accumulate cationic NPs more than anionic or neutral NPs with the majority of the NPs localized to the gills and intestine [11]. The gills and intestine both secrete protective mucus made up of negatively charged components, which favors attraction of cationic NPs [61]. I suspect that the larger uptake rate is primarily due to higher sorption of cationic NPs to the mucus and that internalization of the NPs is minimal due to the intentionally short exposure period. It is likely that with longer exposure duration the mucus reserves may run out [61] allowing for greater internal accumulation as noted in several of the liver/gallbladder samples and in studies

that extended the exposure period past 14 hours [38,55,62-63]. Despite a lack of attraction or competing electrostatic forces, anionic and neutral NPs have a proclivity for accumulating in these organs [11] as well as the liver [38,55,62]. My zwitterionic distribution study agreed with these findings indicating that zwitterionic NPs were indeed accumulated in the gills, intestine, and, for one replicate, in the liver/gallbladder.

Unlike uptake, elimination of cationic and zwitterionic NPs by *D. magna* was unaffected by WW incubation, a trend that persisted under a longer exposure period. Similarities in the slow elimination rate constant for both NPs suggested that WW did not influence absorption or that the absorbed fraction is small compared to the NP burden in the gut tract. Zwitterionic elimination was similar between treatments because the intrinsic particle characteristics were unaffected by the presence of wastewater. Cationic NPs are clearly affected by the WW coating after ingestion as evident by the equilibrium binding constants and TEM images (Figure 3.8c and d). *D. magna* efficiently eliminate DOC after ingestion with minimal internalization; therefore, *D. magna* would be expected to depurate NPs associated with DOC more quickly than in an exposure without DOC [59]. The discrepancy between this assumption and our data could be explained by the propensity for gold NPs to sorb to debris in the gut tract [64]. Gold NPs associated with debris and DOC remaining in the gut tract would be eliminated uniformly in the presence of a food source.

Once again I found evidence to conclude that surface charge played an important role in NP elimination by *D. magna*. There was a significant disparity between the elimination of cationic NPs and zwitterionic NPs after 14 hours that became more apparent after the 24-hour exposure. Daphnids exposed to zwitterionic NPs retained a significant concentration of NPs (~10% of original body burden) compared to the cationic NPs (~0.01%) after 48 hours in clean MHW with a bountiful food supply. In the previous chapter I observed a similar trend and attributed the fast elimination of the cationic NPs to its greater propensity for attaching to debris in the middle of the gut tract. The slow elimination of zwitterionic NPs, on the other hand, is not as easily explained. The particles have a slight anionic charge; therefore, their behavior after ingestion may be similar to the anionic charged spheres and rod in the previous chapter. I did not produce images to indicate if the particles were absorbed but it is unlikely given that the zwitterionic surface ligand also improves evasion of cellular uptake mechanisms [49]. As this would likely increase the

elimination rate, zwitterionic NPs must be initiating another unidentified mechanism for retarding movement through the gut tract.

Accumulation of NPs by *D. magna* is often restricted to external compartments such as the gut tract and carapace. Several studies have demonstrated NP translocation across cell membranes in the gut of a daphnid for quantum dots [8] and polystyrene beads [65] but to date no studies have identified a similar mechanism for gold [64,66]. The previous chapter highlighted work on *D. magna* uptake of gold NPs coated with anionic and cationic ligands and did not yield evidence to indicate internal accumulation of these particles. However, cationic NPs used in this study were found in epithelial cells regardless of treatment (Figure 3.6a-b). Though all NPs used for these exposures were natively 2 nm in diameter, particles observed crossing the gut tract were at least an order of magnitude larger. Human cell lines preferentially take up larger gold NPs [49,67] and it is plausible that *D. magna* epithelial cells harbor the same proclivities. On the other hand, identifying 20 nm NP is much simpler than finding 2 nm NPs and it is possible that smaller NPs were also trans-located but could not be separately identified. Regardless the efficiency of elimination suggests that the internally accumulated NPs are a small fraction of the total NPs taken up in the exposure period.

The ability of these NPs to cross when others could not may have to do with the ligand construction in addition to the surface chemistry. The NPs used in this study are specifically designed for cellular uptake and drug delivery applications [68] whereas the particles used in the previous chapter were more rudimentary. The spherical and rod shaped particles from the previous chapter had the attributes necessary for cellular uptake [67] yet it I did not find evidence of internalization. The additional modifications on the ligand of the particles used in this study likely increased the probability of internal absorption. These possible stipulations argue for a more holistic approach when separating particles into distinct subgroups. Reducing a NP to a small set of characteristics (size, shape, surface charge) overlooks other important characteristic influences that will collectively provide a more concrete prediction of fate and behavior [8,69].

Deriving elimination rate constants for *P. promelas* proved difficult due to the variability in the data especially in the zwitterionic exposures. As with uptake, elimination was affected by particle charge

but not by treatment. The similarity between treatments and disparity between particle configurations suggested that, as with uptake, elimination by *P. promelas* is not sensitive to minute changes in particle size but is greatly affected by the charge on the particle. Elimination of NPs is dependent on both the speed of mucus sloughing and food availability [61]. In a similar study, cationic particles were eliminated from the intestine of Japanese medaka at an analogous rate when food was not provided [11] successfully clearing their gut content by the end of the 120-hour depuration experiment. The similarities to my study suggested that sloughing of the mucus is the main motive force in elimination. The zwitterionic NPs are not expected to have a strong attraction to the negatively charged mucus, which may be the reason for quicker elimination. Without a strong attachment to surfaces in the gut tract the zwitterionic NPs may have been more easily removed by passing food. Likewise constant water flowing across the gills would more easily disrupt the weaker electrostatic attraction between the zwitterionic NPs and the gill mucus. These results are consistent with observations from the Zhu et al. study for negative and neutrally charged NPs [11]. The speed at which NPs were eliminated in our exposure and the Zhu et al. [11] study suggested that fish are adept at depurating gold NPs even in situations where food is scarce.

To my knowledge this is the first attempt at applying the biodynamic model to nanomaterials targeting a vertebrate species. Digestion methods for organisms with higher lipid content added complexity to the analysis of the fish data compared to the daphnia analysis. We attempted several digestion methods to identify a single method that would provide complete digestion of with the least amount of variability between samples. Digestions using only Aqua Regia in a microwave digester were seemingly effective in the percent recovery experiments. However, a significant portion of the lipid content went undigested; therefore, this method might under predict the fish accumulation in the actual experiments. A second method where fish were dry ashed first in a muffle furnace then digested with nitric acid and hydrogen peroxide was employed. This second method was clearly superior to the first with regards to lipid digestion. However, the percent recovery, while consistent, was lower than the first method. The second method involved many sample transfers increasing the probability of losing gold between steps. Additionally, though most lipids were digested some recalcitrant lipids precipitated during the dilution step,

which may have lowered the percent recovery. Nevertheless the second method was preferred because it was consistent and provided a more complete digestion of the sample.

Consistency between our percent recovery experiments for both methods suggested that the high variability between individual replicates was related to the fish and not the digestion method. The NPs used in these experiments were more complex and thus required a longer production period and yielded smaller volumes. Small exposure volumes were used to maximize output of experiments from the obtained NPs. The high variability between individual fish exposed in the same aquaria was likely a result of stress induced by crowding in the small volumes. Fish can take up waterborne NPs either in the process of pushing water across their gills or through swallowing water [38,61]. Fish that are stressed will increase their ventilation rate and are more likely to swallow greater amounts of water accelerating the rate of NP accumulation. Stress induced drinking was associated with increased intestinal concentrations of TiO_2 NPs [70] and carbon nanotubes [71]. The stress on fish in my study did not seem to be universal and thus created significant variability between our replicates. The zwitterionic exposures added additional analytical problems because uptake was quite low and, especially at lower concentrations and after several hours of depuration, replicates were often near or below the detection limit of the ICP-MS (0.250 ug Au/L). As a result the derived biodynamic constants may under predict the actual values and conceal possible differences between treatments. Based on my work I recommend that future studies utilize smaller fish and larger exposure volume. Smaller fish (< 0.2 g) would minimize stress induced from crowding, ensure a more complete digestion, and diminish any matrix effects caused by residual lipids during analysis.

Bioconcentration factors calculated for each organism and each treatment revealed distinct accumulation patterns that align with the previous discussion on uptake and elimination. Given a constant exposure of NPs both organisms are expected to accumulate a higher concentration of cationic NPs. In the case of *D. magn*a uptake is the dominant force behind the high BCF while in *P. promelas* both higher uptake and slower elimination combine to increase the accumulation of NPs from the water column. These trends hold true regardless of the exposure media used in this experiment but may not translate to all water quality scenarios. Changes in pH, ionic strength and different sources of organic matter [15,72] could change the bioavailability of the NPs subverting the predicted biodynamics. Knowledge of both the

characteristic transformations of NPs that pass through wastewater treatment and the aquatic ecosystem on the receiving end of the effluent will be crucial in accurately assessing the deleterious effects of NPs released from WWTPs.

The NP wastewater dynamic appeared to be largely beneficial to the model organisms or, at worst, inconsequential. Accumulation of NPs from WW effluent decreased by approximately a third in *D. magna* compared to an exposure consisting of pristine particles from a direct release. Furthermore, the reduction in BCF for the *D. magna* WW treatment suggested that WW incubation may reduce the toxicity of cationic NPs to *D. magna*. The protective effect is not as apparent in the fathead minnow experiments. Nevertheless, WW incubation did not increase the accumulation of NPs in *P. promelas*, rather they experienced the same accumulation regardless of how they were exposed. One caveat of the study is that I designed the experiments around a scenario where the NPs were combined with WW at the point of entry into an aquatic ecosystem excluding processes that might occur during transit to and through a WWTP. Muth-Kohne et al. observed decreased silver NP toxicity to zebrafish embryos when they mixed the particles with effluent that was released from a simulated WWTP [73]. However, when they subjected the silver NPs to the entire WWTP process, the toxicity of the silver NPs increased which they attributed to an increase in silver ion potency. While these results do not translate directly to particle that is less prone to dissolution such as gold they do demonstrate a need for examining the contributions of NPs to the effluent whether it is an increase in ion release or the transformed particle itself. Effluents are one of the principal sources of NPs into the aquatic and terrestrial environment [6]. My study emphasizes the need to utilize knowledge of pre-exposure processes to better understand the subsequent downstream consequences in exposed organisms rather than basing decisions on data from pristine NPs. Regulators would be remiss to exclude these data from risk analysis as they both provide a more realistic release scenario and clearly impact the extent of accumulation in aquatic organisms. Several studies have already demonstrated nanosized particles in wastewater effluent samples collected in the field [27,74]; therefore, it is urgent that we turn our attention toward bridging these gaps before NPs join the ranks of other legacy pollutants.

Conclusions

The concentration of NPs entering wastewater treatment plants will intensify as nanotechnology becomes more pervasive in consumer products. WWTPs are efficient at removing NPs from the influent; however, a small percentage are still capable of escaping in the effluent and posing a risk to aquatic organisms in receiving bodies of water. The conditions found in a WWTP induce changes in the particle characteristics that can have downstream consequences on behavior, bioavailability and toxicity upon release into the environment. My study demonstrated that the intrinsic NPs characteristics affect the extent of transformation in the presence of wastewater. Furthermore, the downstream consequences of these transformations on particle accumulation were species specific. *D. magna* was more sensitive to the WW induced change in particle characteristics as evident by a reduction in the bioconcentration potential. On the other hand, *P. promelas* were unaffected by changes in particle characteristics and overall were more effective at depurating NPs. The particle and species-specific nature of the WW effects highlights an urgent need for more research on NPs released in WWTP effluent that inspect other organisms and particle configurations. These datasets are essential to the development of robust and defendable fate and behavior models as they relay a more accurate depiction of the NP's actions leading up to its release into the environment.

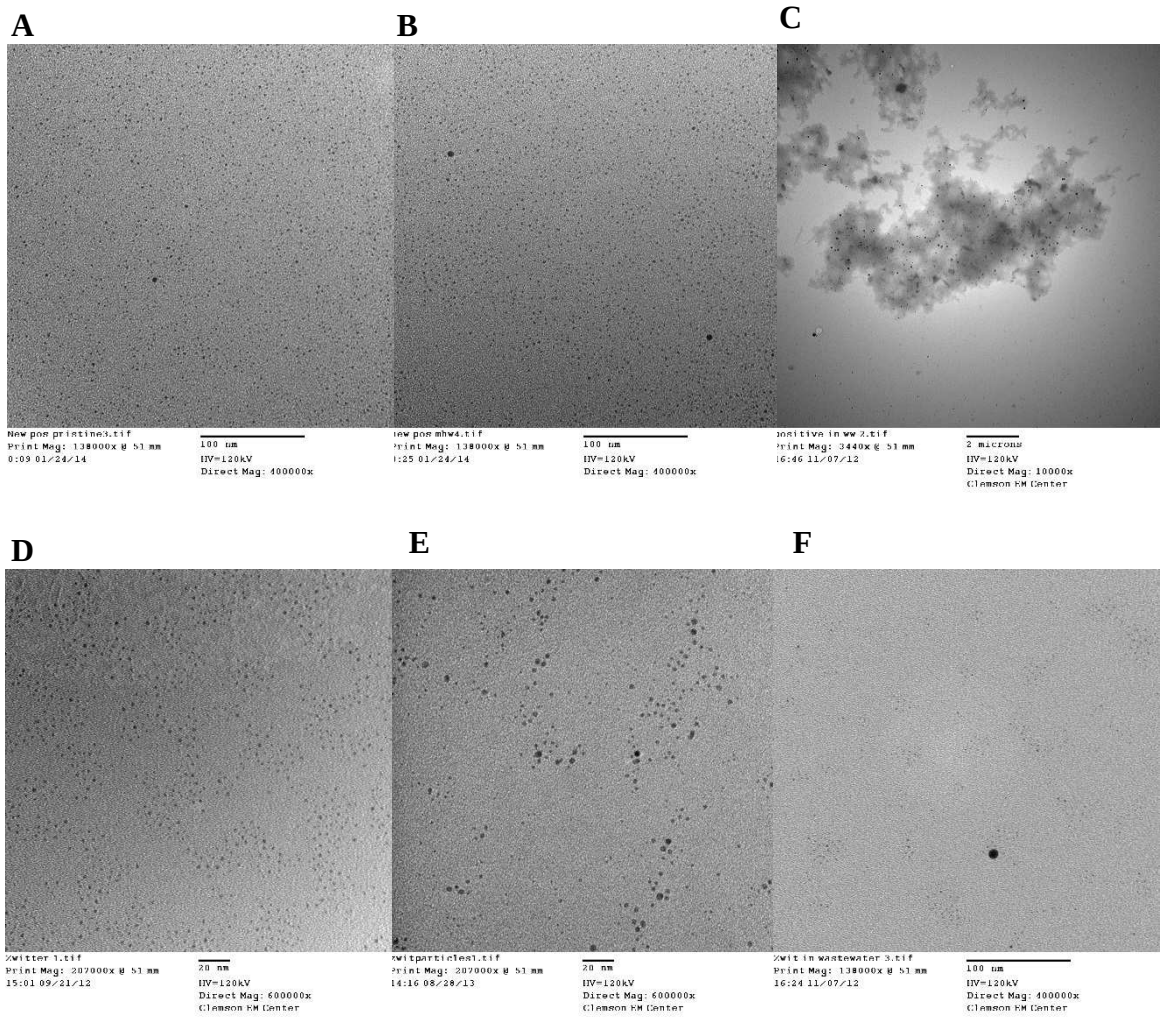

Figure 3.1: TEM images of cationic and zwitterionic gold NPs in stock solution, moderately hard water and wastewater

TEM micrographs of (A) stock cationic gold nanoparticles (NPs), (B) cationic NPs in moderately hard water (MHW), (C) cationic NPs in wastewater (WW), (D) stock zwitterionic NPs, (E) zwitterionic NPs in MHW (F) zwitterionic NPs in WW.

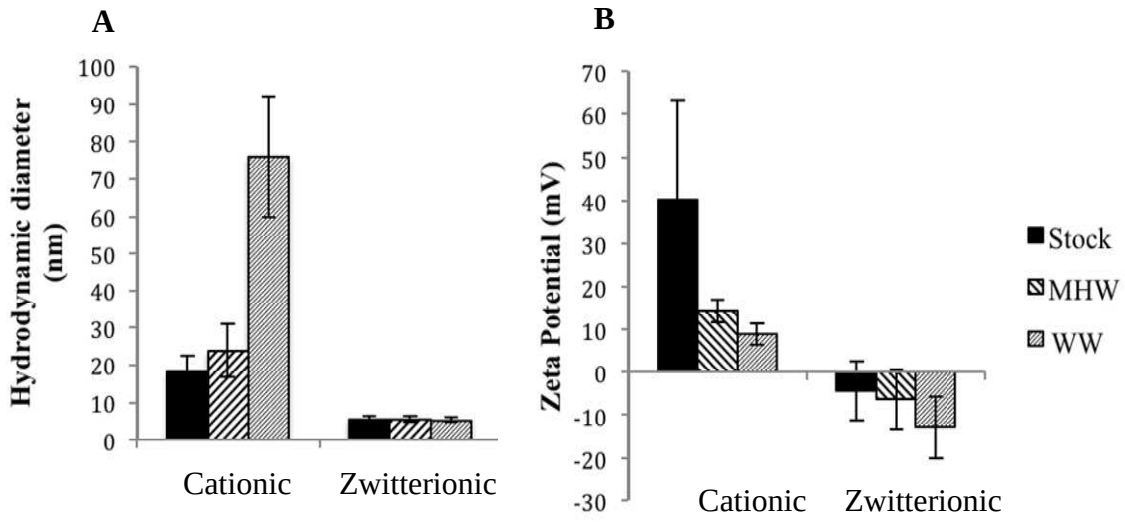

Figure 3.2: Characterization of cationic and zwitterionic gold NPs in each exposure media
Hydrodynamic diameter (A) and zeta potential (B) for both nanoparticles in stock solution, moderately hard water and wastewater (after 1 hour). Each bar represents the average of three runs ± 1 standard deviation.

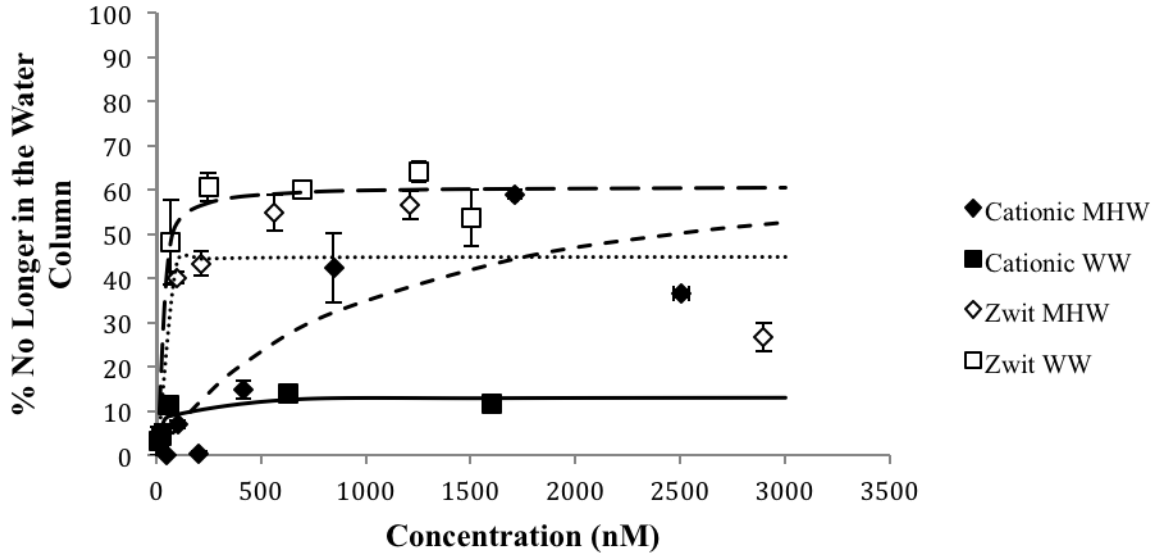

Figure 3.3: Stability of cationic and zwitterionic gold NPs in each exposure media
Estimation of percent sedimentation for each treatment after 14 hours in exposure chambers lacking organisms. Data points represent averages of 3 replicates ± 1 standard deviation. Data were fit to the Michaelis-Menten model to determine the max percent of NPs leaving the water column for the cationic MHW (short dashed line), cationic WW (solid line), zwitterionic MHW (dotted line), and zwitterionic WW (long dashed line).

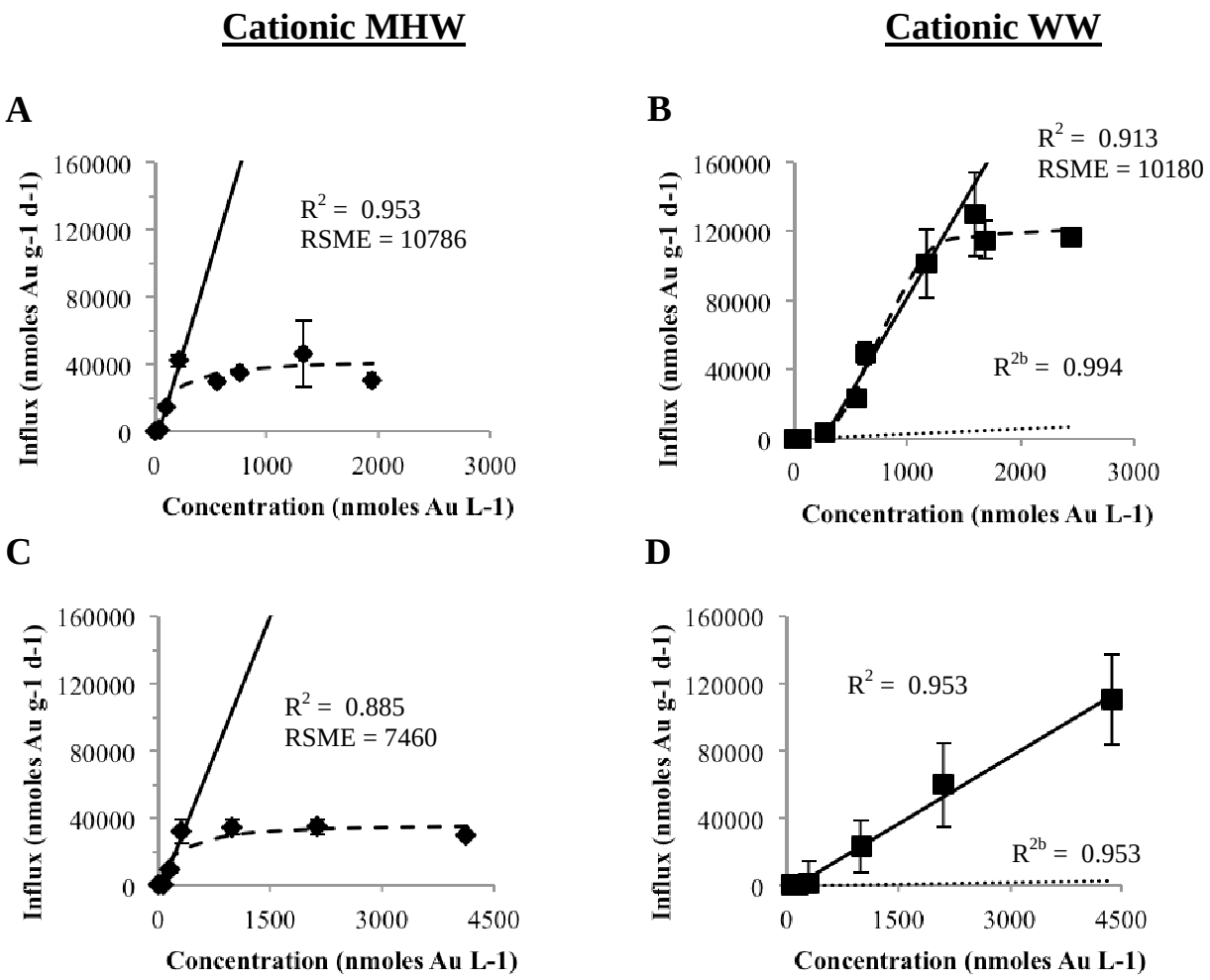

Figure 3.4. Uptake of cationic gold NPs by *Daphnia magna* from two different exposure media

Uptake of cationic nanoparticles by *D. magna* exposed for 14 hours in MHW (A) and WW (B) and 24 hours in MHW (C) and WW (D). Solid lines represent the linear model used to calculate the k_{uw1}. Dotted lines represent the linear model used to calculated k_{uw2}. Dashed lines represent the non-linear regression model used to calculated equilibrium constants. R^2 and RSME values describe the quality of fit for the linear and non-linear models, respectively. Data points represent average of 3-6 replicates $\pm$1 standard deviation.

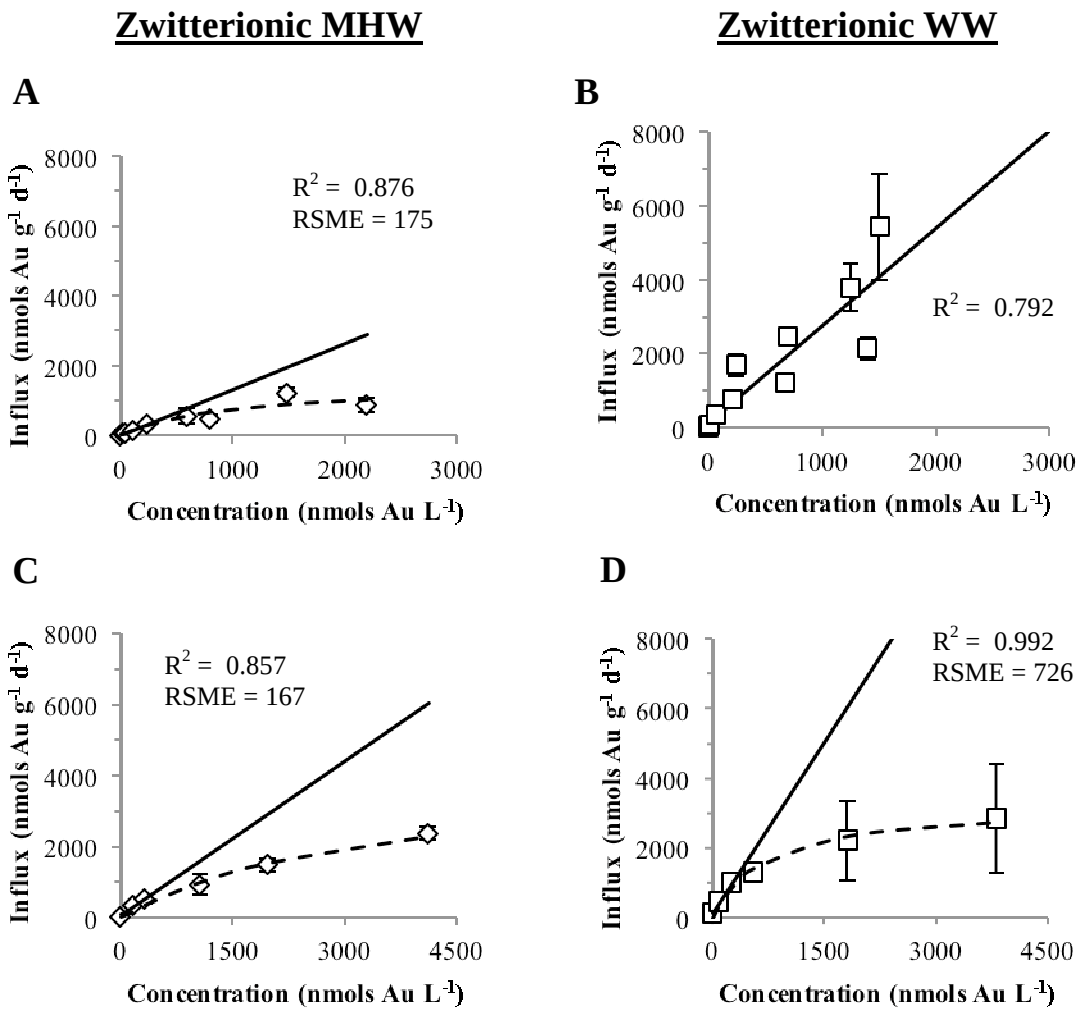

Figure 3.5: Uptake of zwitterionic gold NPs by *Daphnia magna* from two different exposure media

Uptake of zwitterionic nanoparticles by *D. magna* exposed for 14 hours in MHW (A) and WW (B) and 24 hours in MHW (D) and WW (D). Solid lines represent the linear model used to calculate the k_{uw1}. Dashed lines represent the non-linear regression model used to calculated equilibrium constants. R^2 and RSME values describe the quality of fit for the linear and non-linear models, respectively. Data points represent average of 3-6 replicates $\pm$1 standard deviation.

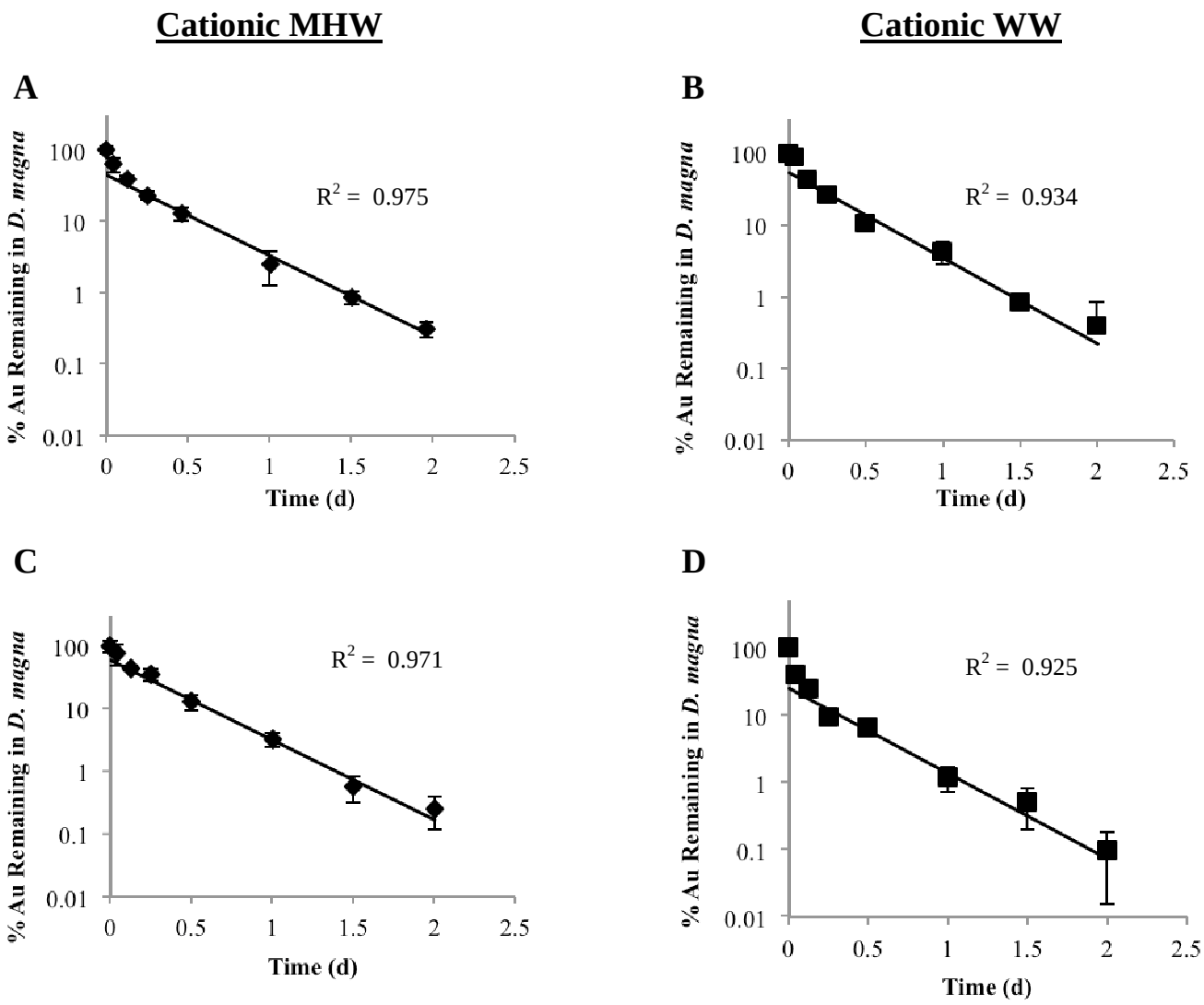

Figure 3.6: Elimination of cationic gold NPs by *Daphnia magna* from two different exposure media

Elimination of cationic nanoparticles by *D. magna* after exposure for 14 hours in MHW (A) and WW (B) and 24 hours in MHW (C) and WW (D). All elimination experiments took place in fresh MHW with ample food supply. Solid lines represent the linear model used to calculate the k_e. R^2 values describe the quality of fit for the linear model. Data points represent average of 3-6 replicates $\pm$1 standard deviation.

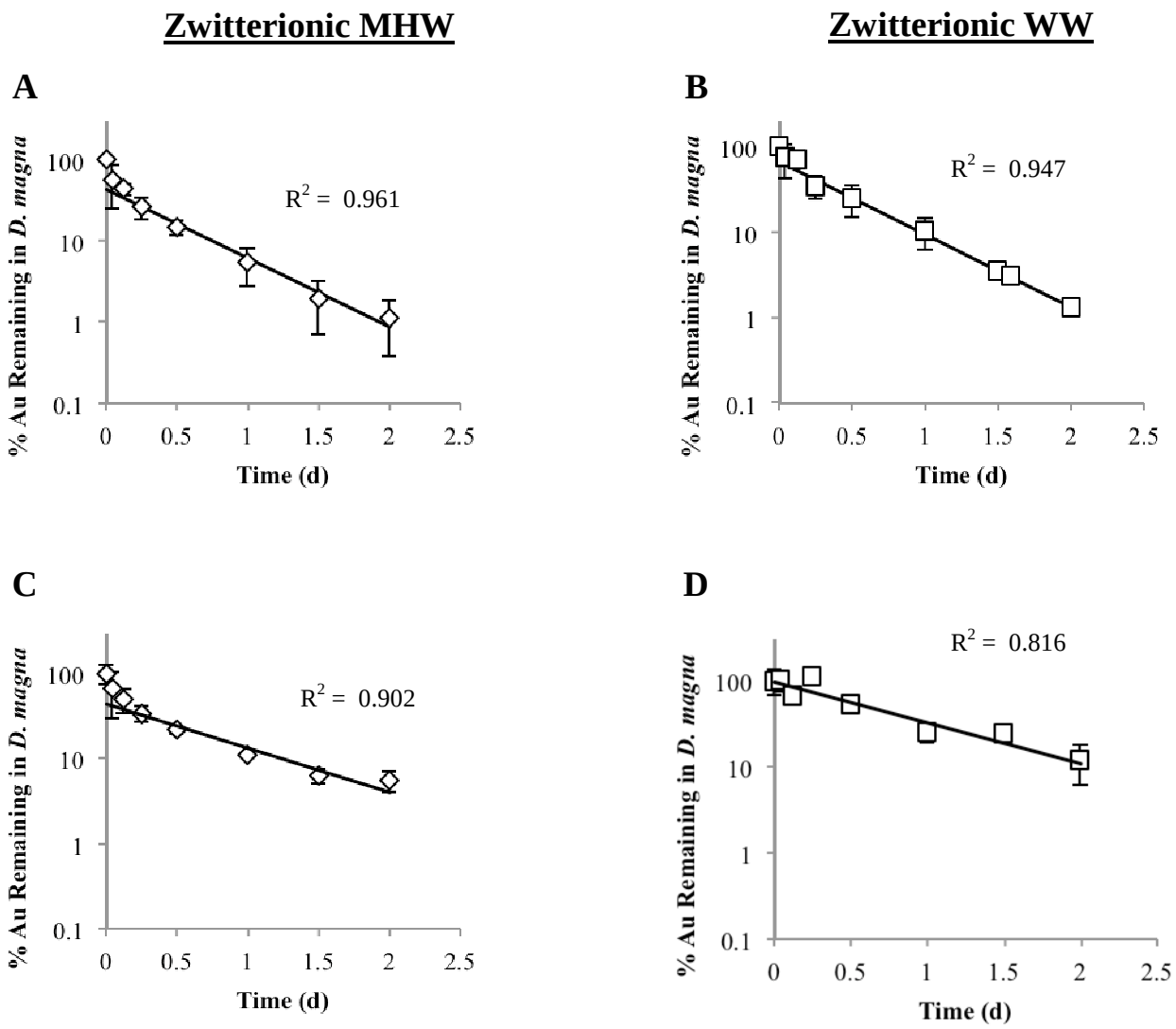

Figure 3.7: Elimination of zwitterionic gold NPs by *Daphnia magna* from two different exposure media

Elimination of zwitterionic nanoparticles by *D. magna* after exposure for 14 hours in moderately hard water (A) (MHW) and wastewater (B) (WW) and 24 hours in MHW (C) and WW (D). All elimination experiments took place in fresh MHW with ample food supply. Solid lines represent the linear model used to calculate the k_e. R^2 values describe the quality of fit for the linear model. Data points represent average of 3-6 replicates $\pm$1 standard deviation.

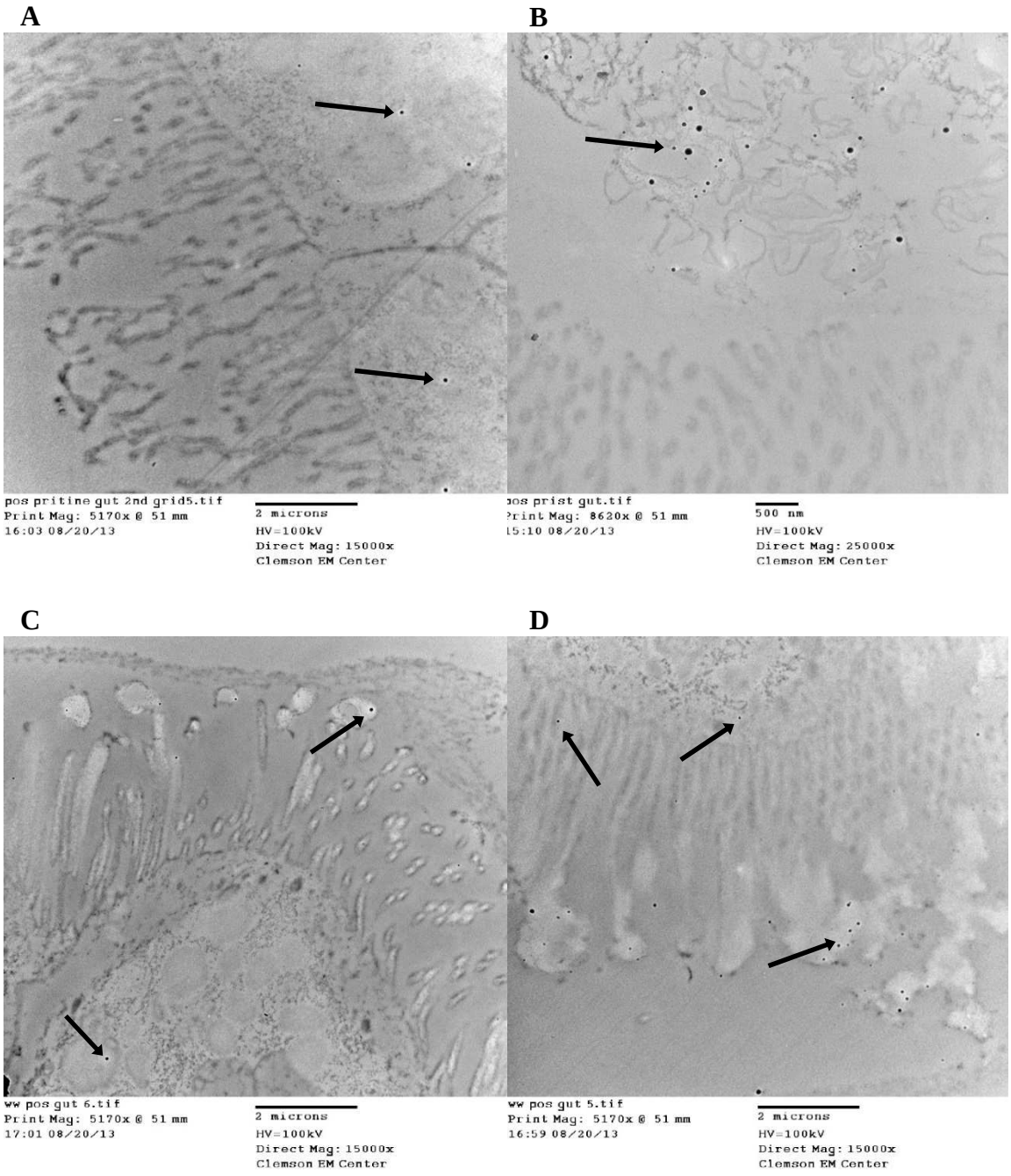

Figure 3.8: TEM images of gut tract from *Daphnia magna* exposed to cationic gold NPs

TEM micrographs of the gut tract of *D. magna* exposed to cationic NPs in moderately hard water (A, B) and wastewater (C, D). All identified nanostructures were separately confirmed to have gold signatures with EDX analysis. Arrows = gold nanoparticles.

Figure 3.9: TEM image of gut tract from *Daphnia magna* exposed to zwitterionic gold NPs
TEM micrograph of the gut tract of *D. magna* exposed to zwitterionic NPs in wastewater. Black spheres are not gold NPs as confirmed with EDX analysis.

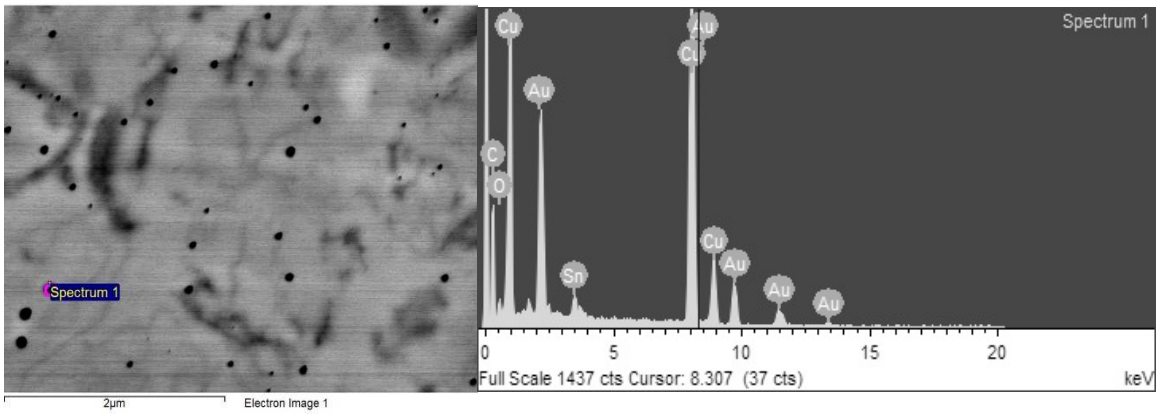

Figure 3.10: Representative elemental analysis of gut tract image from *Daphnia magna* exposed to cationic gold NPs
Representative EDX analysis of *D. magna* gut TEM micrographs. Gold is clearly present in the selected nanoparticle along with other elements that are expected in the EDX analysis. Example is from a daphnid exposed to cationic NPs in MHW.

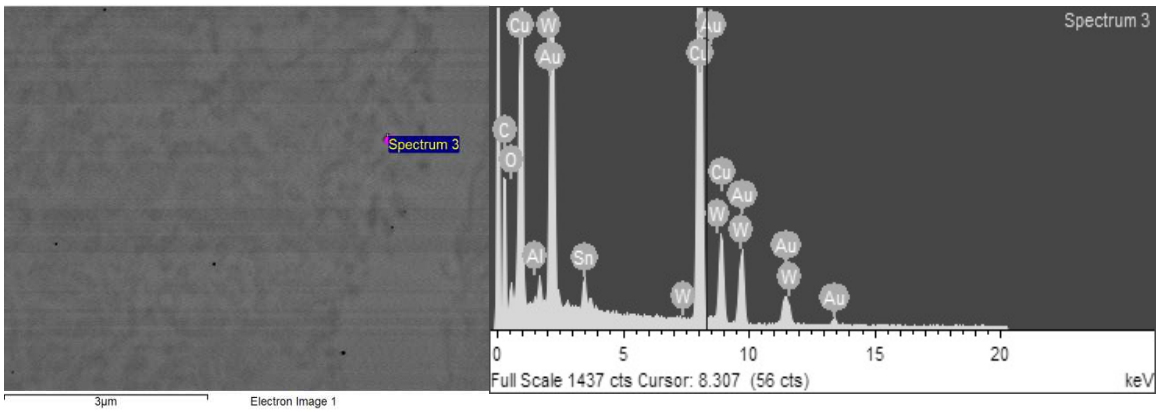

Figure 3.11: Representative elemental analysis of gut epithelial tissue image from *Daphnia magna* exposed to cationic gold NPs
EDX analysis of nanospheres located epithelial cells of *D. magna* exposed to cationic NPs in MHW. Gold is clearly present in the selected nanoparticle along with other elements that are expected in the EDX analysis and minimal signals from Al, Sn and W.

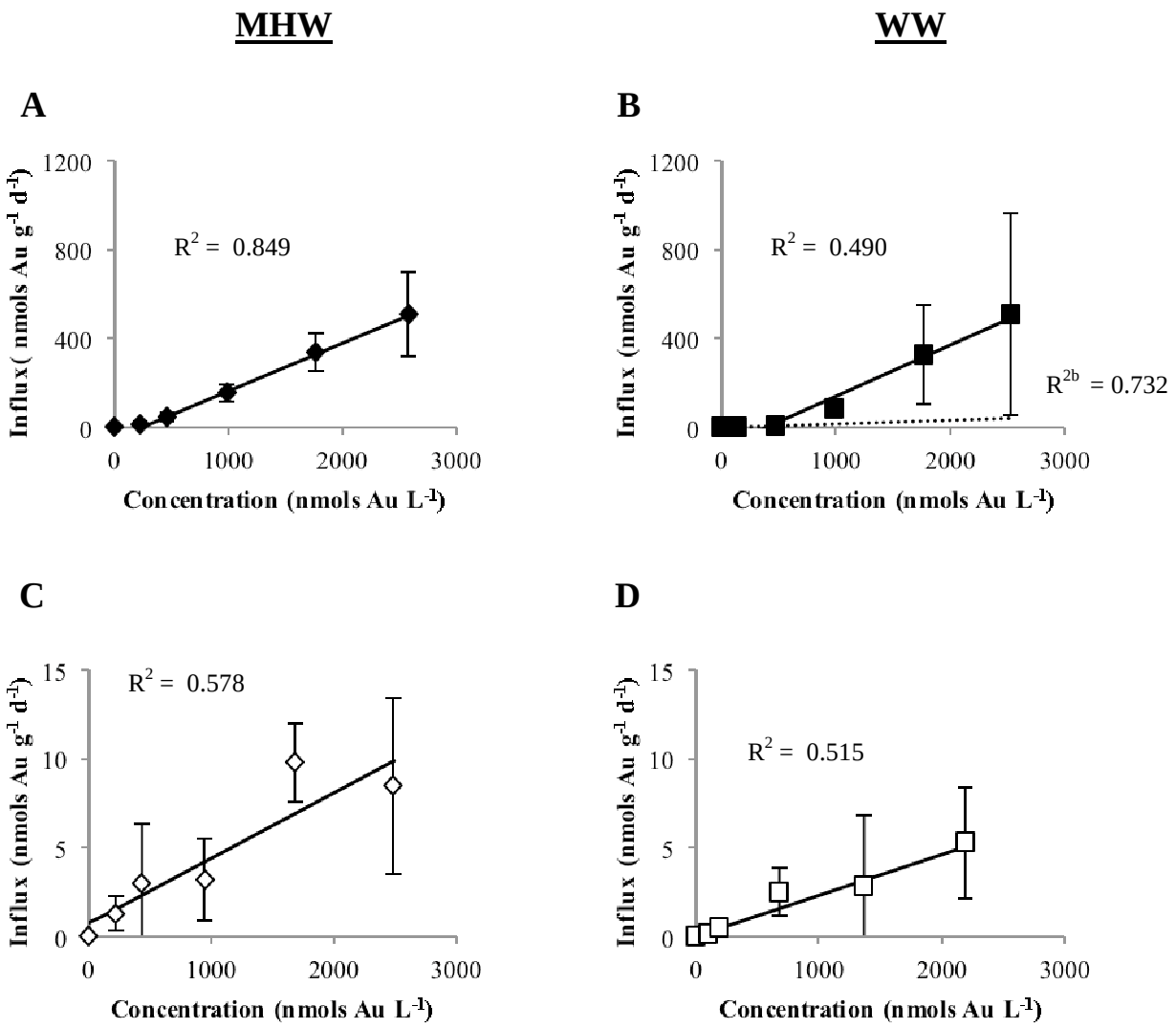

Figure 3.12: Uptake of gold NPs with two unique surface charges by *Pimephales promelas* from two different exposure media

Uptake of cationic nanoparticles by *P. promelas* exposed for 14 hours in moderately hard water (A) (MHW) and wastewater (B) (WW) and zwitterionic nanoparticles after exposure for 14 hours in MHW (C) and WW (D). Solid lines represent the linear model used to calculate the k_{uw1}. Dotted lines represent the linear model used to calculated k_{uw2}. R^2 values describe the quality of fit for the linear models. Data points reflect average of 3 replicates $\pm$1 standard deviation.

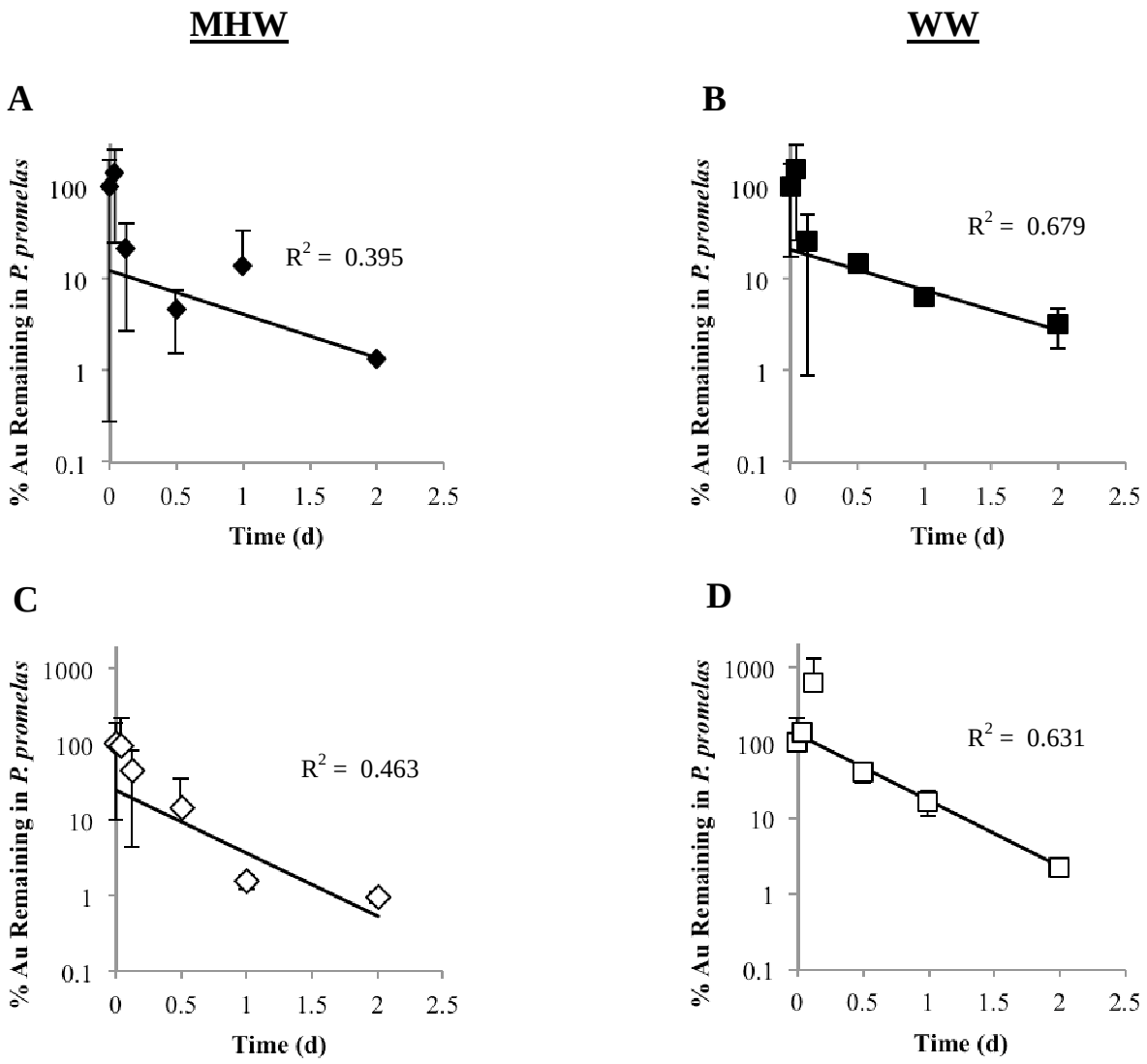

Figure 3.13: Elimination of gold NPs with two unique surface charges by *Pimephales promelas* from two different exposure media

Elimination of cationic nanoparticles by *P. promelas* after exposure for 14 hours in moderately hard water (A) (MHW) and wastewater (B) (WW) and zwitterionic NPs after exposure for 14 hours in MHW (C) and WW (D). All elimination experiments took place in fresh MHW with ample food supply. Solid lines represent the linear model used to calculate the k_e. R^2 values describe the quality of fit for the linear model. Data points represent average of 3 replicates $\pm$1 standard deviation.

	14 hours				24 hours			
	Cationic MHW	**Cationic WW**	**Zwitterion MHW**	**Zwitterion WW**	**Cationic MHW**	**Cationic WW**	**Zwitterion MHW**	**Zwitterion WW**
k_{uw1} (L g^{-1} d^{-1})	218.1 ± 16.1^{abc}	110.3 ± 10.8^{abc}	1.32 ± 0.14^{c}	1.46 ± 0.24^{bc}	110.6 ± 13.3^{abc}	26.5 ± 2.3^{abc}	1.46 ± 0.24^{ac}	3.28 ± 0.12^{abc}
k_{uw2} (L g^{-1} d^{-1})	n/a	2.95 ± 0.26^{b}		n/a	n/a	0.74 ± 0.08^{b}	n/a	n/a
B_{max} (nmol g^{-1})	43350 ± 5430^{ac}	121700 + 5450^{a}	1524 ± 287.2^{b}	n/a	37730 ± 3710^{c}	n/a	4192 ± 717.6^{c}	3239 ± 652.8
K_d (nmol L^{-1})	137.9 ± 69.9^{ac}	729.1 ± 46.3^{a}	988.2 ± 406.7	n/a	240.9 ± 93.2^{c}	n/a	3398 ± 1017^{c}	704 ± 426.2
k_e (d^{-1})	2.64 ± 0.08^{c}	2.73 ± 0.14^{c}	1.96 ± 0.07^{b}	1.98 ± 0.09^{b}	2.93 ± 0.13^{c}	2.90 ± 0.21^{c}	1.18 ± 0.10^{bc}	1.08 ± 0.13^{bc}
% Fast/% Slow	55/45	47/53	56/44	32/68	39/61	75/25	56/44	3/97
BCF (L kg^{-1})	82610	40410	673	1328	37710	9132	1242	2962

Table 3.1: Biodynamic parameters, equilibrium binding characteristics and BCF for *Daphnia magna* exposed to gold NPs

Uptake (k_{uw} ± SE) and elimination rate constants (k_e ± SE), binding capacity (B_{max} ± SE), binding site affinity (K_d ± SE), compartment distribution (%Fast / %Slow) and bioconcentration factors (BCF) for gold nanoparticle exposures in moderately hard water (MHW) and wastewater (WW) lasting 14 and 24 hours .

N/A not applicable for this treatment based on model selection.

[a] significantly different based on exposure media.

[b] significantly different based on exposure duration.

[c] significantly different based on particle charge.

	Cationic MHW	Cationic WW	Zwitterionic MHW	Zwitterionic WW
k_{uw1} (L g^{-1} d^{-1})	0.215 ± 0.025[b]	0.228 ± 0.059[b]	0.0037 ± 0.001[b]	0.0023 ± 0.0006[b]
k_{uw2} (L g^{-1} d^{-1})	n/a	0.017 ± 0.004	n/a	n/a
k_e (d^{-1})	1.11 ± 0.44[b]	1.00 ± 0.22[b]	1.93 ± 0.52[b]	2.05 ± 0.57[b]
% Fast/% Slow	87/13	79/21	76/25	0/127
BCF (L kg^{-1})	194	228	1.92	1.12

Table 3.2: Biodynamic parameters and BCF for *Pimephales promelas* exposed to gold NPs
Uptake (k_{uw} ± SE) and elimination rate, compartment distribution (%Fast / %Slow) and bioconcentration factors (BCF) for gold nanoparticle exposures in moderately hard water (MHW) and wastewater (WW).
N/A not applicable for this treatment based on model selection.
[a] significantly different based on exposure media.
[b] significantly different based on particle charge. For all rate constant comparisons a p value < 0.05 was considered significant

Organ	Control	Cationic MHW	Cationic WW	Zwitterionic MHW	Zwitterionic WW
Brain[b]	N.D.	N.D.	N.D.	N.D.	N.D.
Heart[b]	N.D.	N.D.	N.D.	N.D.	N.D.
Liver/Gallbladder[b]	N.D.	62.93 ± 44.23	2.40 ± 1.70	0.68 ± 0.48	N.D.
Intestine	0.380 ± 0.276	333.34 ± 39.40*	380.39 ± 178.29*	39.59 ± 9.17	31.33 ± 10.08
Gill	1.22 ± 1.22	13.92 ± 3.80*	2.08 ± 0.46	4.96 ± 1.61	1.53 ± 0.43

Table 3.3: Gold concentration (nmoles Au g_{org}^{-1}) in select organs from *Pimephales promelas* exposed to two types of gold NPs

Brain, heart, combined liver and gallbladder, intestine and gill tissue from fathead minnows exposed to cationic and zwitterionic gold nanoparticles in moderately hard water (MHW) and wastewater (WW).

N.D. – none of the replicates contained detectable levels of gold for ICP-MS analysis.

*significantly different ($p < 0.05$) from control

[b]pooled samples into three replicates instead of six.

References

1. Künniger T, Gerecke AC, Ulrich A, Huch A, Vonbank R, Heeb M, Wichser A, Haag R, Kunz P, Faller M. 2014. Release and environmental impact of silver nanoparticles and conventional organic biocides from coated wooden facades. *Environ Pollut* 184: 464-471.

2. Benn T, Cavanagh B, Hristovski K, Posner JD, Westerhoff P. 2010. The release of nanosilver from consumer products used in the home. *J Environ Qual* 39:1875-1882.

3. Kaegi R, Sinnet B, Zuleeg S, Hagendorfer H, Mueller E, Vonbank R, Boller M, Burkhardt M. 2010. Release of silver nanoparticles from outdoor facades. *Environ Pollut* 158: 2900-2905.

4. Kaegi R, Ulrich A, Sinnet B, Vonbank R, Wichser A, Zuleeg S, Simmler H, Brunner S, Vonmont H, Burkhardt M, Boller M. 2008. Synthetic TiO_2 nanoparticle emission from exterior facades into the aquatic environment. *Environ Pollut* 156: 233-239.

5. Benn TM, Westerhoff P. Nanoparticle silver released into water from commercially available sock fabrics. *Environ Sci Technol* 2008, 42, 4133–4139.

6. Gottschalk F, Sonderer T, Scholz RW, Nowack B. 2009. Modeled environmental concentrations of engineered nanomaterials (TiO_2, ZnO, Ag, CNT, Fullerenes) for different regions. *Environ Sci Technol* 43: 9216-9222.

7. Burns JM, Pennignton PL, Sisco PN, Frey R, Kashiwada S, Fulton MH, Scott GI, Decho AW, Murphy CJ, Shaw TJ, Ferry JL. 2013. Surface charge controls the fate of Au nanorods in saline estuaries. *Environ Sci Technol* 47:12844-12851.

8. Feswick A, Griffitt RJ, Siebein K, Barber DS. 2013. Uptake, retention and internalization of quantum dots in *Daphnia* is influenced by particle surface functionalization. *Aquat Toxicol* 130-131:210-218.

9. Glenn JB, Klaine SJ. 2013. Abiotic and biotic factors that influence the bioavailability of nanoparticles to aquatic macrophytes. *Environ Sci Technol* 47:10223-10230.

10. Glenn JB, White SA, Klaine SJ. 2012. Interactions of gold nanoparticles with freshwater aquatic macrophytes are size and species dependent. *Environ Toxicol Chem* 31:194-201.

11. Zhu Z, Carboni R, Quercio Jr. MJ, Yan B, Miranda OR, Anderton DL, Arcaro KF, Rotello VM, Vachet RW. 2010. Surface properties dictate uptake, distribution, excretion, and toxicity of NPs in fish. *Small* 6:2261-2265.

12. Ferry JL, Craig P, Hexel C, Sisco P, Frey R, Pennington P, Fulton M, Scott G, Decho A, Kashiwada S, Murphy C, Shaw TJ. 2009. Transfer of gold nanoparticles from the water column to the estuarine food web. *Nat Nanotechnol* 157:1-4.

13. Stankus DP, Lhose SE, Hutchison JE, Nason JA. 2011. Interactions between natural organic matter and gold nanoparticles stabilized with different organic capping agents. *Environ Sci Technol* 45: 3238-3244.

14. Hotze EM, Phenrat T, Lowry GV. 2010. Nanoparticle aggregation: Challenges to understanding transport and reactivity in the environment. *J Environ Qual* 39: 1909-1924.

15. Lin D, Tian X, Wu F, Xing B. 2010. Fate and transport of engineered nanomaterials in the environment. *J Environ Qual* 39: 1896-1908.

16. Mukherjee B, Weaver JW. 2010. Aggregation and charge behavior of metallic and nonmetallic nanoparticles in the presence of competing similarly-charged inorganic ions. *Environ Sci Technol* 44: 3332-3338.

17. Auffan M, Rose J, Wiesner MR, Bottero J. 2009. Chemical stability of metallic nanoparticles: A parameter controlling potential cellular toxicity in vitro. *Environ Pollut* 157: 1127-1133.
18. Röcker C, Pötzl M, Zhang F, Parak WJ, Nienhaus GU. 2009. A quantitative fluorescence study of protein monolayer formation on colloidal nanoparticles. *Nat Nanotechnol* 4: 577-580.

19. Diegoli S, Manciulea AL, Begum S, Jones IP, Lead JR, Preece JA. 2008. Interaction between manufactured gold nanoparticles and naturally occurring organic macromolecules. *Sci Total Environ* 402: 51-61.
20. Limbach LK, Bereiter R, Muller E, Krebs R, Galli R, Stark WJ. 2008. Removal of oxide nanoparticles in a model wastewater treatment plant: Influence of agglomeration and surfactants on clearing efficiency. *Environ Sci Technol* 42: 5828-5833.

21. Nowack B, Ranville JF, Diamond S, Gallego-Urrea JA, Metcalfe C, Rose J, Horne N, Koelmans AA, Klaine SJ. 2012. Potential scenarios for nanomaterial release and subsequent alteration in the environment. *Environ Toxicol Chem* 31: 50-59.

22. Kaegi R, Voegelin A, Ort C, Sinnet B, Thalmann B, Krismer J, Hagendorfer H, Elumelu M, Mueller E. 2013. Fate and transformation of silver nanoparticles in urban wastewater systems. *Water Res* 47:3866−3877.

23. Brar SK, Verma M, Tyagi RD, Surampalli RY. 2010. Engineered nanoparticles in wastewater and wastewater sludge – Evidence and impacts. *Waste Manage* 30: 504-520.

24. Westerhoff PK, Kiser MA, Hristovski K. 2013. Nanomaterial removal and transformation during biological wastewater treatment. *Environ Eng Sci* 30:109-117.

25. Ma R, Levard C, Judy JD, Unrine JM, Durenkamp M, Martin B, Jefferson B, Lowry GV. 2014. Fate of zinc oxide and silver nanoparticles in a pilot wastewater treatment plant and in processed biosolids. *Environ Sci Technol* 48:104-112.

26. Hou L, Li K, Ding Y, Li Y, Chen J, Wu X, Li X. 2012. Removal of silver nanoparticles in simulated wastewater treatment processes and its impact on COD and NH4 reduction. *Chemosphere* 87:248-252.

27. Westerhoff P, Song G, Hristovski K, Kiser MA. 2011. Occurrence and removal of titanium at full scale wastewater treatment plants: Implications for TiO_2 nanomaterials. *J Environ Monit* 13:1195-1203.

28. Park H, Kim HY, Cha S, Ahn CH, Roh J, Park S, Kim S, Choi K, Yi J, Kim Y, Yoon J. 2013. Removal characteristics of engineered nanoparticles by activated sludge. *Chemosphere* 92:524-528.

29. Kiser MA, Ryu H, Jang H, Hristovski K, Westerhoff P. 2010. Biosorption of nanoparticles to heterotrophic wastewater biomass. *Water Res* 44:4105-4114.

30. Hendren CO, Badireddy AR, Casman E, Wiesner MR. 2013. Modeling nanomaterial fate in wastewater treatment: Monte Carlo simulation of silver nanoparticles (nano-Ag). *Sci Total Environ* 449:418-425.

31. Kiser MA, Westerhoff P, Benn T, Wang Y, Pe´rez-Rivera J, Hristovski K. 2009. Titanium nanomaterial removal and release from wastewater treatment plants. *Environ Sci Technol* 43:6757–6763.

32. Lee KJ, Browning LM, Nallathamby PD, Desai T, Cherukuri PK, Xu XN. 2012. In vivo quantitative study of sized-dependent transport and toxicity of single silver nanoparticles using zebrafish embryos. *Chem Res Toxicol* 25:1029-1046.

33. Pan J, Buffet P, Poirier L, Amiard-Triquet C, Gilliland D, Joubert Y, Pilet P, Guibbolini, M, Risso de Faverney C, Roméo M, Valsami-Jones E, Mouneyrac C. 2012. Size dependent bioaccumulation and ecotoxicity of gold NPs in an endobenthic invertebrate: The Tellinid clam *Scrobicularia plana*. *Environ Pollut* 168:37-43.

34. Hull M, Chaurand P, Rose J, Auffan M, Bottero J, Jones JC, Schultz IR, Vikesland PJ. 2011. Filter-feeding bivalves store and biodeposit colloidally stable gold NPs. *Environ Toxicol Chem* 45:6592-6599.

35. McLaughlin J, Bonzongo JC. 2011. Effects of natural water chemistry on nanosilver behavior and toxicity to *Ceriodaphnia dubia* and *Pseudokirchneriella subcapitata*. *Environ Toxicol Chem* 31:168-175.

36. Allen HJ, Impellitteri CA, Macke DA, Heckman JL, Poynton HC, Lazorchak JM, Govindaswamy S, Roose DL, Nadagouda MN. 2010. Effects from filtration, capping agents and presence/absence of food on the toxicity of silver nanoparticles to *Daphnia magna*. *Environ Toxicol Chem* 29:2742-2750.

37. Johnston BD, Scown TM, Moger J, Cumberland SA, Baalousha M, Linge K, van Aerle R, Jarvis K, Lead JR, Tyler CR. 2010. Bioavailability of nanoscale metal oxides TiO_2, CeO_2, and ZnO to fish. *Environ Sci Technol* 44:1144-1151.

38. Scown TM, Santos EM, Johnston BD, Gaiser B, Baalousha M, Mitov S, Lead JR, Stone V, Fernandes TF, Jepson M, van Aerle R, Tyler CR. 2010. Effects of aqueous exposure to silver nanoparticles of different sizes in rainbow trout. *Toxicol Sci* 115:521-534.

39. Peng X, Palma S, Fisher NS, Wong SS. 2011. Effect of morphology of ZnO nanostructures on their toxicity to marine diatoms. *Aquat Toxicol* 102:186-196.

40. Pal S, Tak YK, Song JM. 2007. Does the antibacterial activity of silver nanoparticles depend on the shape of the nanoparticle? A study of the gram-negative bacterium *Escherichia coli*. *Appl Environ Microbiol* 73:1712-1720.

41. Lee KJ, Browning LM, Nallathamby PD, Xu XN. 2013. Study of charge-dependent transport and toxicity of peptide functionalized silver nanoparticles using zebrafish embryos single nanoparticle plasmonic spectroscopy. *Chem Res Toxicol* 26:904-917.

42. El Badawy AM, Silva RG, Morris B, Scheckel KG, Suidan MT, Tolaymat TM. 2011. Surface charge-dependent toxicity of silver nanoparticles. *Environ Sci Technol* 45:283-287.

43. Bone AJ, Colman BP, Gondikas AP, Newton KM, Harrold KH, Cory RM, Unrine JM, Klaine SJ, Matson CW, Di Giulio RT. 2012. Biotic and abiotic interactions in aquatic microcosms determine fate and toxicity of Ag nanoparticles: Part 2 - toxicity and Ag speciation. *Environ Sci Technol* 46:6925-6933.

44. Croteau M, Misra SK, Luoma SN, Valsami-Jones E. 2011. Silver bioaccumulation dynamics in a freshwater invertebrate after aqueous and dietary exposures to nanosized and ionic Ag. *Environ Sci Technol* 45:6600-6607.

45. U.S. EPA. 2008. OPPTS 835.3240 Simulation test- aerobic sewage treatment: A. Activated sludge units. EPA 712-C-08-004.

46. U.S. EPA. 2002. Methods for measuring the acute toxicity of effluents and receiving waters to freshwater and marine organisms. 5th Ed. 1-275.

47. Lacerda SHD, Park JJ, Meuse C, Pristinski D, Becker ML, Karim A, Douglas JF. 2010. Interaction of gold nanoparticles with common human blood proteins. *ACS Nano* 4: 365-379.

48. Brewer SH, Glomm WR, Johnson MC, Knag MK, Franzen S. 2005. Probing BSA binding to citrate-coated gold nanoparticles and surfaces. *Langmuir* 21: 9303-9307.

49. Duncan B, Kim C, Rotello VM. 2010. Gold nanoparticle platforms as drug and biomacromolecule delivery systems. *J Control Release* 148: 122-127.

50. Rouhana LL, Jaber JA, Schlenoff JB. 2007. Aggregation-resistant water-soluble gold nanoparticles. *Langmuir* 23:12799–12801.

51. Khan FR, Misra SK, Garcia-Alonso J, Smith BD, Stekopytov S, Rainbow PS, Luoma SN, Valsami-Jones E. 2012. Bioaccumulation dynamics and modeling in an estuarine invertebrate following aqueous exposure to nanosized and dissolved silver. *Environ Sci Technol* 46:7621-7628.

52. Zhao C, Wang W. 2010. Biokinetic uptake and efflux of silver nanoparticles in *Daphnia magna*. *Environ Sci Technol* 44:7699-7704.

53. Wang Y, Huang J, Gao Y. 2013. Subcellular accumulation of different concentrations of cadmium, nickel, copper in Indian mustard and application of a sigmoidal model. *J Environ Qual* 42: 1142-1150.

54. Miao A, Wang N, Yang L, Wang, W. 2012. Accumulation kinetics of arsenic in Daphnia magna under different phosphorus and food density regimes. *Environ Toxicol Chem* 31: 1283-1291.

55. Gaiser BK, Fernandes TF, Jepson MA, Lead JR, Tyler CR, Baalousha M, Biswas A, Britton GJ, Cole PA, Johnston BD, Ju-Nam Y, Rosenkranz P, Scown TM, Stone V. 2012. Interspecies comparisons on the uptake and toxicity of silver and cerium oxide nanoparticles. *Environ Toxicol Chem* 31:144-154.

56. Zhao C, Wang W. 2012. Size-dependent uptake of silver nanoparticles in *Daphnia magna*. *Environ Sci Technol* 46: 11345-11351.

57. Lee S, Kim K, Shon HK, Kim SD, Cho J. 2011. Biotoxicity of nanoparticles: Effect of natural organic matter. *J Nanopart Res* 13: 3051-3061.

58. Jiang S, Cao Z. 2010. Ultralow-fouling, functionalizable, and hydrolysable zwitterionic materials and their derivatives for biological applications. *Adv Mater* 22:920-932.

59. Speas DW, Duffy WG. 1998. Uptake of dissolved organic carbon (DOC) by *Daphnia pulex*. *J Freshwater Ecol* 13: 457-463.

60. Santore RC, Di Toro DM, Paquin PR, Allen HE, Meyer JS. 2001. Biotic ligand model of the acute toxicity of metals. 2. Application to acute copper toxicity in fresh water fish and *Daphnia*. *Environ Toxicol Chem* 20: 2397-2402.

61. Handy RD, Henry TB, Scown TM, Johnston BD, Tyler CR. 2008. Manufactured nanoparticles: Their uptake and effects on fish-a mechanistic analysis. *Ecotoxicology* 17:396-409.

62. Jung Y, Kim K, Kim JY, Yang S, Lee B, Kim SD. 2014. Bioconcentration and distribution of silver nanoparticles in Japanese medaka (*Oryzias latipes*). *J Hazard Mater* 267: 206-213.

63. Zhao J, Wang Z, Liu X, Xie X, Zhang K, Xing B. 2011. Distribution of CuO nanoparticles in juvenile carp (*Cyprinus carpio*) and their potential toxicity. *J Hazard Mater* 197: 304-310.

64. Khan FR, Kennaway GM, Croteau M, Dybowska A, Smith BD, Nogueira AJA, Rainbow PS, Luoma SN, Valsami-Jones E. 2014. *In vivo* retention of ingested Au NPs by *Daphnia magna*: No evidence for trans-epithelial alimentary uptake. *Chemosphere* 100:97-104.

65. Rosenkranz P, Chaudhry Q, Stone V, Fernandes TF. 2009. A comparison of nanoparticle and fine particle uptake by *Daphnia magna*. *Environ Toxicol Chem* 28:2142-2149.

66. Lovern SB, Owen HA, Klaper R. 2008. Electron microscopy of gold nanoparticle intake in the gut of *Daphnia magna*. *Nanotoxicology* 2:43-48.

67. Chithrani BD, Ghazani AA, Chan WCW. 2006. Determining the size and shape dependence of gold nanoparticle uptake into mammalian cells. *Nano Lett* 6:662-668.

68. Moyano DF, Rotello VM. 2011. Nano meets biology: Structure and function at the nanoparticle interface. *Langmuir* 27: 10376-10385.

69. Harper S, Usenko C, Hutchison JE, Maddux BLS, Tanguay RL. 2008. *In vivo* biodistribution and toxicity depends on nanomaterial composition size, surface functionalization and route of exposure. *J Exp Nanosci* 3: 195-206.

70. Federici G, Shaw BJ, Handy RD. 2007. Toxicity of titanium dioxide nanoparticles to rainbow trout (*Oncorhynchus mykiss*): Gill injury, oxidative stress, and other physiological effects. *Aquat Toxicol* 84:415-430.

71. Smith CJ, Shaw BJ, Handy RD. 2007. Toxicity of single walled carbon nanotubes to rainbow trout, (*Oncorhynchus mykiss*): Respiratory toxicity, organ pathologies and other physiological effects. *Aquat Toxicol* 82: 94-109.

72. Edgington AJ, Roberts AP, Taylor LM, Alloy MM, Reppert J, Rao AM, Mao J, Klaine SJ. 2010. The influence of natural organic matter on the toxicity of multiwalled carbon nanotubes. *Environ Toxicol Chem* 29:2511-2518.

73. Muth-Kohne E, Sonnack L, Schlich K, Hischen F, Baumgartner W, Hund-Rinke K, Schafers C, Fenske M. 2013. The toxicity of silver nanoparticles to zebrafish embryos increases through sewage treatment processes. *Ecotoxicology*. 22: 1264-1277.

74. Li L, Hartmann G, Doblinger M, Schuster M. 2013. Quantification of nanoscale silver particles removal and release from municipal wastewater treatment plants in Germany. *Environ Sci Technol* 47:7317-7323.

CHAPTER FOUR

ACCUMULATION AND DISTRIBUTION OF DOXORUBICIN AND NANO-DOXORUBICIN IN *PIMEPHALES PROMELAS*

Introduction

The inception of the pharmaceutical industry was a watershed movement for modern medicine arming physicians with powerful tools to eradicate diseases, delay terminal illness and improve overall quality of life. It is difficult to argue that our society would have advanced to its current state without the omniscient pharmaceutical business, yet the benefits of traditional medicine have reached a plateau plagued by several caveats that limit the effectiveness of an otherwise revolutionary tool. Specifically, traditional medicine is hampered by a lack of control over internal distribution. As a result introduced pharmaceuticals and invasive treatment procedures run afoul of the defensive mechanisms in our bodies in route to the desired site of action. Generally this requires a cost benefit analysis where the efficacy of the pharmaceutical is weighed against its toxicity to find the highest effective dose that causes the least amount of toxicity. The high dose requirements of most pharmaceuticals are the root cause of myriad side effects that are, at best, uncomfortable and in extreme cases can be lethal. These high dose requirements along with improper disposal and recycling of waste material are the major contributors to the growing presence of pharmaceuticals in the environment [1].

One major source of pharmaceuticals entering the aqueous environment is expected point source discharges affiliated with waste treatment and disposal. Ubiquitous availability and excessive use of pharmaceuticals elevate concentrations in waste streams to levels that place strain upon ill-equipped WWTPs. The efficiency of pharmaceutical removal from wastewater influent is linked to the design of the WWTP and the chemical structure of the pharmaceutical [2]. As a result, analysis of WWTP effluents has registered pharmaceutical concentrations that range from ng/L to ug/L [3]. This is a cause for concern because the measured exposure concentrations align with known sub lethal toxic responses in aquatic organisms. Previous studies have observed disrupted growth and reproduction for crustaceans, growth in

bacteria and algae [1] for various pharmaceuticals at the ppb exposure level and altered behavior in hybrid striped bass exposed to anti-depressants [4]. With the current consumption rates concentrations of pharmaceuticals in aquatic ecosystems will continue to increase in perpetuity until a suitable alternative is developed. Further, these same pharmaceuticals have been measured in drinking water systems downstream from wastewater effluents [5].

Over the past decade scientists and engineers have turned to nanotechnology to address the problems inherent with traditional medicine. Nanoparticles (NPs) provide long-term circulation, enhanced stability and increased capability with respect to the lone drug [6]. Manipulation of the intrinsic properties of NPs confers unprecedented control over distribution of the attached pharmaceutical. The fidelity of these nanomaterial drug delivery systems enables targeting of specific organs [7-9], cell types [10-11], and cellular organelles [12]. Moreover, nanomaterial treatments are purposefully engineered to avoid internal defense mechanisms [13-14] and release the attached compound based on predetermined physiological conditions or external stimuli [8,10,15-17] to avoid toxicity in non-target organs.

A myriad of nanomaterials are undergoing extensive study to establish their biological compatibility and viability as a biomedical tool. Gold nanomaterials are considered an excellent candidate for biomedical applications based on the ease of production, tissue and tumor specific targeting capabilities and the relatively low toxicity compared to other particle types [8,15]. Gold nanomaterials have been shown to successfully and accurately transport chemotherapy agents [10], antibiotics and biomolecules [8,15]. Furthermore, the unique properties of gold nanomaterials allow for improved resolution in tissue imaging and have spurred development of unconventional cancer therapies [18-19]. Improving the absorption of the compound by adding NP shells or carriers will make a notable difference to quality of life because they will foster lower dose requirements. Likewise, environmental concentrations of the pharmaceutical should decrease because these lower dose requirements will reduce the magnitude of incidental release via excretion. However, a percentage of this initial nanomedicine dose will be excreted into waste streams despite the improved fidelity of drug delivery. The fate and behavior of this mixed contaminant in waste streams and the aquatic environment remain unexplored. Once nanomedicines are

approved for mass distribution the pharmaceutical use paradigm will likely shift toward these new treatment options potentially introducing a unique and unpredictable contaminant into aquatic ecosystems.

We currently lack definitive evidence for how NP conjugates compare to traditional pharmaceuticals both in behavior and effects to non-target species and environmental systems. Nanomaterial drug delivery design is based on human consumption thus non-target organisms may respond differently to a nanomaterial-drug conjugate than expected based on mammalian research. Removing the uncertainty surrounding routes of entry into the environment and subsequent effects will be necessary for proper regulation of this indispensable biomedical tool. This study was designed to address the environmental implications of embracing nanomedicines as a suitable replacement for traditional pharmaceutical treatments. The methods and results from this study built upon previous research that examined nanomaterial accumulation and distribution for filter feeding invertebrates and fish. Spherical gold nanomaterials conjugated with the chemotherapy agent doxorubicin were utilized as a model pharmaceutical-nanomaterial to examine accumulation and distribution of these intertwined contaminants in *Pimephales promelas*. Results were compared to exposures of the lone pharmaceutical to explore how conjugation to a NP changes the internal distribution and if this new paradigm is protective or harmful to the organism.

Materials and Methods

Doxorubicin NP Synthesis and Characterization

Gulen Yesilbag and Daniel Moyano, University of Massachusetts-Amherst, graciously provided the nanomaterials used in this study. Particle synthesis followed methods outlined in Kim et al. [10] and Zhu et al. [20]. The doxorubicin nanoparticles (DoxNPs) used in this study were constructed from 2 nm spherical gold cores. The cores were coated with a ligand (identical to the ligand construction for the cationic NPs used in Chapter 3) that contained a quaternary amine conferring a cationic charge to the particle. A doxorubicin molecule was attached via an acid labile hydrazone bond to some but not all of the ligands on each particle transforming the particle into a drug delivery vehicle.

Size, surface charge and number of doxorubicin molecules per NP were characterized for all DoxNPs received from the University of Mass- Amherst. Hydrodynamic diameter and zeta potential were calculated with a Malvern Zetasizer in triplicate. Core diameter was confirmed with transmission electron microscopy (Hitachi 7600 TEM). DOXNP solutions of known NP concentration were diluted in Milli-Q, acidified with 0.1% HCl and analyzed on a SpectraMax GEMINI Fluorescence Microplate Reader with an excitation wavelength of 470 nm and emission wavelength of 590 nm. The concentration of doxorubicin was then calculated from a standard curve and divided by the number of NPs to quantify the average number of doxorubicin molecules per NP. Hydrodynamic diameter was measured at hour 0, 1 and 24 to assess changes in size that may indicate aggregation over the course of the exposure.

Culturing Pimephales promelas

Pimephales promelas were cultured in accordance with an animal use protocol approved by the Clemson University Animal Use Committee that followed established protocols [21]. *P. promelas* were grown and bred in a spacious flow through system that maintained the temperature between 23 -27 °C, pH between 7.5-8, and minimized nitrate and ammonia levels. Organisms were fed daily and kept under a 16:8 light/dark cycle. All fish were allowed to acclimate to the exposure containers and reconstituted moderately hard water (MHW) for 48 hours prior to exposure to alleviate any stress induced by the change in water hardness and alkalinity, and the additional stress caused by the transfer process. All adult fish used in uptake and organ accumulation experiments were 6-10 months old.

Preparation of Exposure Media

Doxorubicin HCl (Dox) and internal standard danuorubicin HCl (IS) stocks were prepared at 1mg/ml in methanol. Doxorubicin HCl and Danuorubicin HCl were purchased from Sigma Aldrich. Exposures were conducted in MHW and synthetic wastewater (WW) to compare direct and indirect release scenarios. Pristine MHW media was produced using the EPA standard method and then spiked with 25 ug/L doxorubicin (Dox) or the equivalent Dox concentration for gold NPs carrying doxorubicin molecules (DoxNP). Synthetic wastewater (WW) was formulated following a recipe outlined in the EPA guidelines for simulating aerobic treatment in wastewater treatment studies [22]. The contents were as follows:

peptone casein pancreatic digest (Sigma), 144 mg; meat extract (Sigma), 99 mg; urea (Sigma), 27 mg; dipotassium hydrogen phosphate (Fisher), 25 mg; sodium chloride (Fisher), 7 mg; calcium chloride (Fisher), 4 mg; magnesium sulfate (Sigma), 2 mg. The solution was brought to a final volume of 900 mL with Milli-Q water. The stock WW (~100 mg/L DOC) was then diluted to 6.5 mg DOC/L with MHW and filter sterilized through a 0.22 um Supra® membrane. Wastewater media was then spiked with the appropriated volume of Dox and DoxNP and allowed to equilibrate with gentle stirring for 1 hour prior to exposure. All exposures including controls were diluted so that the final methanol concentration was below the ASTM recommendation of 1 mL/L. No lethality or unusual behavior was observed in the controls at this methanol concentration.

Exposure for Organ Distribution Study

Prior to exposure, adult *P. promelas* (6-8 month old) from the main culture were conditioned to the exposure chambers for 48 hours. After conditioning three organisms were transferred in 1.2 L of the appropriate spiked exposure media for 48 hours. Each exposure was run in duplicate to give a total sample size of six. After 48 hours the adults were euthanized with buffered 4 % Tricane MS-222 and dissected to remove brain, liver/gallbladder, heart, gills and intestine. Brain, liver/gallbladder and heart samples were pooled in sets of two while the intestine and gills were analyzed separately. Organs were weighed and stored in -80 C until HPLC analysis.

Preliminary studies indicated that Dox degraded rapidly in our exposure media with approximately 80% reduction in concentration after 8 hours based on fluorescence measurements. All Dox treatments were respiked every 8 hours to maintain a relatively constant concentration of 25ug/L over the 48-hour exposure. Due to a lack of supplies the DoxNP exposures were not respiked every 8 hours. Water samples were collected every 8 hours for the Dox experiments and every 24 hours for the DoxNP experiments. Doxorubicin concentration in the Dox and DoxNP experiments was quantified with SpectraMax GEMINI Fluorescence Microplate Reader with an excitation wavelength of 470 nm and emission wavelength of 590 nm. Dox samples were analyzed without further processing. DoxNP water samples were amended with 0.1% HCl and allowed to incubate at 54 °C for 24 hours prior to analysis.

Separate Dox NP water samples were combined with concentrated Aqua Regia and analyzed for gold content on a Thermo Scientific XSeries2 Inductively Coupled Plasma Mass Spectrometer.

The *P. promelas* distribution experiments were performed with constant aeration to maintain acceptable dissolved oxygen concentrations during the exposure. Clemson Animal Use Committee (IACUC) approved the experimental design and euthanasia procedure used in all vertebrate testing for this study.

Sample Preparation

Organs were removed from the -80 °C freezer and thawed at room temperature. Organs were then homogenized with a Tissue Tearor for 30 seconds in acidified methanol (0.1% HCl). Liver/gallbladder and heart samples were homogenized in 1 mL of acidified methanol while brain, intestine and gill samples were homogenized in 2 mL. After homogenization samples were placed in -20 °C for 24 hours. Each sample was then spiked with 20 ug/L IS, vortexed for 30 seconds and incubated at 54 °C for 24 hours. After incubation samples were centrifuged at 4500 rpm for 15 minutes and 500 uL aliquots of the supernatant stored in sample vials for HPLC analysis.

HPLC Analysis

Working stock solutions of 1 mg/L were prepared each day of analysis from the doxorubicin and danuorubicin stock solutions. Standards for HPLC analysis were prepared in acidified methanol (0.1% HCl) from the working Dox stock solution at concentrations of 0, 2, 5, 10, 25, and 50, 100 and 500 ug/L doxorubicin. All standards were spiked with 20 uL of the 1 mg/L IS to give a final internal standard concentration of 20 ug/L. HPLC analysis was conducted with a Waters 1525 Binary HPLC Pump, a Waters 717 Plus auto sampler and a Waters 2475 Multi wavelength fluorescence detector. Separation was achieved with a Varian Polaris C-18A reverse phase analytical column (250 mm x 4.6 mm) and guard column. The mobile phase was a 35:65 mixture of HPLC grade acetonitrile: Milli-Q water, pH 3.5 adjusted with glacial acetic acid and supplemented with 0.1% triethylamine. Prior to analysis, the mobile phase was filtered with 0.45 micron nylon filter and degassed in a sonication bath. Sample analysis ran for 12 minutes at a flow rate of 1 mL/min with a 40 uL sample injection volume. Fluorescence signals were collected at excitation

wavelength 470 nm and emission wavelength 590 nm. Retention time ranged from 4.96 – 5.1 minutes for doxorubicin and from 7.45 - 7.86 for danuorubicin (Figure A.2).

Statistical Analysis

All treatments were compared to the control values using students-t test. Two-way ANOVA analysis was conducted in JMP 10.0 to identify significance influences from the main effects (exposure media, form of contaminant) on accumulation of doxorubicin in each organ. For all data analysis a p value of ≤ 0.05 was considered statistically significant.

Results

Particle Characterization in Exposure Media

Gold NPs with doxorubicin attached were 2 nm (Figure 4.1) and held a cationic surface charge. The hydrodynamic diameter, 18.44 ± 9.5 nm, and zeta potential, $+13.53 \pm 2.52$ mV of the Dox-NPs in MHW were similar to the measurements of the cationic NPs in Chapter 3 (Figure 4.2). In WW the Dox-NPs the surface charge remained at $+13.73 \pm 2.24$ mV despite a size increase to 263.37 ± 162.96 nm (Figure 4.2). The gold NPs in the DoxNP exposure contained on average 11 ± 1 doxorubicin molecules/particle.

As outlined in the methods, degradation of doxorubicin was rapid in the exposure chambers. Replenishment of doxorubicin every 8 hours was intended to maintain a constant concentration of Dox around 25 ug/L, which was analogous to the initial Dox concentration in the DoxNP exposures. The two exposures are inherently different because I did not have the supplies to maintain a constant concentration of DoxNPs in the exposure solution. Over the course of the experiment the concentration of Dox in the DoxNP solutions decreased by 85% in the MHW exposure and 70% in the WW exposure as gold NPs were either taken up by the fish or fell out of solution. Furthermore the ratio of doxorubicin molecules to gold dropped by ~50% over the 24 hour period in MHW but remained stable for the last 24 hour period. In contrast the shift in ratio of DoxNPs in the WW exposure was more gradual dropping to 76% after 24 hours and 63% of the original ratio after 48 hours.

Organ Accumulation

The intestine was the only organ to accumulated Dox above the LOD (1.4 ug Dox/L) in at least one replicate across all treatments (Table 1). Doxorubicin accumulation from the MHW Dox exposure, 0.198 $\pm$ 0.046 ug/g, was the only organ from all the treatments that was significantly different from the controls. Even though HPLC analysis identified measurable doxorubicin in the intestine of each replicate fish exposed to Dox in WW, 0.111 $\pm$ 0.032 ug/g, the average value was not significantly different from the control. Along with higher variability average accumulation of Dox in the intestines was greater for the DoxNP exposures with concentrations of 1.65 $\pm$ 1.34 ug/g and 1.83 $\pm$ 1.79 ug/g for DoxNP MHW and DoxNP WW exposures, respectively. Due to the high variability the two DoxNP exposures were not significantly different from the controls. None of the liver, gill, heart and brain samples for any treatment were significantly different from the controls. Organ accumulation data for each treatment including the controls are compiled in Table 1.

Accumulation was not determined to be different based on the form of the pharmaceutical or the exposure media and no interaction between the main effects was found in any organ. It should be noted that many of the heart, liver and brain replicates did not contain detectable doxorubicin; therefore, the concentration in these organs was highly dependent on the precision of the calibration curve and the inherent variability in creating a new standard curve for each run. High variability in the DoxNP exposures confounded my ability to differentiate based on form for each of the organs that were often not considered statistically different from the controls. Nevertheless, several trends were apparent in the data that given a larger sample size may have provided evidence for influences based on form and exposure media. Accumulation of Dox in the intestines from the NP form was highly variable in both exposure media; yet, the average accumulated Dox was an order of magnitude higher from DoxNP compared to the Dox only exposure (Figure 4.3). Moreover, the gills of fish from the DoxNP MHW exposure tended to accumulated more than the Dox MHW exposure. In general accumulation of Dox in the WW exposures was lower for the intestines. Only two of the six replicate intestines in the DoxNP WW exposure produced a measureable signal on the HPLC. In contrast, five of six intestines returned signals that were above the LOD for the

DoxNP MHW exposure. Likewise intestines from fish in the Dox MHW on average accumulated more Dox than fish from the Dox WW exposure though the differences were not significant.

Several other interesting trends appeared in the other organs that were not significant but may be suggestive for identifying distributional differences between exposure scenarios. Doxorubicin content found in either the brain, liver, or heart would indicate internalization of doxorubicin. Of the three liver replicates for each treatment, only one liver in the DoxNP MHW, 0.117 ug/g, returned a signal above the LOD (Figure 4.4). Likewise only one of the Dox WW heart replicates, 0.088 ug/g, produced a signal above the LOD. Analysis of the brain samples from each treatment did not return values above the detection limit implying that this organ is not important in doxorubicin distribution in *P. promelas*.

In the intestine and the liver several unique peaks not observed in the control samples appeared during analysis (Figure 4.5). The most common peak, retention time between 4.6 and 4.8 minutes, was found in eight of the 24 intestines and appeared to scale with the concentration of doxorubicin in the intestine. We observed a similar peak at 4.713 minutes in one of the liver replicates for the Dox MHW exposure. Other peaks were found that did not appear in the control samples but did occasionally show up as unknown peaks in some of the higher concentration standards. Four of the 12 intestines in the DoxNP exposures produced a signal that scaled with doxorubicin concentration at retention time 5.9 to 6.2 minutes. These peaks were not observed in any of the Dox exposures. Two of the liver samples in the DoxNP exposure, one liver and one heart in the Dox WW exposure produced signals with retention time between 7.1 and 7.3 minutes. A final unique peak, retention time between 9.2 and 9.7 minutes, was observed in five of the 24 intestines and in the only liver sample (Figure 5) that registered a concentration above the LOD. Further characterization of these peaks with the appropriate standards and more sensitive analytical equipment is required before I can confidently identify them.

Discussion

Gold NPs with doxorubicin attached to their surface responded to WW incubation in a manner similar to the cationic gold NPs without the pharmaceutical. As both particles were cationic, this suggests that the WW incubation is indeed a function of the surface charge. No stability studies were performed for

the DoxNPs; however, previous work identified a stabilizing effect at low concentration of WW over a 14-hour period that likely maintained over the duration of the experiment. Sample collection at 48 hours confirmed that a higher number of DoxNPs were in the water column; however, this may be indicative of lower uptake in the fish rather than a more stable gold NP solution.

I observed an unexpected decrease in the ratio of doxorubicin molecules per NP in both DoxNP exposures over the duration of the experiment. The change in ratio could be indicative of either a cleaving of the doxorubicin-NP linkage, degradation of the molecule or both. Even with uptake from fish the Dox NP exposures retained between 15 and 30% of the initial Dox exposure after 48 hours whereas the Dox only exposures lost approximately 80% after 8 hours suggesting that the Dox attached to the NP was protected to some extent from known degradation mechanisms in aqueous media [23]. Gold NPs might mitigate the photodegradation of doxorubicin through nanosurface energy transfer that quenches the fluorescent signal associated with free doxorubicin [24]. As a result degradation of doxorubicin tethered to the surface of the gold NPs likely contributed little to the change in doxorubicin ratio. However, doxorubicin released from the particle would be highly susceptible to photodegradation process as I observed in the Dox exposures. Previous work correlated an increase in hydrolysis of the bond connecting the doxorubicin to the NP with decreasing pH [25-26]. Less than 10% of the attached Dox was found to release from copolymers and micelles at pH 7.4 and 8.0 [25-26]. The pH of both exposure media in my study remained between 7.9 and 8.1 over the 48-hour experiment; therefore, the pH likely did not facilitate substantial release of Dox from the NPs in the exposure media. The exact cause of the ratio change in the media is unknown but I speculate that the change is related to water quality. Dissolved oxygen is involved in the degradation and toxicity of doxorubicin [23] and may impact the doxorubicin linkage. Additionally, the presence of organic matter reduced the rate of change in the ratio suggesting that in addition to stabilizing the particle surface the organic coating may restrict release of attached molecules from the NP surface.

Accumulation of doxorubicin in *P. promelas* was almost entirely localized in the intestine for all treatments. Swallowing water is common for fish in a high stress environment and is a common route for NPs and other contaminants to reach the intestine [27]. It is likely that the fish in this study were stressed

given the low volume exposures required and the propensity for accumulation in the intestine. Several peaks were observed in the gills in the DoxNP MHW exposure indicating this organ may be an important accumulation site. However, the four signals returned concentration values below the LOD suggesting they could just as easily be false positives. Despite similar conditions for all treatments, only one of the 12 fish exposed to free doxorubicin produced a measurable signal in the gills suggesting that this was not an important site in the Dox only exposures. Signals in the heart and liver indicated that doxorubicin was absorbed across intestinal and/or gill epithelial cells. The heart is a known target for doxorubicin [28] and I did observe a single peak in the Dox WW exposure. Yet a dearth of peaks in our other treatments suggested that the heart is not a principal accumulation site and low concentration exposures of Dox or DoxNPs will likely incur few deleterious responses in the heart. Fish liver and gallbladder samples from the DoxNP MHW exposure were the only replicates to produce measurable peaks for doxorubicin with no indication of doxorubicin in the livers of fish exposed to the free pharmaceutical. The disparity in these results suggested either a unique accumulation pattern for doxorubicin attached to NPs or that the content in the liver was scaled to the higher total doxorubicin content in the intestine for the DoxNP exposures. In either case the form of the pharmaceutical was a contributing factor.

There were no statistical differences in any of the organs across the four treatments indicating that neither the primary source of doxorubicin in the DoxNP exposures was free form and that the exposure media did not affect accumulation. However, there is evidence in the data to suggest that subtle differences between the forms may be important despite the lack of statistical significance. The high variability in the DoxNP intestines compared to the Dox only exposures imply that the content in the intestine of DoxNP fish cannot be attributed to the free form alone. My previous work identified the intestine as the primary site of cationic gold NP accumulation and encountered similar replicate variability further supporting the hypothesis that the NP is at least partially dictating the extent of doxorubicin accumulation in the intestine. Interestingly, the high variability of the DoxNP exposure also suggested that the NP can either enhance accumulation as in the case of the outliers or act in a protective manner as evident by the replicates near or below the LOD. A similar form-dependent effect was evident in the gills. The gills are another sink for NPs [20,29-31] and based on the signals from the HPLC it appeared that the DoxNP were accumulating at this

site more than the Dox only exposures. These trends outlined above are nothing more than that at the moment. More exposures at higher concentrations with more replicates are required to determine if these observations belie more important relationships between the form, exposure media, and accumulation.

The analytical methods were designed to give information on total doxorubicin content in each organ; therefore, it is difficult to determine if the doxorubicin in the liver for the DoxNP experiments is an example of the Trojan horse effect [32] or uptake of Dox that was cleaved from the NP either in the media or after ingestion. Doxorubicin that was cleaved prior to ingestion would be highly susceptible to degradation; therefore, I suspect that the contribution from this form of doxorubicin was minimal. While certain NPs are accumulated in the liver [30-31,33], a study on organ distribution with gold NP did not find significant concentrations of NPs in the liver of Japanese medaka [20]. Interestingly, I did find measurable gold in several of the liver/gallbladder samples from *P. promelas* exposed to cationic gold NPs in the last chapter. However, high variability and the Zhu et al. [20] study suggests that translocation of gold NPs to the liver is uncommon. As mentioned above the hydrazone bond is a pH liable linkage that is susceptible to lower pH environments. The intestinal pH of related species, *C. pauciradii* and *N. leptocephalus*, fall between 6.7 and 7.0 which is common for species in the Cyprinidae family of which *P. promelas* is a member [34]. Some degradation of the hydrazone bond (<10%) is likely to occur especially at the lower end of this pH range [25]; therefore, we suspect the Dox in the liver is the free form rather than attached to the NP.

Extra peaks were observed in the liver and intestine samples that were not associated with control samples or other organs. The most common peak found among the intestine samples, retention time between 4.6 and 4.8, eluted more quickly than doxorubicin, danuorubicin and the other peaks (Figure 6b-c). This peak likely represented doxorubicinol, a common metabolite of doxorubicin, based on its position relative to doxorubicin on the chromatograph [35]. The presence of this metabolite in the intestinal tissues could originate from direct metabolism in the intestinal tract and/or release of the compound from the liver into the intestinal tract after metabolism. The first scenario would suggest that the intestinal tract is capable of cleaving the hydrazone bond, as doxorubicin will not be metabolized if it remains attached to the gold NP. The second scenario could also indicate cleaving in the gut but might also suggest that the NPs are

transporting doxorubicin to the liver. In humans, doxorubicin is metabolized to doxorubicinol by aldoketoreductases and carbonyl reductase enzymes, which are found in the liver, kidney and gastrointestinal tract [36-37]. Homologues of the mammalian aldoketoreductase enzymes were identified in fish liver and intestines [38-39]. The relative concentrations of metabolite scaled to the concentration of doxorubicin in the intestine and support the argument for metabolism in the intestinal tract. Furthermore, liver samples did not always indicate the presence of the parent compound or the metabolite in fish replicates that demonstrated significant doxorubicin accumulation in their intestines. This does not rule out the possibility of doxorubicin cleaving from NPs after cellular uptake; however, as mentioned previously there is little evidence to support internal accumulation of gold NPs in fish [20]. The other peaks may represent other known metabolites of doxorubicin [35]. However, it is equally possible that these peaks are some other artifact in the doxorubicin or danuorubicin stocks as several of the extra peaks overlapped with peaks in the standards and one peak was difficult to differentiate from the IS peak.

The acidification of each organ prior to analysis precluded distinctions between the amount of free doxorubicin and the doxorubicin attached to the NP. As a result the concentrations of doxorubicin quantified in the DoxNP exposures represents a worst case scenario where all of the doxorubicin was released from the NP in each organ. As previously discussed this is an unlikely scenario for *P. promelas* because they lack a stomach and the pH of their intestine is close to neutral. The results are more reflective of a fish that has a stomach, such as salmon, where the pH drops to ~3 [40]. Even if absorption is expected to be low, the accumulated fraction of DoxNP in *P. promelas* will be a source of contamination for higher trophic level fish that do have a stomach.

There is a paucity of data in the literature on the environmental implications of nano-pharmaceuticals despite its popularity in the biomedical field. Release of nano-pharmaceuticals into waste streams should not be as extensive as traditional pharmaceuticals based on the perceived efficacy of the nano formulation and lower dose requirements. Regardless, a percentage of that dose will be excreted and transported to a WWTP on its way to environmental release. Wastewater treatment of doxorubicin range from highly effective (>90%) to woefully inept (~0%), yet effluent concentrations remain in the low ng/L range [41-43]. Nanomaterials are more effectively treated by WWTP but the removal efficiency can vary

based on the particle characteristics and the complexity of the plant design [44-46]. Current estimates of nanomaterials in the environment cover the low ug/L to the high ng/L range [47] thus attachment of doxorubicin to NPs could increase the concentration of the pharmaceutical as well as its persistence in the environment.

Conclusions

The biomedical industry has already benefited immensely from the influence of nanotechnology based on the unprecedented control over in vivo distribution. Many of the nano-pharmaceuticals are still in the research and development phase but within the next decade it is likely that there will be an influx of approved nano-medicines on the market. Research on the environmental implications of nanomaterials has evolved rapidly over the last few years and recently turned focus toward NPs released from consumer products in more environmentally relevant scenarios. This study examined the differences in accumulation and distribution in *P. promelas* exposed to doxorubicin in the free and NP form. Statistical analysis of the data indicated that neither the form nor the exposure media was influential to accumulation. However, high variability especially in the DoxNP exposure, masked several trends in the data that, with an expanded experimental design, may implicate form and exposure media as important factors for Dox accumulation. Extra peaks found in the liver and intestines indicated that doxorubicin was metabolized in fish exposed to both free Dox and DoxNP. Release of doxorubicin from DoxNP was suspected to occur primarily in the intestine; however, more studies are required to confirm this hypothesis. The results from this study demonstrate that NPs have the potential to affect the uptake and distribution of pharmaceuticals in the environment, which could elicit a toxic response depending on the construction of the nano-pharmaceutical and the organism physiology. With the nano revolution in traditional medicine looming on the horizon it is imperative that we conduct an exhaustive assessment of the environmental implications of this mixed contaminant before it becomes commonplace in our society.

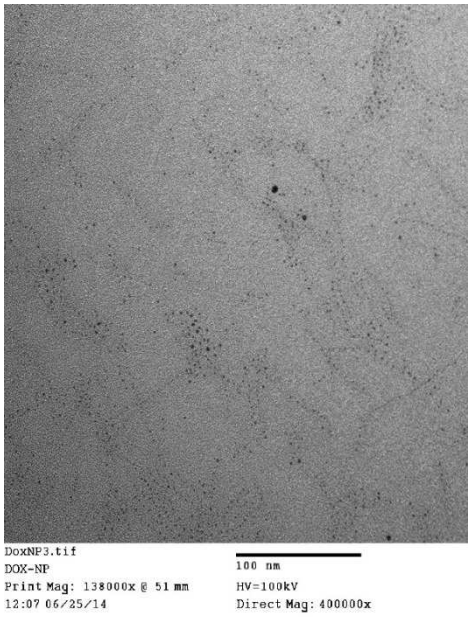

Figure 4.1: TEM micrograph of stock doxorubicin nanoparticles
Micrograph of DoxNP dried on a copper grid. Particles are fairly monodispersed with a nominal core diameter of 2 nm.

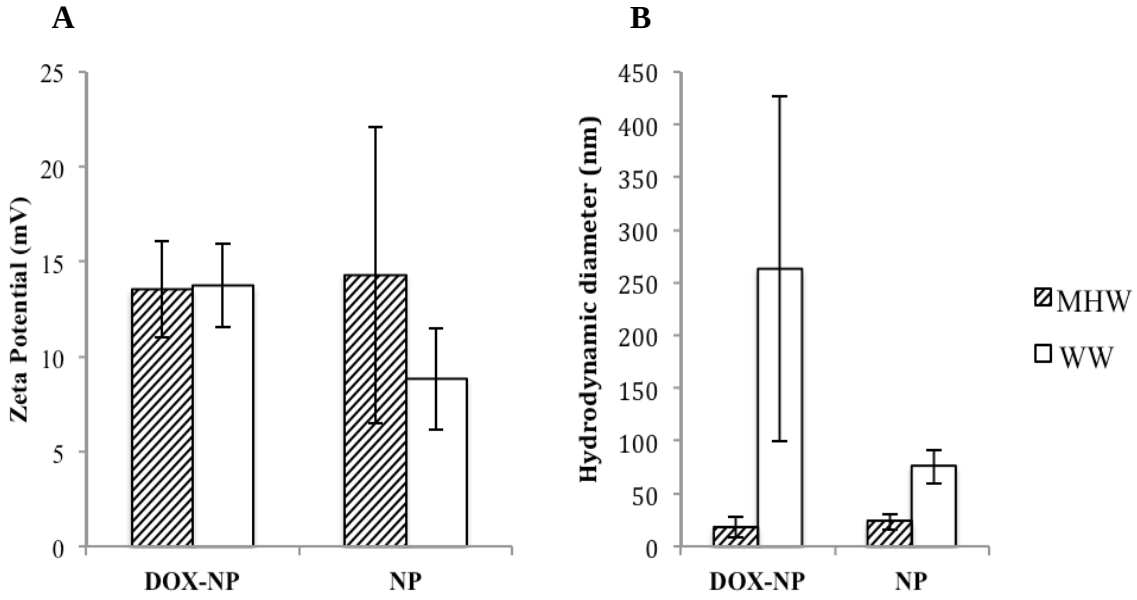

Figure 4.2: Characterization of doxorubicin nanoparticles and cationic gold NPs from Chapter 3
(A) Hydrodynamic diameter and (B) zeta potential for doxorubicin nanoparticles (DOX-NP) and cationic gold NPs (NP) from Chapter 3 in moderately hard water (MHW) and wastewater (WW). Each bar represents the average of 2-4 runs $\pm$ 1 standard deviation.

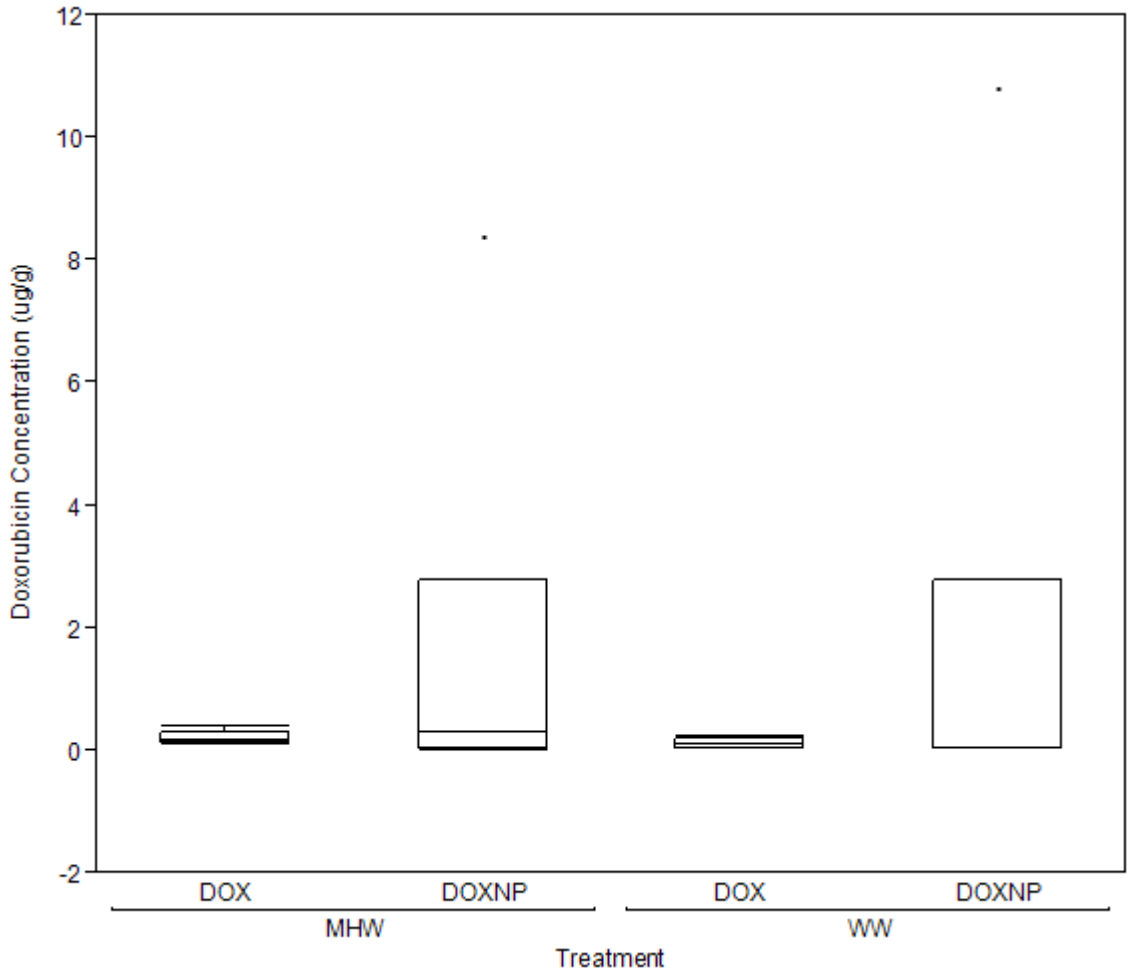

Figure 4.3: Doxorubicin accumulation in the intestine of fish from each treatment
Box plot displaying the distribution of analyzed doxorubicin concentration for intestines from fish exposed to the free doxorubicin (DOX) and doxorubicin attached to cationic gold NPs (DOXNP) in moderately hard water (MHW) and wastewater (WW). Values not connected to the box plot are considered outliers.

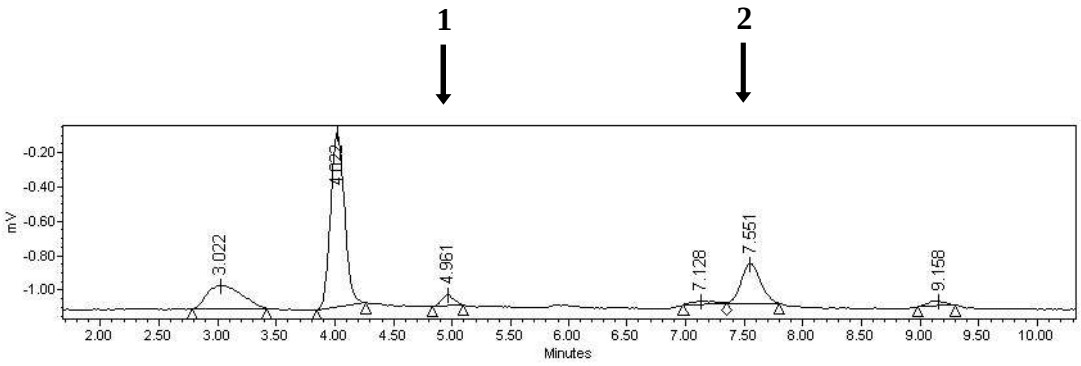

Figure 4.4: HPLC chromatograph of liver/gallbladder sample from fish exposed to doxorubicin nanoparticles

Chromatograph for a pooled liver/gallbladder sample from fish exposed to Dox-NP in MHW. **1**: peak for doxorubicin, retention time 4.96 – 5.10 minutes. **2**: peak for danuorubicin, retention time 7.45 – 7.86 minutes.

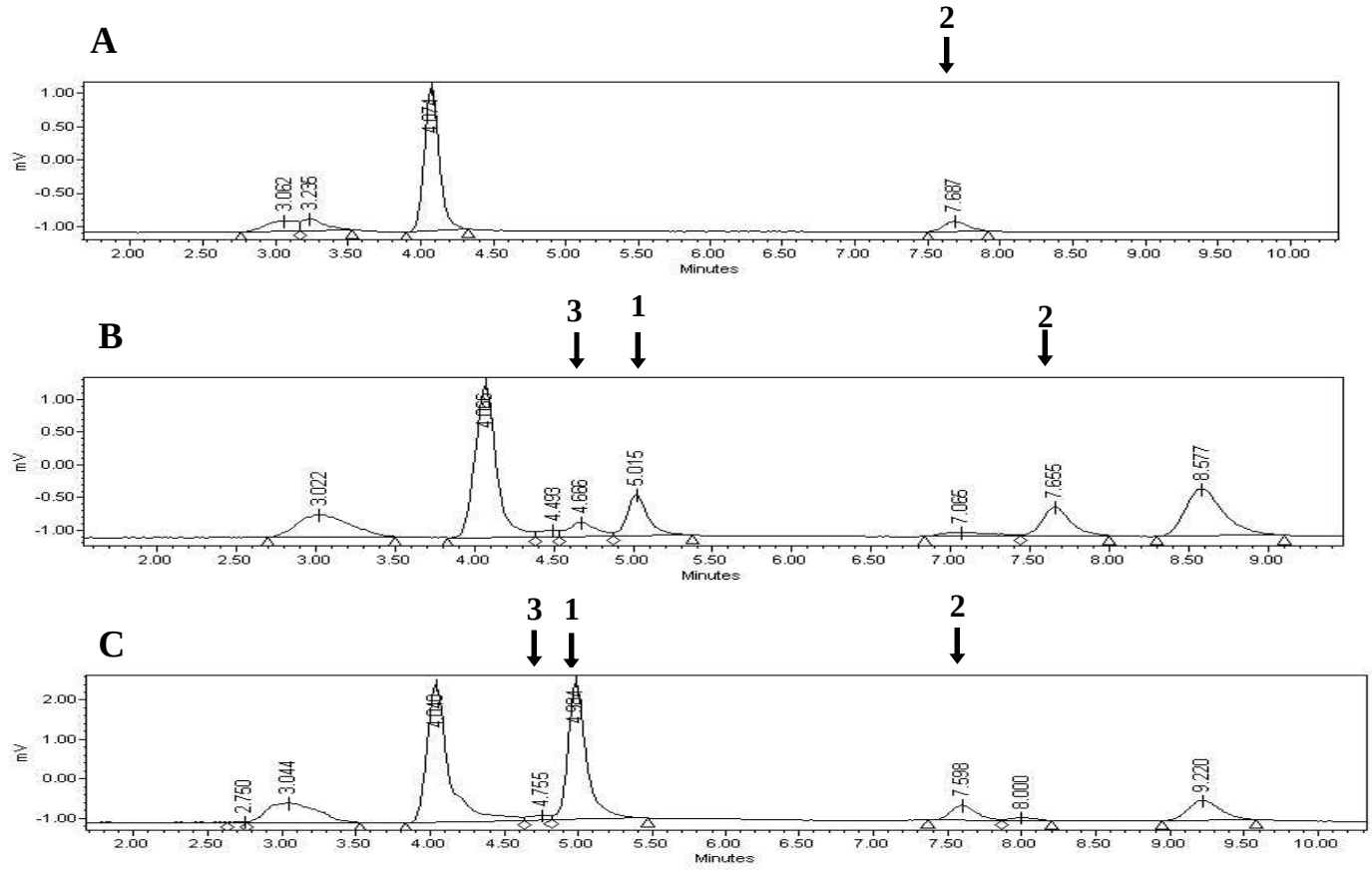

Figure 4.5: HPLC chromatograph of fish intestines from control, Dox and DoxNP exposures
Sample chromatographs of intestines for fish from (A) control, (B) free doxorubicin (Dox), and (C) doxorubicin attached to gold nanoparticles (DoxNP) exposures. **1**: peak for doxorubicin, retention time 4.96 – 5.10 minutes. **2**: peak for danuorubicin, retention time 7.45 – 7.86 minutes. **3:** unknown peak, possibly doxorubicinol, retention time 4.6 – 4.8 minutes.

	Doxorubicin Concentration (ug Dox g^{-1})				
	Control	**Dox MHW**	**Dox WW**	**DoxNP MHW**	**DoxNP WW**
Brain[a]	0.074 ± 0.074	N.D.	0.004 ± 0.004	N.D.	N.D.
Heart[a]	0.033 ± 0.033	N.D.	0.036 ± 0.027	N.D.	N.D.
Liver/Gallblader[a]	0.008 ± 0.008	N.D.	0.009 ± 0.009	0.039 ± 0.039	N.D.
Intestine	0.004 ± 0.002	0.198 ± 0.046[b]	0.111 ± 0.032	1.65 ± 1.34	1.83 ± 1.79
Gill	0.013 ± 0.009	0.008 ± 0.008	N.D.	0.029 ± 0.021	N.D.

Table 4.1: Doxorubicin concentration in select organs from five different treatments
Doxorubicin concentration in each organ (± SE) of *Pimephales promelas* exposed to no contaminant (control) free doxorubicin (Dox) and doxorubicin attached to cationic gold NPs (DoxNP) in moderately hard water (MHW) and wastewater (WW) for 48 hours
N.D. non-detect
[a] pooled samples into three replicates instead of six
[b] organ concentration is significantly different from the control
[c] organ concentration is significantly different based form of the pharmaceutical
[d] organ concentration is significantly different based on the exposure media

References

1. Santos LHMLM, Araujo AN, Fachini A, Pena A, Delerue-Matos C, Montenegro MCBSM. 2010. Ecotoxicological aspects related to the presence of pharmaceuticals in the aquatic environment. *J Hazard Mater* 175: 45-95.

2. Luo Y, Guo W, Ngo HH, Nghiem LD, Hai FI, Zhang J, Liang S, Wang XC. 2014. A review on the occurrence of micropollutants in the aquatic environment and their fate and removal during wastewater treatment. *Sci Total Environ* 473-474: 619-641.

3. Kummerer K. 2010. Pharmaceuticals in the environment. *Annu Rev Environ Resour* 35: 57-75.

4. Gaworecki KM, Klaine SJ. 2008. Behavioral and biochemical responses of hybrid striped bass during and after fluoxetine exposure. *Aquat Toxicol* 88: 207-213.

5. Stackelberg PE, Furlong ET, Meyer MT, Zaugg SD, Henderson AK, Reissman DB. 2004. Persistence of pharmaceutical compounds and other organic wastewater contaminants in a conventional drinking-water-treatment plant. *Sci Total Environ* 329: 99-113.

6. Khelbstov N, Dykman L. 2011. Biodistribution and toxicity of engineered gold nanoparticles: A review of in vitro and in vivo studies. *Chem Soc Rev* 40: 1647-1671.

7. Chen PC, Mwakwari SC, Oyelere AK. 2008. Gold nanoparticles: From nanomedicine to nanosensing, *Nanotech Sci Appl* 1:45–66.

8. Ghosh P, Han G, De M, Kim CK, Rotello VM. 2008. Gold nanoparticle in delivery applications. *Adv Drug Deliv Rev* 60:1307–1315.

9. Pissuwan D, Valenzuela SM, Killingsworth MC, Xu X, Cortie MB. 2007. Targeted destruction of murine macrophage cells with bioconjugated gold nanorods, *J Nanopart Res* 9:1109–1124.

10. Kim B, Han G, Toley BJ, Kim C, Rotello VM, Forbes NS. 2010. Tuning payload delivery in tumour cylindroids using gold nanoparticles. *Nat Nanotechnol* 5:465-472.

11. Weissleder R, Kelly K, Sun EY, Shtatland T, Josephson L. 2005. Cell-specific targeting of nanoparticles by multivalent attachment of small molecules. *Nat Biotechnol* 23:1418-1423.

12. Paulo CSO, Pires das Neves R, Ferreira LS. 2011. Nanoparticles for intracellular-targeted drug delivery. *Nanotechnology* 22:1-11.

13. Gu Y, Cheng J, Man CW, Wong W, Cheng SH. 2012. Gold-doxorubicin nanoconjugates for overcoming multidrug resistance. *Nanomed Nanotechnol* 8:204-211.

14. Li M, Al-Jamal KT, Kostarelos K, Reineke J. 2010. Physiologically based pharmacokinetic modeling of nanoparticles. *ACS Nano* 4: 6303-6317.

15. Pissuwan D, Niidome T, Cortie M.B. 2011. The forthcoming applications of gold nanoparticles in drug and gene delivery systems. *J Control Release* 149:65-71.

16. Skirtach AG, Javier AM, Kreft O, Köhler K, Alberola AP, Möhwald H, Parak WJ, Sukhorukov GB, 2006. Laser-induced release of encapsulated materials inside living cells. *Angew Chem* 118:4728–4733.

17. Gupta P, Vermani K, Garg S. 2002. Hydrogels: From controlled release to pH-responsive drug delivery. *Drug Discov Today* 7:569–579.

18. Chen J, Glaus C, Laforest R, Zhang Q, Yang M, Gidding M, Welch MJ, Xia Y. 2010. Gold nanocages as photothermal transducers for cancer treatment. *Small* 6:811-817.

19. Boisselier E, Astruc D. 2009. Gold nanoparticles in nanomedicine: preparations, imaging, diagnostic, therapies and toxicity. *Chem Soc Rev* 38:1759-1782.

20. Zhu Z, Carboni R, Quercio Jr. MJ, Yan B, Miranda OR, Anderton DL, Arcaro KF, Rotello VM, Vachet RW. 2010. Surface properties dictate uptake, distribution, excretion, and toxicity of NPs in fish. *Small* 6:2261-2265.

21. U.S. EPA. 2002. Methods for measuring the acute toxicity of effluents and receiving waters to freshwater and marine organisms. 5th Ed. 1-275.

22. U.S. EPA. 2008. OPPTS 835.3240 Simulation test- aerobic sewage treatment: A. Activated sludge units. EPA 712-C-08-004.

23. Nawara K, Krysinski P, Blanchard GJ. 2012. Photoinduced reactivity of doxorubicin: Catalysis and degradation. *J Phys Chem A* 116: 4330-4337.

24. Wang F, Wang Y, Dou S, Xiong M, Sun T, Wang J. 2011. Doxorubicin-tethered responsive gold nanoparticles facilitate intracellular drug delivery for overcoming multidrug resistance in cancer cells. *ACS Nano* 5: 3679-3692.

25. Bae Y, Nishiyama N, Fukushima S, Koyama H, Yasuhiro M, Kataoka K. 2005. Preparation and biological characterization of polymeric micelle drug carriers with intracellular pH-triggered drug release property: Tumor permeability, controlled subcellular drug distribution, and enhanced in vivo antitumor efficacy. *Bioconjugate Chem* 16: 122-130.

26. Etrych T, Jelinkova M, Rihova B, Ulbrich K. 2001. New HPMA copolymers containing doxorubicin bound via pH-sensitive linkage: Synthesis and preliminary in vitro and in vivo biological properties. *J Control Release* 73: 89-102.

27. Handy RD, Henry TB, Scown TM, Johnston BD, Tyler CR. 2008. Manufactured nanoparticles: Their uptake and effects on fish-a mechanistic analysis. *Ecotoxicology* 17:396-409.

28. Thorn CF, Oshiro C, Marsh S, Hernandez-Boussard T, McLeod H, Klein TE, Altman RB. 2011. Doxorubicin pathways: pharmacodynamics and adverse effects. *Pharmacogenet Genomics* 21: 440-446.

29. Scown TM, Santos EM, Johnston BD, Gaiser B, Baalousha M, Mitov S, Lead JR, Stone V, Fernandes TF, Jepson M, van Aerle R, Tyler CR. 2010. Effects of aqueous exposure to silver nanoparticles of different sizes in rainbow trout. *Toxicol Sci* 115:521-534.

30. Gaiser BK, Fernandes TF, Jepson MA, Lead JR, Tyler CR, Baalousha M, Biswas A, Britton GJ, Cole PA, Johnston BD, Ju-Nam Y, Rosenkranz P, Scown TM, Stone V. 2012. Interspecies comparisons on the uptake and toxicity of silver and cerium oxide nanoparticles. *Environ Toxicol Chem* 31:144-154.

31. Zhao J, Wang Z, Liu X, Xie X, Zhang K, Xing B. 2011. Distribution of CuO nanoparticles in juvenile carp (*Cyprinus carpio*) and their potential toxicity. *J Hazard Mater* 197: 304-310.

32. Park EJ, Yi J, Kim Y, Choi K, Park K. 2010. Silver nanoparticles induce cytotoxicity by a Trojan-horse type mechanism. *Toxicol in Vitro* 24:872-878.

33. Jung Y, Kim K, Kim JY, Yang S, Lee B, Kim SD. 2014. Bioconcentration and distribution of silver nanoparticles in Japanese medaka (*Oryzias latipes*). *J Hazard Mater* 267: 206-213.

34. German DP, Nagle BC, Villeda JM, Ruiz AM. 2010. Evolution of herbivory in a carnivorous clade of minnows (Teleostei: Cyprinidae): Effects on gut size and digestive physiology. *Physiol Biochem Zool* 83: 1-18.

35. Zhou Q, Chowbay B. 2002. Determination of doxorubicin and its metabolites in rat serum and bile by LC: Application to preclinical pharmacokinetic studies. *J Pharmaceut Biomed* 30: 1063-1074.

36. Kassner N, Huse K, Martin H, Godtel-Armbrust U, Metzger A, Meineke I, Brockmoller J, Klein K, Zanger UM, Maser E, Wojnowski L. 2008. Carbony reductase 1 is a predominant doxorubicin reductase in the human liver. *Drug Metab Dispos* 36:2113-2120.

37. Kivisto KT, Kroemer HK, Eichelbaum M. 1995. The role of human cytochrome P450 enzymes in the metabolism of anticancer agents: Implications for drug interactions. *Br J Clin Pharmacol* 40: 523-530.

38. Lou Z, Johnson JV, James MO. 2002. Intestinal and hepatic microsomal metabolism of testosterone and progesterone by a 3α-hydroxysteroid dehydrogenase to the 3α-hydroxy derivatives in the channel catfish, *Ictalurus punctatus*. *Mol Biol* 82: 413-424.

39. Oppermann UCT, Nagel G, Belai I, Bueld JE, Genti-Raimondi S, Koolman J, Netter KJ, Maser E. 1998. Carbonyl reduction of an anti-insect agent imidazole analogue of metyrapone in soil bacteria, invertebrate and vertebrate species. *Chem-Biol Interact* 114: 211-224.

40. Ringo E, Olsen RE, Mayhew TM, Myklebust R. 2003. Electron microscopy of intestinal microflora of fish. *Aquaculture* 227: 395-415.

41. Martin J, Camacho-Munoz D, Santos JL, Aparicio I, Alonso E. 2014. Occurrence and ecotoxicological risk assessment of 14 cytostatic drugs in wastewater. *Water Air Soil Pollut* 225: 1896-1906.

42. Martin J, Camacho-Munoz D, Santos JL, Aparicio I, Alonso E. 2011. Simultaneous determination of a selected group of cytostatic drugs in water using high-performance liquid chromatography-triple quadrupole mass spectrometry. *J Se Sci* 34: 3166-3177.

43. Mahnik SN, Lenz K, Weissenbacher N, Mader RM, Fuerhacker M. 2007. Fate of 5-fluorouracil, doxorubicin, epirubicin, and daunorubicin in hospital wastewater and their elimination by activated sludge and treatment in a membrane-bio-reactor system. *Chemosphere* 66:30-37.

44. Park H, Kim HY, Cha S, Ahn CH, Roh J, Park S, Kim S, Choi K, Yi J, Kim Y, Yoon J. 2013. Removal characteristics of engineered nanoparticles by activated sludge. *Chemosphere* 92:524-528.

45. Kiser MA, Ryu H, Jang H, Hristovski K, Westerhoff P. 2010. Biosorption of nanoparticles to heterotrophic wastewater biomass. *Water Res* 44:4105-4114.

46. Limbach LK, Bereiter R, Muller E, Krebs R, Galli R, Stark WJ. 2008. Removal of oxide nanoparticles in a model wastewater treatment plant: Influence of agglomeration and surfactants on clearing efficiency. *Environ Sci Technol* 42: 5828-5833.

47. Gottschalk F, Sonderer T, Scholz RW, Nowack B. 2009. Modeled environmental concentrations of engineered nanomaterials (TiO_2, ZnO, Ag, CNT, Fullerenes) for different regions. *Environ Sci Technol* 43: 9216-9222.

CHAPTER FIVE

CONCLUSIONS

Modeling the influence of physicochemical properties on particle uptake and elimination in *Daphnia magna*

1. Accumulation mechanisms in *D. magna* are sensitive to changes in size and surface charge while shape has relatively little influence over biodynamics.
2. When challenged in environmental conditions similar to those in my experiments, *D. manga* will accumulate a higher NP body burden from exposure to larger cationic NPs ($\geq$ 20 nm) compared to smaller anionic particles (< 20 nm).
3. Nanoparticles with the configurations used in this study were not internalized; therefore, the calculated BCF represent the relative contributions of the ingestion and adsorption rate and NP interactions with permanent (gut epithelial membranes) and transient (peritrophic membrane and debris) structures in the gut tract.

Transformation of nanoparticles in the presence of wastewater and its impact on accumulation in *Daphnia magna* and *Pimephales promelas*

1. Transformation of NPs during WW incubation varied based on initial particle charge and DOC concentration.
2. Incubation of NPs with a low concentration of WW reduced accumulation of cationic gold by *D. magna* but had little impact on zwitterionic accumulation.
3. The cationic NPs used in this study were constructed with properties that encouraged internalization by *D. magna* regardless of the exposure scenario.
4. *P. promelas* biodymnaics were affected by the intrinsic particle charge on the gold NP but were not sensitive to the transformative changes triggered by incubation with WW.

Accumulation and distribution of doxorubicin and nano-doxorubicin in *Pimephales promelas*

1. Doxorubicin attached to gold NPs was more resistant to degradation in both exposure solutions compared to the free doxorubicin.
2. Uptake of doxorubicin was not statistically different based on the form of the pharmaceutical or the exposure conditions.
3. Doxorubicin was primarily distributed to the intestine of *P. promelas* with some evidence of lesser accumulation in the liver and gill.

The purpose of this dissertation was to call attention to several areas of NP research that have yet to be fully explored. Creating specific models for each NP configuration is both time and cost intensive task based on the sheer number of possible combinations therefore reducing a NP to its primary characteristics is an excellent strategy for defining risk. I demonstrated that not all characteristics are created equal in biodynamic processes. Furthermore, while I examined only the three most discussed properties, comparisons to other studies in the literature stressed the importance of several other characteristics such as core and surface chemistry that need to be weighed in a similar manner to prioritize risk of NPs. Further refinement of risk prioritization will need to take into account the water chemistry not only at the point of exposure but also during the steps prior to release to more accurately predict the toxic potential of the NP. The journey of a NP from production to environmental release is fraught with influences that are capable of changing the identity of the nanomaterial. I demonstrated that certain particle configurations are more susceptible to these transformations and that these transformations do not affect accumulation in all species. The final chapter of this dissertation emphasized the subtle differences between accumulation of the nano and molecular forms of pharmaceuticals. A quick literature search for nano-medicines reveals a technology that has rapidly grown in popularity over the last decade without consideration for environmental consequences. The data are preliminary but the results argue that this mixed contaminant warrants further scrutiny.

APPENDIX

Appendix A

Extra Figures and Tables

	Method 1	Method 2
Procedure	1. Homogenize fish 2. 6 mL 35% Aqua Regia (AR) + 1 mL H_2O_2 (TraceGrade 30% v/v) 3. Microwave Digest - 170 °C for 25 minutes 4. Dilute to 30 mL with Milli Q	1. Dry Ash in 450 °C for 26 hrs 2. Dissolve ash in 5 mL concentrated HNO_3 (Tracegrade 70% v/v) 3. Dilute to 35% acid with Milli-Q 4. Microwave Digest - 170 °C for 25 minutes 5. Combine with 5 mL 100% AR let sit for 1 hour 6. Evaporate to near dryness in PFA digestion chambers 7. Dissolve residue in 100% AR 8. Dilute to 6 or 10 mL with Milli-Q
Percent Recovery	**89.44 ± 36.17 %**	**73.03 ± 3.58 %**

Table A.1: *Pimephales promelas* digestion methods
Two methods used including the microwave digester procedure and the percent recovery with standard error. Percent recovery was calculated from 5-7 replicates.

	Method 1	Method 2	Method 3
Procedure	1. Digest overnight in 3 mL HNO_3 (Tracegrade 70% v/v) 2. Add 1 mL H_2O_2 (TraceGrade 30% v/v) and 2 mL Milli Q water 3. Microwave Digest - 170 °C for 25 minutes 4. Evaporate to near dryness in PFA digestion chambers 5. Dissolve residue in 0.720 or 1.1 mL of 100% AR 6. Dilute to 6 or 10 mL with Milli-Q	1. Combine organ with 2.5 mL HNO_3 (Tracegrade 35% v/v) and 0.5 mL H_2O_2 (TraceGrade 30% v/v) 2. Hot Plate Digest - ~100 °C for 35 minutes 3. Combine with 4 mL HCl (Tracegrade 36% v/v), let sit for 1 hour 4. Evaporate to near dryness in PFA digestion chambers 5. Dissolve residue in 0.250 mL of 100% AR 6. Dilute to 10 mL with Milli-Q	1. Digest overnight in 3 mL HNO_3 (Tracegrade 70% v/v) 2. Add 1 mL H_2O_2 (TraceGrade 30% v/v) and 2 mL Milli Q water 3. Microwave Digest - 170 °C for 25 minutes 4. Add 2.5 mL 100% Aqua Regia, let sit for 1 hour 5. Evaporate to near dryness in PFA digestion chambers 6. Dissolve residue in 0.720 or 1.1 mL of 100% AR 7. Dilute to 6 or 10 mL with Milli-Q
Percent Recovery	**90.79 ± 3.0 %**	**78.63 ± 8.66 %**	**95.68 ± 3.93 %**

Table A.2: Organ digestion methods with percent recovery
Percent recovery experiment used to identify the best method for analyzing the gold content in *P. promelas* organs. Each method includes detailed steps and percent recovery with standard error. Percent recovery was calculated from 2-4 replicates.

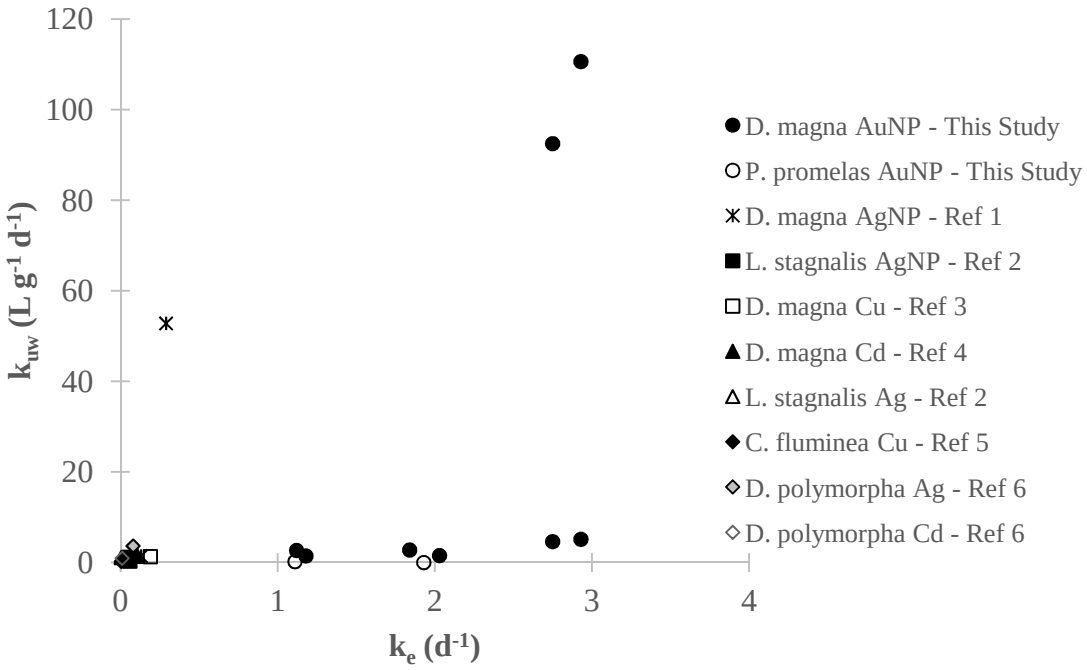

Figure A.1: Comparision of biodynamic constants from this dissteration and the literature

Biodynamic parameters from various literature sources (references on page 146) are compared to the biodynamic parameters derived in this dissertation. Uptake rate constant (k_{uw}) is ploted against elimination rate constant (k_e) to demonstrate the significant difference between the parameters I derived and those from other types of metallic contaminants and other important model species.

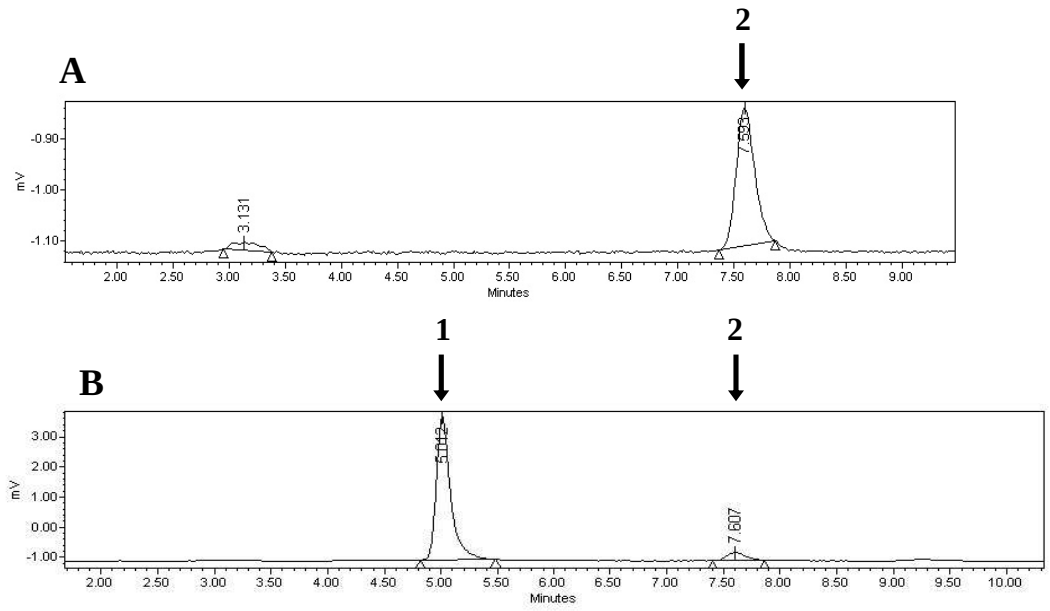

Figure A.2: HPLC chromatograph of doxorubicin standards
Sample chromatographs of 0 (A) and 100 (B) ppb doxorubicin standards spiked with 20 ppb danuorubicin internal standard. **1**: peak for doxorubicin, retention time 4.96 – 5.10 minutes. **2**: peak for danuorubicin, retention time 7.45 – 7.86 minutes.

	Method
Procedure	1. Homogenize organs in acidified MeOH (0.1% HCl) for 30 seconds 2. Sit overnight in -20 °C 3. Vortex 30 seconds 4. Incubate in drying oven at 54 °C for 24 hours 5. Centrifuge at 4500 rpm for 15 minutes 6. Remove 500 uL aliquout of supernantant for analysis
Percent Recovery	**90.50 ± 5.45 %**

Table A.3: Doxorubicin extraction method with percent recovery
Method used for extracting doxorubicin and doxorubicin-NPs from *P. promelas* organs. Method includes detailed steps and the percent recovery with standard error. Percent recovery was calculated from 4 replicates.

References

1. Zhao C, Wang W. 2010. Biokinetic uptake and efflux of silver nanoparticles in *Daphnia magna*. *Environ Sci Technol* 44:7699-7704.

2. Croteau M, Misra SK, Luoma SN, Valsami-Jones E. 2011. Silver bioaccumulation dynamics in a freshwater invertebrate after aqueous and dietary exposures to nanosized and ionic Ag. *Environ Sci Technol* 45:6600-6607.

3. Zhao CM, Fan WH, Wang WX. 2010. Aquesous and dietary copper uptake and elimination in *Daphnia magna* determined by the ^{67}Cu radiotracer. *Environ Toxicol Chem* 28: 2360-2366.

4. Guan R, Wang WX. 2006. Multiphase biokinetic modeling of cadmium accumulation in *Daphnia magna* from dietary and aqueous sources. *Environ Toxicol Chem* 25: 2840-2846.

5. Croteau MN, Luoma SN, Topping BR, Lopez CB. 2004. Stable metal isotopes reveal copper accumulation and loss dynamics in the freshwater bivalve *Corbicula*. *Environ Sci Technol* 38: 5002-5009.

6. Roditi HA, Fisher NS, Sañudo-Wilhelmy SA. 2000. Field testing a bioaccumulation model for zebra mussels. *Environ Sci Technol 34*: 2817−2825.